MGT FLUE GAS CHARACTERIZATION & TREATMENT BY PLASMA-CATALYST

NATURAL GAS MICRO-GAS TURBINE COMBUSTION FLUE GAS
CHARACTERIZATION AND AFTER-TREATMENT BY NON-
THERMAL PLASMA-CATALYST REACTOR

By

SCOTT AMBRIDGE, B.ENG.

A Thesis

Submitted to the School of Graduate Studies

In Partial Fulfillment of the Requirements

For the Degree

Master of Applied Science

McMaster University

MASTER OF APPLIED SCIENCE (2004)
(Engineering Physics)

McMaster University
Hamilton, Ontario

TITLE: Natural Gas Micro-Gas Turbine Combustion Flue Gas
Characterization and After- Treatment by Non-Thermal Plasma-Catalyst
Reactor

AUTHOR: Scott Ambridge, B.Eng. (Carleton University)

SUPERVISOR: Professor Jen-Shih Chang

NUMBER OF PAGES: 140

Abstract

With the increasing need for alternative power sources in the future, the growth of the distributed energy sector will play an important role for meeting future world energy needs. One potential source of distributed energy is the natural gas combustion micro-gas turbine (MGT). Although natural gas is considered a cleaner source of energy than some solid and liquid fuels, there are still significant pollutant emissions. In order to determine the potential pollution from MGTs, two types of MGTs were characterized for their emissions; one single stage moderate lean burn combustion type MGT and one dual stage lean burn combustion type MGT. Furthermore, a novel pollution control device, a trench type non-thermal plasma-catalyst reactor, was examined for potential effectiveness of treating gaseous pollutants in MGT type flue gas.

The MGT characterization of the exhaust flue gas revealed that the pollutants of greatest concern for the single stage combustion type MGT were nitrogen oxides (NO_x) and volatile organic compounds (VOCs), with steady state concentrations of 15ppm (~510 g[NO_x]/MWh) and 120ppm at a full load of 101.2kW, respectively. VOCs were observed to be higher in the dual stage MGT's flue gas with a maximum steady state concentration of 140ppm at a full load of 70kW. It was observed that the dual stage MGT had a significant amount of particulate matter emission for a diameter smaller than 29nm.

Preliminary MGT simulated exhaust gas treatment results for the trench type non-thermal plasma-catalyst reactor were observed to be effective for converting NO to: NO_2, N_2, O_2, CO_2 and H_2O. Further tests need to be completed on real natural gas combustion exhaust in order to determine the effectiveness of the non-thermal plasma catalyst for treating MGT exhaust.

Acknowledgements

TABLE OF CONTENTS

LIST OF FIGURES

x

LIST OF TABLES

Chapter 1: Introduction

1.1 Micro-Gas Turbines: a Source for Distributed Energy Generation

In recent years increasing demand for cost-effective energy has made the need for alternative power generation solutions apparent. One possible solution to the ever-increasing demand for energy is on-site energy production, otherwise known as distributed energy generation. The energy crisis in California that began in the spring 2000 and the North-eastern North American Blackout of 2003 has heightened the interest in distributed energy sources. The most common solution to generating on-site power is the use of diesel generators; however this application has numerous drawbacks. Diesel generators in many instances are not well optimized and under-regulated and thus create considerable pollution in the form of nitrogen oxides (NO_x) and particulate matter (soot). One of the sources of distributed energy on the forefront of research, development and commercialization is the natural gas micro-gas turbine (MGT). Kerosene and propane can also be used to power MGTs, however natural gas has proven to be the fuel most commonly used because it is cleaner burning and readily available in most markets. MGTs are exactly as the name implies: a small scale gas turbine, which typically produces anywhere from 30kW to 300kW of electric energy [1].

Since micro-gas turbines were first sold on the market a multitude of applications for MGTs have been established. The use of MGTs for all applications can be classified by five broad categories, which are: emergency power, cogeneration, peak shaving, grid support and stand alone power [1]. Emergency power application would typically be institutions that require power if faced with a power outage, such as hospitals or phone companies such as Sprint in the United States [2]. Cogeneration involves using the power from the MGT for electricity and

1

capturing the heat produced by the exhaust for other applications, such as plant or building heating. MGTs can be used for peak shaving and brought online during peak hours of the day, when cost of electricity from the utility exceeds the cost of operating the MGT. As well utility companies can use MGTs for the same purpose in order to meet peak demand, when generation capacity of the utility is not sufficiently high. Utilities can also use MGTs for grid support in remote locations where the gird is not fully developed to meet the demands of the users. Furthermore, MGTs can be used for stand alone on-site power generation. One industry that has been quick to take advantage of the versatility of the MGT is the oil and gas industry. This industry operates many remote facilities, such as oil drilling rigs. MGTs are currently being used by companies in Alberta, Texas and Colorado for this purpose [3]. Another novel use for MGTs is to produce power from otherwise wasted natural gas, produced by landfills or wastewater treatment plants. MGTs have been used in these industries in California with successful operations [4]. Some researches have even suggested using a MGT to power individual households may be the way of the future energy market [5].

As stated previously, a MGT is a small-scale gas fired turbine producing electrical power between 30kW and 300kW and generally has four major components. The first component is a compressor used to compress the air mixture as it enters the combustion chamber. The air is often preheated to increase the overall efficiency of the combustion process. The other components include a combustion chamber, where the combustion occurs, a rotating turbine and a generator for the production of electrical power [6]. MGTs also operate under high pressure, generating continuous combustion. Two main types of MGTs exist today: a single stage combustion type and a dual stage combustion type MGT. In the single stage MGT there is only one turbine that drives both the

compressor and the generator via a single shaft, as shown in Figure 1-1(a). In a dual stage MGT, such as the Ingersoll-Rand 70kW MGT, there are two turbines. Once the combustion gas leaves the combustor it enters a turbine that powers the compressor. The combustion gas then enters a second turbine that drives the generator [7], as shown in Figure 1-1(b). MGTs also operate at extremely high rotating speeds or rotations per minute (RPM). For example, the Ingersoll-Rand 70kW MGT operates at 44,000rpm [7] and the Capstone 60kW MGT operates at 96,000rpm [8]. The smaller size of MGTs and the extremely high rotation speeds separates MGTs from standard gas fired turbines.
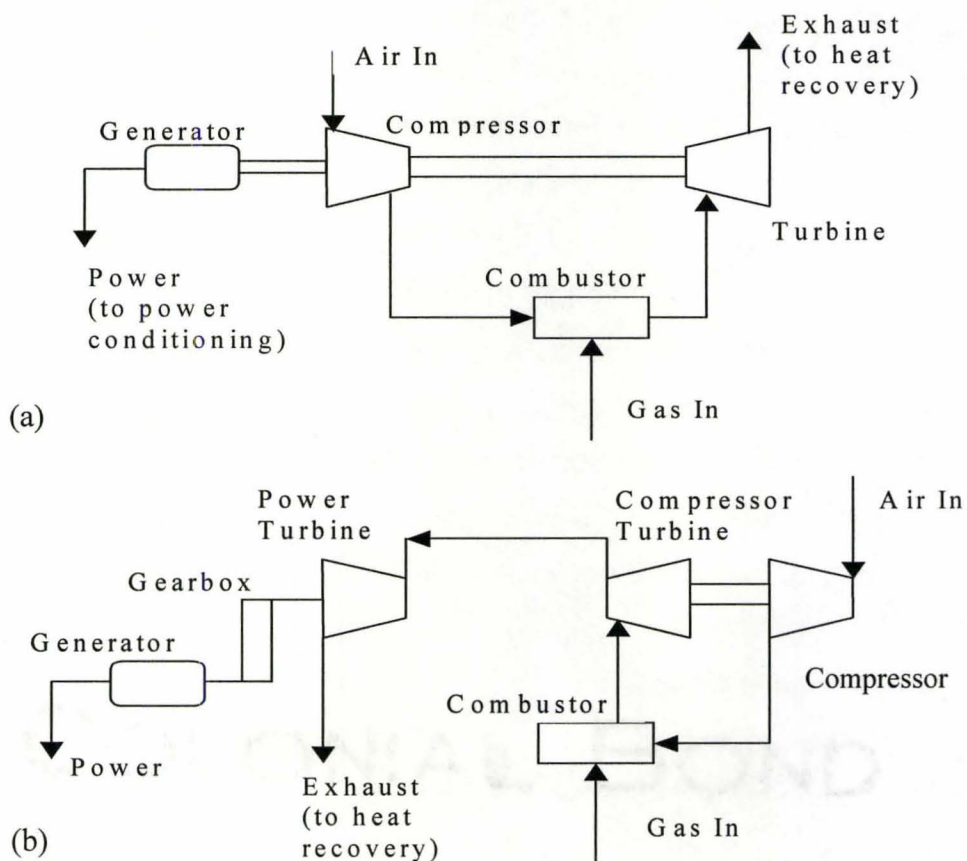
Figure 1-1: Basic overview of (a) single stage combustion type micro-gas turbine and (b) dual stage combustion type micro-gas turbine

1.2 Emission Regulations for Stationary Sources

Given the wide range of applications that MGTs can be used for as well as the consistent growth in the MGT marketplace, it is evident that MGTs will play a large role in the energy sector of the future. Thus the emissions created by MGTs needs to be closely monitored. As MGTs are relatively new to the marketplace, regulations have not kept pace with the constantly evolving technology sector. In many, if not most, jurisdictions regulations for MGTs are lenient or non-existent. The exception is the State of California, which recently had stringent new regulations come into effect.

In most cases regulations cover nitrogen oxides (NO_x) and carbon monoxide (CO), two of the pollutants of great concern from combustion processes. Other emissions from stationary sources do occur, such as volatile organic compounds (VOCs), unburnt hydrocarbons (HC) and particulate matter (PM); although in many jurisdictions these emissions remain unregulated from stationary sources. Sulphur dioxide (SO_2) is also covered by all stationary source regulations primarily because a large amount can be produced by coal-fired power plants. SO_2 will be mentioned in the stationary source regulations covered in the following sections, although SO_2 is not a great concern for natural gas combustion as natural gas usually has a negligible sulphur content.

1.2.1 Regulations in Canada

In 1992 the Canadian Council of Ministers of the Environment (CCME) adopted a guideline for emissions from stationary sources. The guidelines were subsequently adopted by the provinces as emissions regulations. The guideline covers three major pollutants: NO_x, CO and SO_2. The guidelines are given in units of weight (grams) of pollutants per

unit of useful output energy (GJ). The guidelines for NO_x allowances from natural gas combustion are given in Table 1-1.

Table 1-1: Emissions standards for NO_x from natural gas combustion in Canada [9]

Non-Peaking Turbines	Natural Gas (g/GJ output)	@ 25% efficiency (ppm)	@ 30% efficiency (ppm)	@ 35% efficiency (ppm)
Under 3MW	500	74	88	103
2-20MW	240	35	42	49
Over 20MW	140	21	25	29
Peaking Turbines	**Natural Gas g/GJ**	**@ 25% efficiency ppm**	**@ 30% efficiency ppm**	**@ 35% efficiency ppm**
Less than 3MW	Exempt	Exempt	Exempt	Exempt
Over 3MW	280	41	49	58

Calculations for parts per million (ppm) are based on the assumption that 1 ISO ppm is equivalent to 1.70 grams of NO_2 per GJ of heat input at 15% oxygen levels [9]. MGTs would fall under the first category, non-peaking turbines less than 3MW. As is summarized in Table 1, MGTs are required to emit no more than 500g/GJ of output energy or 88ppm at 30% efficiency (typical MGT efficiencies range from 25-30% [8, 10, 11]).

The guidelines also state that CO emissions should not exceed 50ppm at 15% oxygen in the exhaust. However when the guidelines were adopted in Ontario this regulation was increased to 60ppm because:

"Recent information from users/manufacturers of combustion turbines indicates that a level of 50ppm [of CO] is barely achievable at lower NO_x levels. Therefore a tolerance of 20% (10ppm) has been added. The CO limit of 60ppm may be adjusted in the future, depending on the actual performance data." [12]

At the present time the regulation remains unchanged and the limit for CO from MGTs is 60ppm.

The regulations also state that for non-peaking turbines the SO_2 emissions must be less than 800g/GJ or 970g/GJ for peaking units. However given the current purity of natural gas supplies with respects to fuel born sulphur, MGTs produce a negligible amount sulphur dioxide. The only case were sulphur dioxide could be a issue for MGTs is when they are used with "sour gas" (unpurified natural gas, high in sulphur) on natural gas fields, however in this case the guideline states that such units are exempt from SO_2 criteria.

It is important to note that at the present time in Canada there are no regulations for MGTs with respect to VOCs, hydrocarbons or particulate matter emissions. However, Environment Canada has recently started public consultation on new guidelines for new stationary sources. These regulations once again focus primarily on large stationary facilities and not micro power production, such as MGTs. The proposed limit for NO_x is to be changed to 0.47- 0.66 kg/MWh output (~130 - 183g/GJ or 23 - 32ppm). The limit for NO_x is proposed to be realigned with the strictest current standard; natural gas turbines over 20MW (see Table 1-1). This limit will apply to both liquid and solid fuels, both of which currently have much

higher NO_x limits than natural gas. This is in an effort to make cleaner burning fuels more attractive that other currently used liquid and solid fuels, such as coal. The limit for SO_2 is to be changed to between 0.47 - 4.9 kg/MWh of output (~130-1360g/GJ). The SO_2 emission standard, unlike the NO_x guideline, will still be based on the type of fuel, thus solid fuels will be allowed larger emissions than liquid or gaseous fuels. The proposed legislation also outlines particulate matter standards to be 0.075 - 0.12 g/MWh output. There has been no proposal of reducing the current CO requirement below 50ppm. The ratings are also based on the best economically achievable efficiency of a current coal power plant where 9.4GJ yields 1 MWh [13] or an efficiency of approximately 38%.

1.2.2 United States Emission Regulations for Stationary Sources

1.2.2.1 National Emission Standards

The United States amended the guidelines for the National New Source Performance Standards (NSPS) in the Clean Air Act in 1998 to enforce stricter NO_x emissions standards. The NO_x regulations for any new stationary sources emissions must be no more than 1.6lb/MWh or 0.73kg/MWh. Unlike the Canadian regulations these standards are based on an overall plant efficiency of 32.5% instead of 38%. This is the minimum standard for NO_x, however the United States uses the philosophy of "best available control technologies" (BACT). This philosophy allows the market, not the government to determine the best emissions control technology. The concept implies that once an emission technology is proven in one given plant operation, it should be applied to all other similar plants, thus slowly improving pollution prevention as control technology evolves [14]. The emissions limits are therefore based on the BACT and are rated on an individual basis depending on the

specific industrial application. Currently in the United States the NO_x emissions limit for a stationary source would most likely be around 1.05lb/MWh or 0.48kg/MWh based on the BACT, even though the actual minimum by law is 1.6lb/MWh [13].

The SO_2 regulations are still based on the type of fuel divided into two categories: solid and liquid/gaseous. For solid fuels the emissions must not exceed either of the following standards: (1) 5.7kg/MWh and a 90% reduction uncontrolled SO_2 emissions or (2) 2.9kg/MWh and a 70% reduction in uncontrolled SO_2 emissions. Uncontrolled SO_2 emissions are the emissions of SO_2 based on the fuel and process that would occur with no abatement technology. For liquid or gaseous fuels the emissions must not exceed either of the following standards: (1) 3.8kg/MWh and a 90% reduction in uncontrolled SO_2 emissions or (2) 0.95kg/MWh [13]. However, recent stationary sources permits following the BACT philosophy have shown that the SO_2 limit is continuously dropping, with one of the stricter permits requiring 0.47kg/MWh [13].

The United States' regulations also specify that stationary sources shall not emit more than 0.144kg/MWh of particulate matter. Once again with the application of the BACT philosophy this standard has dropped to between 0.09kg/MWh and 0.10kg/MWh for new applications. There are no requirements for hydrocarbons or VOCs at the present time for stationary combustion sources.

1.2.2.2 State of California Emission Regulations for Stationary Sources

The state of California has long been known as a groundbreaker of environmental law. Faced with increasingly high levels of pollution, especially in metropolitan areas such as Los Angeles, the state of California has become a forerunner in environmental policy by necessity. California has created regulations specifically for distributed energy

sources including MGTs. The law was implemented in November of 2001 and created a distributed energy certification program run by the Air Resources Board (ARB) of California. This program required that all new sources of distributed energy must meet strict new emissions laws in order to be used in that state [15].

The new California guidelines concentrate on 3 major pollutants: NO_x, CO and VOCs. The regulations were based on the BACT achieved in practice. The recommended guidelines for the aforementioned pollutants are presented in Table 1-2.

Table 1-2: BACT emissions from stationary combustion turbines for turbines producing less than 50MW electrical energy [16]

Category	NO_X (ppm 15%O_2)	VOC (ppm @15% O_2)	CO (ppm @15% O_2)
< 3MW	9	5	10
3 – 50MW			
Combined cycle	2.5	2	6
Simple cycle	5	2	6

However, as in all of the prior cases these regulations are for larger scale turbines that have higher efficiencies (between 40-56%) [16] than MGTs (between 25-30%). Therefore it would be difficult for MGTs at the present time to meet these stringent regulations. The California guidelines state the MGTs are "an emerging technology generally sized below the permitting threshold for gas turbines". As such there is not BACT emission criteria set out in the guidelines. The BACT emission criteria were determined when MGTs from Ingersoll-Rand and Capstone were tested and certified in 2003 by the ARB. The results from the testing established the BACT limits for MGTs in California. The emission

guidelines are presented in Table 1-3. The values in parts per million assume a MGT efficiency of 28%.

Table 1-3: Emission criteria for micro gas turbines in California [17, 18]

Pollutant/Units	kg/MWh	ppm @ 15% O_2
NO_x	0.227	11
VOC	0.454	61
CO	2.724	189

As can be seen from Table 1-2 and Table 1-3 the limits for both VOCs and CO are much higher in MGTs than in regular gas turbines. Although this is in part because turbines have greater efficiencies that MGTs, it is also because at the present time there is not cost effective after treatment for MGTs for the abatement of pollutants, thus MGTs do not employ any control technologies. At the present time the BACT for MGTs is simply no after treatment, yet with the growing MGT market share cost effective after treatment of MGT exhaust will become necessary to reduce the amount of NO_x, VOCs and CO emitted into the atmosphere.

1.2.3 European Regulations for Stationary Sources

European emissions regulations are similar to those found in Canada and the United States. There are currently no regulations specific to MGTs, as in other jurisdictions only regulations for large gas turbines. Like the United States, Europe also applies the BACT philosophy to emission control technologies. The pollutants regulated for gas fired turbines are: NO_x, SO_2, CO and PM. The European guidelines for natural gas fired turbines for these pollutants are given in Table 1-4.

Table 1-4: European regulations for natural gas turbines [19]

Emission/ Units	mg/Nm^3	ppm @ 15% O_2, STP
NO_x	20-50	10-25
CO	5-30	4-24
SO_2	10	3.5
PM	5	NA

1.2.4 Summary of Regulations

As described in the preceding sections most jurisdictions (with the exception of California) do not have emission regulations specific to MGTs. This is mostly due to MGTs still being a relatively new technology on the commercial market and regulations can take years to catch up with new innovations. However the state of California is generally seen as a leader in the area on environmental regulations and many other states, provinces and countries are likely to follow the proposed strict emission regulations for NO_x, CO and VOCs in the years to come. Therefore it will be necessary for MGTs to improve their performance with regards to the efficiency and emissions of the device.

1.3 Health and Environmental Impacts by Pollutants from Stationary Natural Gas Combustion Sources

Although natural gas combustion can be seen as cleaner burning than other fuel sources such as diesel or coal, there are still significant emissions. These emissions can cause both human health issues, as well as serious environmental impacts. The major pollutants of concern are, as expected, those associated with stationary source regulations. The pollutants are SO_2, NO_x, CO, PM and VOCs and unburnt hydrocarbons. NO_x in the past has stood for the amount of nitrogen monoxide (NO) and

nitrogen dioxide (NO_2) emitted. More recently the amount NO_x has also incorporated N_yO_x compounds, such as nitrous oxide (N_2O) in to the definition. Table 1-5 provides a summary of the possible health and environmental effects of natural gas combustion emissions.

Table 1-5: Impact of natural gas combustion generated emissions [14, 20]

Pollutant	Impact
NO_x	Acid rain, ozone formation, greenhouse effects, visibility impairment, respiratory effects, eutrophication of ecosystems, formation of toxins
CO	Toxic
SO_2	Acid rain, respiratory effects
PM	Respiratory effects, visibility impairment, component of smog, damages buildings
VOCs	Ozone formation, some carcinogenic compounds
CH_4	Greenhouse gas

Table 1-5 summarizes the wide range of effects that natural gas combustion generated emissions can have on humans and the environment. When NO and NO_2 are released into the atmosphere they can both be readily converted to nitric acid (HNO_3), thus causing acid rain. Nitric acid vapour can also cause respiratory tract damage in humans. As well, NO and NO_2 can react with VOCs in the atmosphere to create ground level ozone [20]. Ground level ozone is a major component of photochemical smog, which can cause respiratory difficulties for humans

and damage vegetation [21, 22]. N_2O is a greenhouse gas, hence adding to the global warming problem. NO_x can deposit into the environment, potentially overloading the ecosystems with excess nitrogen causing detrimental effects on the ecosystem (eutrophication). NO_x can also obstruct sunlight and react with VOCs to create hazardous chemicals in the atmosphere [20].

Carbon monoxide is known to be toxic to humans. When carbon monoxide enters the respiratory tract it bonds to the haemoglobin in our blood. Haemoglobin normally transports oxygen throughout our body; however haemoglobin has a greater affinity for carbon monoxide than oxygen. Thus if carbon monoxide enters our bloodstream through the lungs it can be potentially fatal if too much oxygen is displaced. According to the American Conference of Governmental Industrial Hygienists the time weighted average maximum concentration of CO should not exceed 25ppm over 8hrs in the workplace [14].

The two largest concerns with the emission of SO_2 into the atmosphere are human respiratory effects and the formation of acid rain. High localized concentrations of SO_2 can cause serious respiratory disease in humans. As well SO_2 can react in the atmosphere with oxygen, NO_x and water to form sulphuric acid, which causes acid rain. However the purity of natural gas is such that natural gas combustion produces virtually no SO_2 (< 1ppm).

Particulate matter produced from the combustion of natural gas can be a serious problem. Although the mass of particulate matter is relatively low when compared to other types of combustion sources, the particulate matter is very small. PM that is smaller than $10\mu m$ can enter the body's airways. Particles that are under $2.5\mu m$ are classified as respirable particles, which means that the particles will enter the lungs. This can cause irritation and illness depending on the particles' composition.

13

Suspended PM in the atmosphere impairs visibility, blocks sunlight and is a component of photochemical smog.

The major concern with the emission of VOCs into the atmosphere is that VOCs can combine with NO_x to form ground-level ozone, which is a component of smog [21]. Some VOCs could potentially be harmful to humans or combine with other compounds in the air to form hazardous compounds. Another major concern for natural gas combustion is the emission of unburnt methane. Most natural gas combustion devices operated with excess oxygen during combustion, thus limiting the amount of unburnt fuel or methane. However methane is a strong (methane is 20 times more effective as a greenhouse gas when compared to CO_2 [14]) greenhouse gas and therefore must be monitored.

1.4 Non-Thermal Plasma-Catalyst Overview

As mentioned previously many natural gas combustion processes including MGTs, operate with excess oxygen (also known as lean burn). Lean burn conditions aid in keeping the NO_x formation low and the amount of unburnt fuel to a minimum. However it poses challenges to current pollution control after treatment technologies, as many current catalysts do not operate well in an excess oxygen environment (conventional technologies are further discussed in Chapter 2). A novel solution to this problem is the use of non-thermal plasma and a catalyst for natural gas combustion after treatment.

There are several different methods for generating non-thermal plasma: pulsed discharge [23, 24], electron beam [25, 26], dc flow stabilized corona [27, 28] and dielectric barrier discharge [29, 30], etc. This research will center on using a trench type non-thermal plasma dielectric barrier discharge reactor [31] for the control of natural gas flue gas pollutants. This section will focus on the fundamental characteristics

observed in barrier discharges in plasma reactors. Plasma discharges are usually placed into two general categories: low pressure discharges and high-pressure discharges. Low pressure discharges occur at pressures below or at 13.3kPa, whereas high pressure discharges occur at atmospheric pressure (101.325kPa) or higher [32]. The type of discharge that occurs in a dielectric barrier discharge non-thermal plasma (NTP) reactor is a corona discharge. These discharges fall under the category of high-pressure discharges as most applications that create corona discharges are at atmospheric pressure.

In a dielectric barrier discharge plasma reactor one or both of the electrodes are covered with a material that has a finite specific dielectric constant larger than 2 [33, 34]. Examples of materials include Pyrex and ceramics such as alumina. The use of a dielectric material to cover an electrode allows a streamer corona to form (when charge is collected on the dielectric barrier) in between the electrodes and prevents spark discharge [31]. Each corona stream creates high mean energy electrons with energies around 1 to 10eV. These high energy electrons then create free radicals, which can reduce, oxidize and/or decompose harmful pollutants [31, 33, 34]. Usually dielectric barrier discharge plasma reactors are operated with voltages between 8-30kV and frequencies between 50-10kHz [31, 33]. In a trench type reactor one electrode has triangular channels, which the gas flows through. A schematic of a trench type NTP reactor is shown in Figure 1-2.
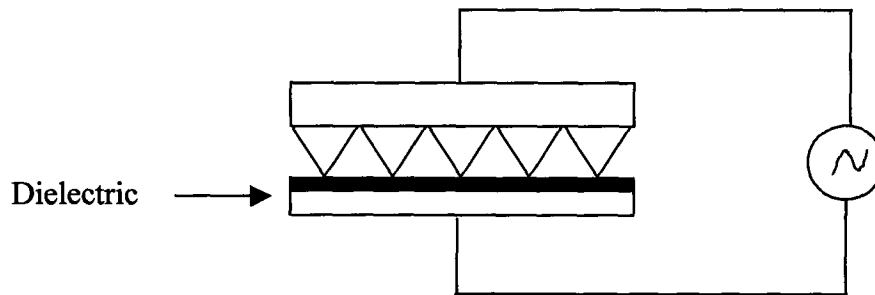
Figure 1-2: A trench type dielectric barrier discharge non-thermal plasma reactor

The corona streamer forms between the tip of the trench electrode and the dielectric material, i.e. highest electric field locations. The typical properties of a corona streamer at atmospheric conditions are shown in Table 1-6.

Table 1-6: Properties of a streamer corona for gaps of 1 to 100cm [34]

Streamer rise time	$\cong 1$ns
Streamer duration	$\cong 1\mu$s
Repetition period	$\cong 1$ns
Streamer diameter	$\cong 20\mu$m
Electric field	$10^{-19} < E/N < 10^{-17}$ Vm^2
Ion temperature	$\cong 10^3$ K

$N = m^{-3}$ (Loschmidt's number), $E = $ V/m

Typically when using dielectric barrier discharge NTP reactors the properties measured in relation to the discharge are: voltage, current and electric charge. Voltage and current are normally measured together in a single plot. The voltage is measured from peak to peak to determine the applied voltage on the plasma reactor and the streamer corona discharges can be observed as peak in the current waveform. Typical voltage-current characteristics for a dielectric barrier discharge NTP reactor are shown in Figure 1-3.
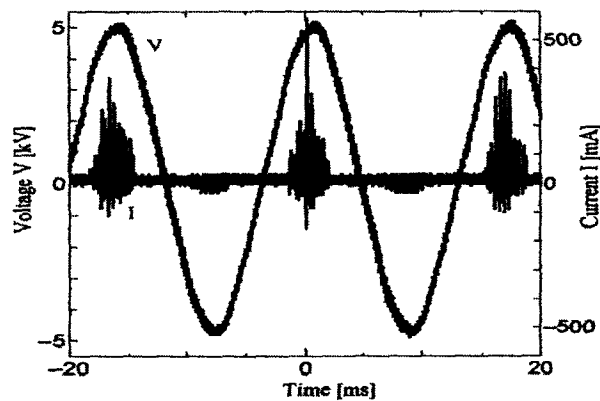
Figure 1-3: Typical voltage-current characteristics from a dielectric barrier non-thermal plasma reactor

Figure 1-2 shows two sinusoidal waveforms versus time. The smooth sinusoidal wave represents the voltage injected into the reactor. The voltage waveform is sinusoidal in this case because the injected electricity is AC. The other waveform represents the current in the plasma reactor. The numerous peaks seen on this waveform correspond to the many micro-discharges (streamer corona) occurring in the reactor.

The electrical power injected to a NTP reactor can also be determined using a X-Y plot of voltage versus charge of the reactor [30, 35-37]. In this case the voltage is plotted on the X-axis and the charge is plotted on the Y-axis to form a Lissajous figure. The area of the diagram represents the electrical power injected into the reactor. A typical Lissajous figure for a NTP reactors is presented in Figure 1-4.
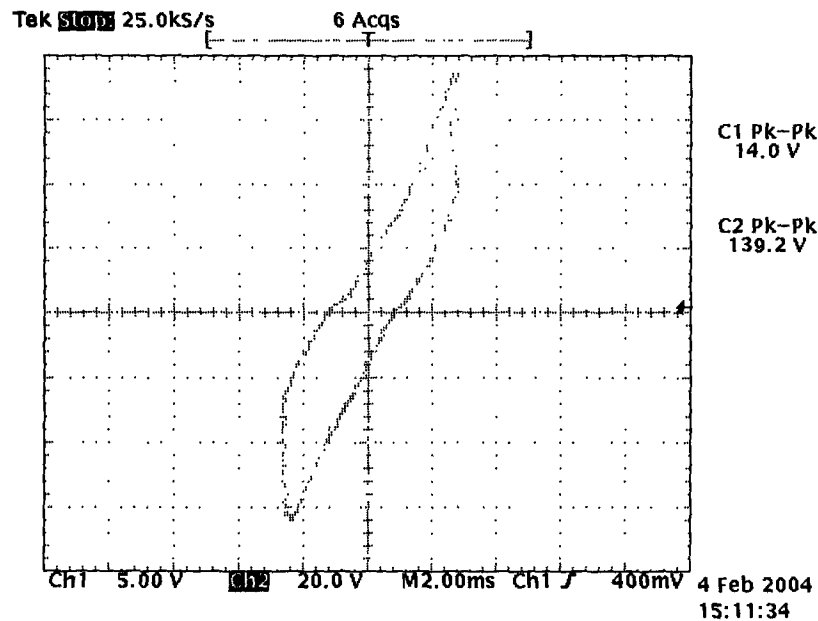
Figure 1-4: Typical voltage-charge characteristics (Lissajous figure) for dielectric barrier non-thermal plasma reactors

This research will focus on the use of a dielectric barrier discharge reactor coupled with a sodium zeolite catalyst activated by aldehydes. A detailed explanation of the methodology and chemistry for the use of non-thermal plasma and plasma catalysts for pollution control will be given in Chapter 2.

1.5 Objectives and Statement of Work

Given that MGTs and other forms of natural gas combustions devices are gaining a greater share in recent years because of their versatility and advantages over diesel generators, the pollutants emitted from natural gas combustion will need to be characterized and controlled to reduce the impacts on human health and the environment. This research will focus on the characterization of the emissions of two types of natural gas MGTs in order to better understand the pollutants emitted by this new technology. Both MGTs operate in lean burn conditions, however

one MGT operates under leaner conditions. The exhaust of the MGTs will be characterized for emissions of NO_x, CO, CO_2, O_2, O_3, particulate matter, VOCs, and hydrocarbons.   Furthermore, this research will undertake the development of a cost-effective and efficient after treatment reactor using a non-thermal plasma-catalyst for the control of natural gas combustion emissions.

The exhaust of a MGT will be simulated using a lab scale test loop and the non-thermal plasma-catalyst will be tested for its efficiency in treating natural gas emissions, where the sodium zeolite (Na-Y) catalyst (coated on a 400cpsi cordierite monolith) activated by aldehydes will be used. The specific objectives of the non-thermal plasma-catalyst are to convert NO_x to less harmful substances such as N_2, O_2 and H_2O. The system also aims to convert CO to CO_2 and covert hydrocarbons and VOCs to aldehydes in order to activate the catalyst. The objectives are summarized in Figure 1-5.

Natural Gas
Combustion
Exhaust

```
                ┌──────────────┐              ┌──────────────┐
                │  Non-Thermal │              │              │
   ──────────▶  │ Plasma (NTP) │ ──────────▶  │   Catalyst   │ ──────────▶
                │   Reactor    │              │              │
                └──────────────┘              └──────────────┘
```

$NO \rightarrow NO_2$ NO_2+Aldehydes$\rightarrow N_2 + O_2 + H_2O$
VOCs, HC $\rightarrow$ Aldehydes N^*, N_2^* +NO_x $\rightarrow N_2$, O_2
$CO \rightarrow CO_2$
$N_2 \rightarrow N^*$, N_2^*
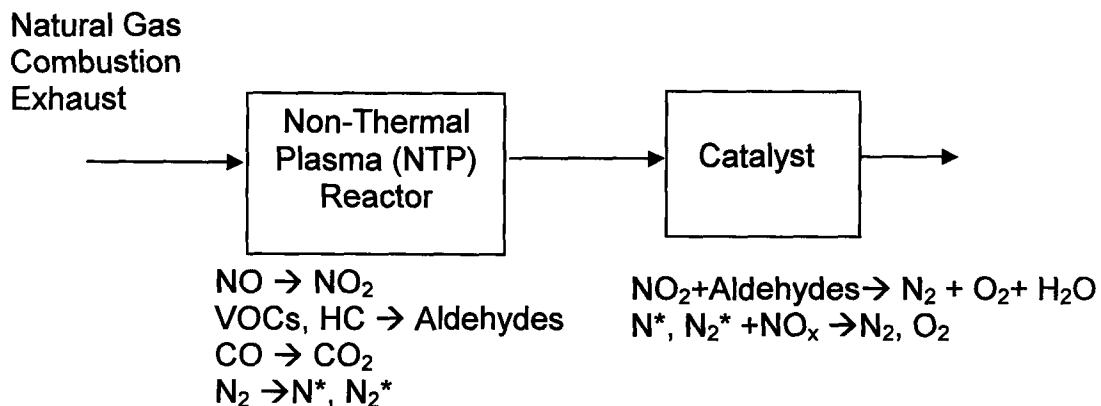
Figure 1-5: Objectives of non-thermal plasma and catalyst hybrid system for the treatment of natural gas combustion exhaust.

Chapter 2 will present background information on results from previous micro-gas turbine characterizations, conventional approaches to the control of natural gas combustion exhaust pollutants and techniques for the control of pollutants by non-thermal plasma-catalysts. Chapter 3 will provide details on the experimental facilities and procedures. Chapter 4 will discuss the results for the characterization of the natural gas combustion exhaust of the two tested MGTs. Chapter 5 will present the findings for the plasma-catalyst tests for the simulated natural gas pollutants test loop. Chapter 6 will provide conclusions of the current research and suggest future work in the area of plasma-catalysts.

Chapter 2: Background

2.1 Micro Gas Turbine Flue Gas Emission Characterization

Given that micro-gas turbines (MGTs) are a relatively new technology, there has not been a substantial amount of scientific studies on the impact of MGTs emissions on the environment. However the Environmental Protection Agency (EPA) of the United States does have an environmental technology verification (ETV) program. The ETV was created by the EPA in an effort to characterize the performance of new commercial technology. The objective is to generate a database of commercial devices' performance to facilitate the accessibility of information to both industry and the public [38]. The ETV has evaluated three natural gas fired MGTs: the Capstone 60kW Microturbine CHP system, the Parallon 75kW Turbogenerator (Honeywell) and the Ingersoll-Rand Powerworks 70kW Microturbine System [38]. The emissions characterization of these MGTs from this program will be presented in this section. Table 2-1 presents the operating parameters of all three MGTs.

Table 2-1: Operating parameters for Capstone 60kW MGT, Ingersoll-Rand 70kW MGT and Honeywell 75kW MGT [8, 10, 11]

Parameter/Manufacturer	Capstone	Ingersoll-Rand	Honeywell
Exhaust Temperature	305°C	232°C	---
Exhaust Mass Flow	0.49kg/s	0.73kg/s	0.70kg/s
Exhaust Flow Rate[1]	$0.408m^3/s$	$0.608m^3/s$	$0.584m^3/s$
Natural Gas Inlet Flow Rate	5.60L/min[2]	5.80L/min[2]	8.40L/min
Normalized Air-to-Fuel Ratio (λ)	7.14	10.2	6.64

[1] Based on STP condition for ideal gas = 22.4L/mol of gas
[2] Based on HHV for methane = $41.2MJ/m^3$

Table 2-1 shows that the exit temperature for the Ingersoll-Rand 70kW MGT is much lower that the Capstone 60kW MGT. The Honeywell 75kW MGT has the lowest normalized air to fuel ratio at 6.64, whereas the Ingersoll-Rand 70kW MGT has the highest at 10.2. This shows that although all MGTs operate on a lean burn combustion cycle ($\lambda > 1$, where λ is the air-to-fuel ratio of the MGT over the stoichiometric air-to-fuel ratio for methane), the Honeywell 75kW MGT operates with the richest amount of fuel of all three MGTs and the Ingersoll-Rand MGT operates with the leanest mixture of fuel. A lean burn combustion operation has the potential advantage of lower NO_x ppm emissions (See section 2.1.4) but may increase the exhaust flow rate as seen in Table 2-1.

As mentioned in Section 1.1 MGTs are generally comprised of four major components: a compressor, combustion chamber, turbine and generator. The Honeywell Parallon 75kW MGT, The Ingersoll-Rand 70kW MGT and the Capstone 60kW MGT all have these major components. In addition all three MGTs use a recuperator (or heat exchanger) to pre-heat the air entering the combustion chamber in order to increase the efficiency of the MGT [39-41]. All three MGT also use the exhaust gas to heat the recuperator. The Honeywell 75kW MGT and the Capstone 60kW MGT have a similar turbine design, where the generator and the turbine are on the same shaft [39, 40]. The Ingersoll-Rand 70kW MGT uses a two-shaft design, which uses a gear box to transfer the work of the turbine to the generator. Both the Honeywell 75kW MGT and the Capstone 60kW MGT are single stage combustion type MGTs, whereas the Ingersoll-Rand 70kW MGT is a two-stage combustion type MGT as previously discussed in Section 1.1. The Honeywell 75kW MGT and the Capstone 60kW MGT use a permanent magnet generator to produce electrical power. The permanent magnet generators produce high-frequency alternating current

22

(AC), which is processed through a rectifier, inverter and filter [39, 40]. The Honeywell 75kW MGT's generator produces 275 AC volts at 50 or 60Hz, whereas the Capstone 60kW MGT produces 480 AC volts at 60Hz [39, 40]. The Ingersoll-Rand 70kW MGT uses an induction generator to produce 480 AC volts at 60Hz [41].

2.1.1 Honeywell Parallon 75kW Turbogenerator Characterization

The first MGT tested was Honeywell's Parallon 75kW Turbogenerator. The Greenhouse Gas Technology center (GHG) of the Southern Research Institute (SRI) evaluated the Parallon MGT [39]. The evaluation was performed at the University of Maryland's College Park Campus where the Parallon MGT was connected to the grid of an office building. The MGT was operated at 50, 75, 90 and 100 percent load and was characterized for four key criteria. The criteria are: electrical power performance, emission performance, power quality performance and operational performance [39]. This section will introduce the emission performance of the MGT observed by this testing.

The emissions characterized by the ETV for the Honeywell Parallon 75kW MGT were: NO_x, CO, total hydrocarbons (THC), carbon dioxide (CO_2), methane (CH_4) and oxygen (O_2). Each load was tested in three separate runs and the average results of the testing are presented in Table 2-2.

Table 2-2: Emission results for the natural gas fired Honeywell 75kW Parallon MGT [39]

Load	Power	NO_x	CO	THC	NO_x	CO	THC	O_2	CO_2
%	kW	ppm @ 15% O_2			g/kWh$_e$ $\times 10^{-3}$			%	
100	75	18.6	1.7	<5.00	442	24	<45	18.72	1.26
90	68	19.7	7.0	<5.00	477	104	<45	18.80	1.21
75	56	27.9	57.2	<5.00	686	858	<52	18.95	1.13
50	38	42.2	781	49.30	1190	13400	481	19.23	1.00

Table 2-2 shows that the amount of load on the MGT directly impacts the amount of pollutants emitted. The lowest emissions were at full load operation of the MGT, whereas the highest were at 50% load. This is expected as the MGT is optimized to be operated at full load continuously, not at 50% load. The amount of CO increased dramatically from 1.7ppm at full load to 781ppm at 50% load. The amount of total hydrocarbons was below the detection limit of the testing equipments used in the study for full load, 90% load and 75% load, but it raised significantly to 49.30ppm when the MGT was at 50% load. However, it was reported that 80% of the THC emissions were methane. Thus most of the THC emissions were simply unburnt fuel because the MGT was not operating at optimal conditions. The amount of CO_2 and O_2 were also recorded during this study. As expected the amount of CO_2 increased with increasing load and the amount of O_2 decreased with increasing load. This is simply because more oxygen was consumed by the oxidation of carbon in the fuel to form CO_2 when the MGT was operating at higher loads [39].

2.1.2 Ingersoll-Rand PowerWorks 70kW Microturbine Characterization

The second MGT tested by the ETV was the Ingersoll-Rand PowerWorks 70kW microturbine. The Ingersoll-Rand MGT was tested by the GHG center in conjunction with the New York State Energy and Development Authority (NYSERDA). The experiment was carried out at a nursing home in New York State, which uses the MGT as its primary energy source [41]. The Ingersoll-Rand MGT was only tested at full load, as it is not possible to change the load on the MGT. Two separate tests were conducted on the MGT. In the first test the MGT was operated under normal site operations of the nursing home. Under normal operating conditions the nursing home uses the heat recovered from the MGT to supplement its boilers. In the second test the MGT was simply run at full load disconnected from the boilers (boilers turned off). The tests evaluated three main categories: heat and power production performance, emissions performance and power quality performance. This section will focus on the emission performance of the MGT recorded by this study [41].

The emissions characterized by the ETV program for the Ingersoll-Rand PowerWorks 70kW MGT were: NO_x, CO, total hydrocarbons (THC), carbon dioxide (CO_2), methane (CH_4) and oxygen (O_2). Each load was tested in three separate runs and the average results of the testing are presented in Table 2-3.

Table 2-3: Emission results for the natural gas Ingersoll-Rand 70kW MGT [41]

Power kW	NO_x	CO	THC	NO_x	CO	THC	O_2	CO_2
	ppm @ 15% O_2			g/kWh$_e$ ×10^{-3}			%	
70 (Normal Site Operation)	0.86	0.62	2.38	21.2	9.49	20.3	18.60	1.21
70 (Only MGT)	1.07	0.65	0.54	26.5	9.72	0.47	18.61	1.32

Table 2-3 clearly indicates that there is very little change in emissions depending on the type of heat recovery application being used. All the emissions were extremely low and would meet the strictest MGT air pollution regulations. As presented in Chapter 1 the Ingersoll-Rand PowerWorks 70 kW MGT was certified under the new California air pollution guidelines [18]. The emissions of methane were also tested in this study, but were observed to be less than the detectable limit of 1ppm of the instrumentation.

2.1.3 Capstone 60kW Microturbine CHP System Characterization

The Capstone 60kW MGT CHP System was the third MGT tested under the ETV program. Like the Ingersoll-Rand MGT, the Capstone MGT was tested by the GHG center in conjunction with NYSERDA. The MGT was tested at a supermarket in New York State [40]. The supermarket uses the MGT on a continuous basis to supply power for lighting and heating operations. The heat that is recovered from the MGT is used to supplement the space heating system installed in the supermarket. Two tests were performed on the MGT. In the first test the MGT was run with the heat recovery system attached to the space heating system of the supermarket. In this test the load was varied at given intervals: 100% load, 75% load, 50% load and 25% load. In the second test the MGT was run separate from the space heating system. In the second test only full load and 50% load were tested. The tests evaluated three main categories: heat and power production performance, emissions performance and power quality performance. This section will focus on the emission performance of the MGT recorded by this study [40].

The emissions characterized by the ETV program for the Capstone 60kW MGT CHP System were: NO_x, CO, THC, CO_2, CH_4 and O_2. Each load was tested in three separate runs and the average results of the

testing are presented in Table 2-4. The emissions of CH_4 from the Capstone 60kW MGT are shown in Table 2-5.

Table 2-4: Emission results for the natural gas Capstone 60kW MGT [40]

Load %	Test	NO_x	CO	THC	NO_x	CO	THC	O_2	CO_2
		ppm @ 15% O_2			g/kWh$_e$ $\times 10^{-3}$			%	
100	Norm Oper.	3.13	3.53	1.06	67.6	46.8	8.04	17.8	1.77
75	Norm Oper.	3.30	154	70.3	77.6	2206	577	18.1	1.56
50	Norm Oper.	4.25	582	1194	121	10260	11850	18.3	1.35
25	Norm Oper.	6.56	338	327	286	8990	4950	18.8	1.11
100	MGT only	3.05	3.90	0.69	66.7	518	5.18	17.7	1.75
50	MGT only	4.50	586	1154	128	10215	11490	18.3	1.34

Table 2-5: CH_4 emission results for the natural gas Capstone 60kW MGT [40]

Load %	Test	CH_4 ppm @ 15% O_2	CH_4 g/kWh$_e$ ×10^{-3}
100	Norm Oper.	<0.9	7.17
75	Norm Oper.	43.5	356
50	Norm Oper.	721	7130
25	Norm Oper.	198	3020
100	MGT only	Not Tested	Not Tested
50	MGT only	678	6720

Table 2-4 and Table 2-5 both show that there was very little change in emissions depending on the heat recovery system. Table 2-3 also shows that NO_x emissions increased with decreasing load, the minimum being 3.05ppm at full load. The same trend was also observed for CO, THC and CH_4 as the emissions, except the emission began to fall again at a load of 25%. The O_2 concentration increased with decreasing load and the CO_2 emissions decreased with decreasing load as expected [40]. All the emissions at full load are low enough to meet the strictest air pollution regulation found in California and as seen in Chapter 1 the Capstone 60kW was certified for use in California last year by the ARB [17].

A comparison of all three MGTs at full load is presented in Table 2-6. The emissions for NO_x, CO and THC are presented in terms of the mass of pollutant produced by a continuously operating MGT for one year per kWh of useful energy produced in order to normalize the emissions.

Table 2-6: Comparison of the emissions from natural gas fired Honeywell 75kW MGT, Ingersoll-Rand 70kW MGT and Capstone 60kW MGT [39-41]

MGT	Load	NO_x	CO	THC	O_2	CO_2
		kg/yr/kWh$_e$			%	
Honeywell 75kW	100%	8.96	0.52	<4.7[a]	18.72	1.26
Ingersoll-Rand 70kW	100%	0.58	0.22	0.57[a]	18.61	1.32
Capstone 60kW	100%	1.29	1.04	0.57[a]	17.7	1.75

[a] THC calculated as hexane (C_6H_{14})

In all the pollutant categories (NO_x, CO, THC) the Ingersoll-Rand MGT had the lowest emissions and the Honeywell MGT had the highest (with the exception of THC as it was below the detection limit of the instrumentation). The NO_x emissions for the Honeywell MGT were an order of magnitude larger than the NO_x emission from the Capstone and Ingersoll-Rand MGTs. However, Honeywell is currently developing an upgraded MGT that will meet NO_x regulations of below 9ppm [39]. The O_2 and CO_2 emissions for the Honeywell and Ingersoll-Rand were similar, whereas the emissions of O_2 were lower and the emissions of CO_2 were higher for the Capstone MGT. Although the combustion of natural gas does emit particulate matter the ETV's verification program for MGTs did not measure particulate matter for any of the MGTs. As particulate matter is a serious concern from combustion sources, research should also focus on characterizing MGTs for particulate matter emissions.

2.2 Conventional Approaches to Natural Gas Combustion Flue Gas Emission Control

The main objectives of the plasma-catalyst system are the control of carbon monoxide, nitrogen oxides and volatile organic compounds. Although other pollutants can be emitted from natural gas combustion this section will focus on conventional methods of controlling NO_x, VOCs and PM from natural gas combustion. CO is generally restricted by controlling the combustion process or by simple catalytic reduction after treatment, hence no detailed discussed will be provided in this section.

2.2.1 Conventional NO_x Controls for Natural Gas Combustion Flue Gas

The control of NO_x from combustion flue gases can be dived into two categories [14]: combustion process modification to reduce the formation of NO_x and post combustion chemical treatment of NO_x. Many combustions process modifications have been made to lower the amount of NO_x formed during combustions. The three variables that most affect NO_x formation during combustion are [14]: the peak temperature that the combustion reaches, the amount of time at an elevated temperature and the amount of excess oxygen present during combustion. These variables are often adapted to lower the amount of NO_x created during combustion. The amount of excess oxygen is the easiest variable to adjust for combustion. Reducing the amount of air during the combustion of fuel will decrease the amount of NO_x formed, simply because there is no oxygen to react with nitrogen to form NO_x. However decreasing the amount of oxygen available for combustion can yield undesirable effects. Reduced oxygen increases the risk that not all the fuel will full combust, which then creates increased levels of VOCs in the form of hydrocarbons and increases the amount of CO formed.

30

There are a number of techniques that modify the combustion process to reduce the combustion temperature. One process is known as fuel reburning or two stage combustion. In this process the fuel is mixed with some air so that the mixture is fuel rich. This mixture is then combusted in the first stage of the process. The exhaust of the first process, which still contains fuel, is then placed into a secondary combustion chamber where it is combusted with excess air. The principle of fuel reburning is that because the combustion of the fuel does not all occur at once the peak temperature is reduced (compared with all the fuel combustion at once), thus reducing the formation of NO_x. A drawback to this process is that complete combustion does not always occur during the second stage, hence leading to VOC and CO formation [14].

Another technique to reduce the formation of NO_x during combustion is flue gas recirculation (FGR) [14]. In this process flue or exhaust gas is re-circulated into the combustion chamber. This reduces NO_x formation by reducing the amount of excess air in the combustion chamber and by reducing the overall temperature. "Low-NO_x" burners [14] usually use two stage combustion and/or FGR to reduce NO_x.

For the after treatment of flue gases to remove NO_x there are two main approaches: catalytic and non-catalytic removal. In the automotive industry three way catalysts (TWC) are normally used to control NO_x emissions. The catalysts are called three-way because they simultaneously remove NO_x, CO and hydrocarbons. However TWCs do not operate well under lean burn or excess oxygen environments. Figure 2-3 demonstrates the conversion efficiency of hydrocarbons (HC), NO_x and CO in a TWC versus the air to fuel ratio.
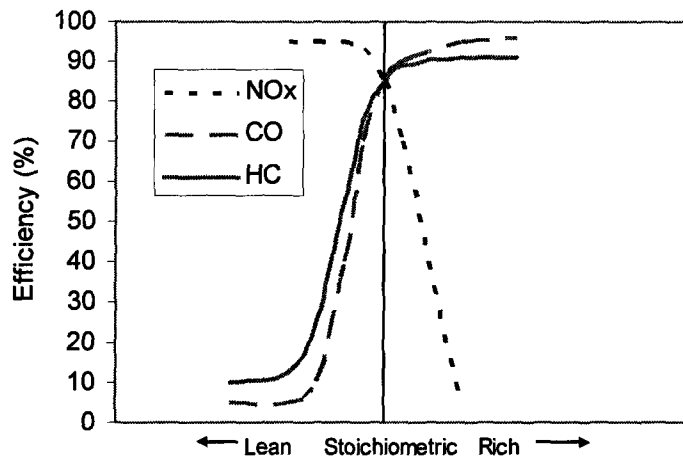
Figure 2-1: Typical conversion efficiency versus air to fuel ratio for a three way catalytic converter for gasoline internal combustion engine [14]

As observed in Figure 2-3 the conversion efficiency of CO and HC for a TWC under lean burn conditions is extremely high, however the conversion of NO_x is very low. For this reason TWC are not well suited to high excess oxygen environments such as MGTs. Another means of catalytic conversion of NO_x from natural gas combustion flue gas is known as selective catalytic reduction (SCR). In this process a reducing agent is used in the presence of a catalyst in order to reduce NO to nitrogen. The reducing agent used is normally ammonia (NH_3) which causes the following reactions to occur [19]:

$$4 \ NO + 4 \ NH_3 + O_2 \xleftarrow{C}\rightarrow 4 \ N_2 + 6 \ H_2O$$

$$6 \ NO_2 + 8 \ NH_3 \xleftarrow{C}\rightarrow 7N_2 + 12 \ H_2O$$
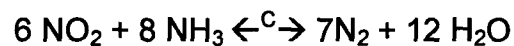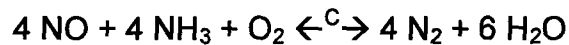
The most common catalysts used in power plants are: heavy metal oxides, zeolites, iron oxides and activated carbon. This process must occur at relatively high temperatures, between 260-420°C and can yield removals of 80-95% of the NO_x in the flue gas [19].

Another technique used for the reduction of NO_x in combustion flue gases in selective non-catalytic reduction (SNCR). This process is similar to SCR as it uses a reducing agent, such as ammonia, except no catalyst is used. When ammonia is used as the reducing agent the following reaction occur [19]:

$$4\ NH_3 + 5\ O_2 \leftrightarrow 4\ NO + 6\ H_2O$$

$$4\ NO + 4\ NH_3 + O_2 \leftrightarrow 4N_2 + 6\ H_2O$$
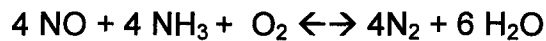
Instead of using a catalyst the reduction relies on higher temperatures to oxidize and reduce NO_x. The temperature range for SNCR is between 850-1050°C and can yield removals of 30-50% of the NO_x in the flue gas [19]. A comparison of SCR and SNCR is presented in Table 2-7.

Table 2-7: Comparison of selective catalytic reduction (SCR) to selective non-catalytic reduction (SNCR) [19]

Parameter	SCR	SNCR
Operating Temperature	260-320°C	850-1050°C
Reduction Agent	Ammonia, Urea	Ammonia, Urea
NH_3/NO_x ratio	0.8-1.0	1.5-2.5
Energy Consumption (% of electric output)	2	0.1-0.3
Pressure Drop	400-1000 Pa	NA
Residence Time within Required Temp.	NA	0.2-0.5s
Operational lifetime	8-10yrs (Natural Gas)	NA

As is shown in Table 2-7 SCR requires more energy to operate than SNCR, however SCR uses less ammonia than SNCR. It can be concluded that SNCR would not be feasible for NO_x control on MGTs due to the extremely high temperature needed, as MGTs usually have exhaust temperatures of approximately between 230-305°C [8, 10, 11]. Furthermore, although SCR could feasibly operate given the exhaust temperatures of MGTs, MGTs are normally used in combined heat and power (CHP) applications. In CHP applications the heat energy of the exhaust gas is used to heat other devices such as boilers or space heaters. This application greatly improves the versatility of the MGT and overall efficiency. However given that the heat energy from the exhaust is removed, this leaves the actual exhaust temperature of the MGT too low to use SCR as an effective after treatment of NO_x.

2.2.2 Conventional VOC Controls for Air Streams

There are numerous methods to remove VOCs from gaseous streams. Condensation can be used to remove VOCs from gases by cooling the air stream, thus condensing the VOCs that can then be removed as a liquid. However condensation cannot be readily applied to hot natural gas combustion exhaust because it requires temperatures below freezing to operate. Therefore a large amount of energy would be required to cool the exhaust gas. Natural gas combustion exhaust also contains a significant amount of water vapour, which would freeze the condensation coils [14].

Adsorption can also be used to collect VOCs from air streams using such materials as activated carbon. Adsorption can yield removals efficiency of up to 90%, however the adsorption systems do have disadvantages. Some drawbacks of an adsorption system include the need to regularly change and dispose of the absorbent [31]. This can lead

to a high maintenance cost. Incineration can also be used to treat air streams with high concentrations of VOCs. In this process VOCs are simply combusted into harmless materials. However if incomplete combustion occurs there is a risk that the exhaust from the incinerator could contain toxic chemicals. Some products that can form from incomplete incineration include dioxins and furans [14], which are some of the most toxic chemicals to known humans. Incineration would also require a significant amount of energy input, therefore if it were used in conjunction with a device that is producing power (such as an MGT), the overall efficiency of the device would be reduced.

Catalytic reduction of VOCs is also a viable for VOC treatment. The air stream with VOCs is sent through a catalyst, which must be at temperatures between 250°C and 400°C. The drawback to stand-alone catalytic treatment of VOCs is that a many different catalysts must be used to target different VOCs. The catalysts must also be continuously replaced and removal efficiencies for catalysts are generally lower than other techniques for removing VOCs [31].

Another technique to reduce VOCs in air streams is known as bio-filtration. Bio-filtration uses micro-organism to oxidize the VOCs into harmless substances. Bio-filtration reactor tends to be quite large and consist of a large reactor with soil containing micro-organisms. The air stream is forced upward through the soil where the VOCs first dissolve in water and then are consumed by the micro-organisms. Some of the disadvantages of these reactors are that they require a significant residence time in order to treat the waste gas stream and in some instances must be conditioned with nutrients to keep a healthy population of micro-organisms [14]. Other techniques that have had some success in removing VOCs from air streams include: ultraviolet oxidation, thermal plasma and high frequency glow discharges [31].

35

2.2.3 Conventional Particulate Matter Control for Air Streams

The simplest method for the removal of particulate matter from air streams is a surface filter. A surface filter is simply a piece of fabric, cloth or paper that has holes smaller than the particulate matter. One of the major drawbacks to this technique is that the diameter of holes within fabric is limited to larger sizes, thus smaller particles are not efficiently collected [14]. For industrial applications surface filters are normally operated in baghouses. A baghouse has a series of cylindrical surface filters arranged in rows that the polluted air streams flows through, thus collecting particulate matter in the filters. One major disadvantage of baghouse is that they cannot be cleaned while in use. Therefore multiple baghouses must be used together so that one baghouse can be taken offline to be cleaned [14].

Another uncomplicated method used to collect particulate matter is a gravity settler. As the name implies theses devices operated by allowing the particulate matter to settle to the bottom of the device by gravity. These devices are easy to build and maintain however there are numerous drawbacks to this technique of PM control. The gravity settler requires a long residence time to settle the particles; as well a gravity settler has only a 50% collection efficiency for particles approximately 40 microns in diameter [14]. Thus gravity settlers cannot be used for applications where smaller particles are a concern. A more efficient gravity settler for collecting particulate matter is known as a cyclone. A cyclone uses centrifugal force to collect particulate matter. By adding centrifugal forces to the particle the settling velocity of the particle is increased, therefore smaller particles can be collected by a cyclone, when compared to a simple gravity settler [14]. However cyclones are still limited to

collection efficiencies of 85-90% and the smallest particles that cyclones can collect are between 5-10 microns [19].

Another approach to PM control is the use of a wet scrubber. A wet scrubber removes PM by forcing the air stream through a mist of water droplets. The particulate matter then adheres to the water droplets and the water is then collected and disposed. This process can be expensive because the flue gas must be cooled before entering the scrubber. Furthermore the collected water must then be treated before it is fully disposed [19].

The most common approach to the removal of PM in an air stream is through a device called an electrostatic precipitator (ESP). In a typical industrial ESP the flue gas is sent through two plate electrodes that are charged by direct current voltage. The negative applied voltage creates a streamer corona that ionizes the flue gas and creates an electric field. This streamer corona thus places a charge on particles, which are then forced to the ground electrode by the electric field within the ESP. The particles adhere to the ground electrode and are removed by cleaning the electrode. ESPs can be a very efficient was of removing particulate matter and are used in 90% of industrial applications in Europe [19]. A comparison of conventional particulate matter control techniques is presented in Table 2-8.

Table 2-8: Comparison of convention techniques for the control of particulate matter [19]

Device / Parameter	Electrostatic Precipitators (ESP)	Surface Filter	Wet Scrubber
Removal Efficiency			
<1μm	>96.5	>99.6	98.5
10μm	>99.95	>99.95	>99.9
Operating Temperature (°C)	120-450	200 (polyester) 280 (fibreglass)	--
Energy Consumption (% of electric capacity)	0.3-1.8	0.08-0.14	Up to 3
Pressure Drop (Pa)	150-300	500-2000	3000-20000
Gas Flow Rate (m³/s)	< 56	> 306	---
Liquid to Gas Ratio (l/m³)	---	---	0.8-2.0

2.3 Technique for Oxidation and Reduction of Gaseous Pollutants by Non-Thermal Plasmas

The development of an after treatment technology for MGTs is critical given the large number of MGTs being used today for commercial and industrial applications is only likely to increase over the next decade. As previously mentioned the three pollutants of greatest concern for MGTs are NO_x, CO and VOCs. Although methods for controlling NO_x are available, none work efficiently in the oxygen rich, low temperature environment created by MGTs. After treatment technologies for VOCs created by MGTs are also limited, given the complexity of VOCs emitted by MGTs and the overall cost of many of these technologies is too high to be cost effective. Given these facts the best solution would be to create a device to treat all pollutants emitted by MGT natural gas combustion at

once. This would create an extremely cost effective method for treating MGT flue gas. One of the technologies at the forefront of research for this application is non-thermal plasma in combination with a catalyst called a plasma-catalyst system. This section will describe the current state of the art for non-thermal plasma reactors and plasma catalyst systems.

2.3.1 NO_x Conversion and Removal by Non-Thermal Plasmas and Plasma-Catalysts

It has been well established that non-thermal plasma reactors can efficiently reduce the NO concentration and convert NO to NO_2 by many researches [24, 35, 42-54]. The corona discharge created in a non-thermal plasma creates high energy electrons and strong electric field. These electrons will then create free radicals that react with the NO_x present in the gas stream. Some research has proposed that in a simple system with only NO and air present some of the following reactions may occur in a non-thermal plasma reactor [46, 55]:

(i) Reduction Reactions

$$N^* + NO \rightarrow N_2 + O \qquad k = 2.9\text{-}6.0 \times 10^{-11}\,cm^3/s \qquad (1)$$

$$N^* + N_2O \rightarrow N_2 + NO \qquad k = 2.2 \times 10^{-12}\text{-}6.0 \times 10^{-14} cm^3/s \qquad (2)$$

$$N_2^* + NO_2 \rightarrow N_2 + O + NO \qquad k = 1.3 \times 10^{-11}\,cm^3/s \qquad (3)$$

$$N_2^* + N_2O \rightarrow 2N_2 + O \qquad k = 6.2 \times 10^{-12}\,cm^3/s \qquad (4)$$

(ii) Oxidation Reactions

$$O^- + NO \rightarrow e + NO_2 \qquad k = 2.8 \times 10^{-10}\,cm^3/s \qquad (5)$$

$$NO + NO + O_2 \rightarrow NO_2 + NO_2 \qquad k = 2.0 \times 10^{-38}\,cm^6/s \qquad (6)$$

$$O_3 + NO \rightarrow NO_2 + O_2 \qquad k = 1.8 \times 10^{-14}\,cm^3/s \qquad (7)$$

$$NO + O + M \rightarrow NO_2 + M \qquad k = 9.0 \times 10^{-32}\,cm^6/s \qquad (8)$$
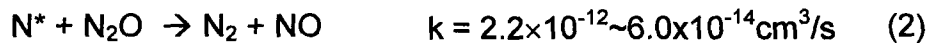
Where * represents an excited atom/molecule and k is the reaction rate. Hence, NO_x can be reduced by nitrogen free radicals and oxidized by

oxygen free radicals. Note that these are only a few of many reactions as the chemistry is very complex and only main reactions are given.

In order to convert the NO and NO_2 to elemental nitrogen and thus a harmless gas, research has focused on combining non-thermal plasmas with reduction or oxidation agents such as hydrocarbon additives [24, 29, 42, 44, 48, 56], sodium sulfides (in a wet scrubber) [54, 57], ammonia [45, 46], hydrogen peroxide [58] and/or catalysts [42, 43, 59-64]. The use of hydrocarbons as reductants in a non-thermal plasma system has been widely studied for two principle reasons. First because most combustion process exhaust usually contain hydrocarbons and secondly because it has been shown by modeling that ammonia can be produced from hydrocarbons [65] in the presence of air. The model by Kilpinen et al showed that ammonia radicals could be formed from methane radicals present in the reburning zone of the combustor in the presence of N, O and H [66]. Theoretically methane radicals can also be produced by the transformation of hydrocarbons by non-thermal plasma and therefore create ammonia radicals. Once ammonia radicals are produced the ammonia can reduce NO_x by some of the following reactions [46, 66]:

$$NO + NH_2 \rightarrow H_2O + N_2 \qquad k = 2.1\times10^{-11}\ cm^3/s \qquad (5)$$

$$NO + NH \rightarrow N_2 + OH \qquad k = 4.7\times10^{-11}\ cm^3/s \qquad (6)$$

$$NO + OH + N_2 \rightarrow HNO_2 + N_2 \qquad k = 6.7\times10^{-31}\ cm^6/s \qquad (7)$$

$$NO + H + H \rightarrow HNO + H \qquad k = 3.5\times10^{-32}\ cm^6/s \qquad (8)$$

$$NO_2 + N_2 \rightarrow OH + NO \qquad k = 1.1\times10^{-10}\ cm^3/s \qquad (9)$$

$$NO_2 + OH + N_2 \rightarrow HNO_3 + N_2 \qquad k = 2.6\times10^{-30}\ cm^6/s \qquad (10)$$

$$NO + H\text{-} \rightarrow HNO + e \qquad k = 4.6\times10^{-10}\ cm^3/s \qquad (11)$$

$$N^* + NO_2 \rightarrow N_2O + O \qquad k = 1.0\times10^{-12}\ cm^3/s \qquad (12)$$
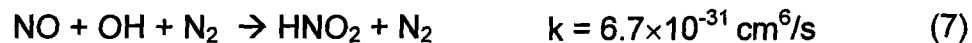
Urashima *et al* [46] studied the effect of ammonia injection on NO_x reduction using a superimposed barrier discharge NTP reactor. Simulated combustion gases were used with the injection of CO_2, O_2, N_2 and 800ppm NO for NO_x. The results showed that the in-phase NO_x reduction was approximately 12.5% at a flow rate of 2L/min, as the level of NO_x dropped from 800ppm to approximately 700ppm. However with the injection of NH_3 at a stoichiometric balance of 1.0 at a flow rate of 1L/min, the NO_x reduction was enhanced. The NO_x reduction with the addition of NH_3 as a reduction agent was 45%, as the NO_x dropped from 800ppm to 440ppm. The NO_x reduction improved further with the addition of more ammonia into the system achieving approximately 50% at an ammonia stoichiometric ratio of 1.25. This study showed that NTP combined with ammonia injection can be an effective mechanism for the reduction of NO_x.

In one case the addition of sodium sulfides in a wet scrubber was studied with non-thermal plasma for NO_x removal [54]. Simulated gases consisting of initial NO_x concentrations on the order of 150ppm were used and were sent through two different types of packed bed dielectric barrier discharge plasma reactors followed by chemical injection via a wet scrubber. The results show that there was 100% NO_x removal when using non-thermal plasma in combination with Na_2SO_3. However there are limitations in this study. The flow rate was extremely with low flow rates of 2-4L/min, the temperature was also low (60°C) and there may have been formation of N_2O and HNO_3, although this was not recorded [54]. This study also used a wet scrubber to remove the NO_x, therefore a large amount of solution would be required in order to fully treat the high flow rates of MGTs, making this solution unfeasible for the treatment of MGT flue gases.

The addition of ethyne (C_2H_2) to a gas stream were tested for of NO_x removal with a dielectric barrier discharge non-thermal plasma reactor [48]. The maximum NO_x removed in this study was approximately 90%, with the addition of 1500ppm C_2H_2 and an initial concentration of 500ppm NO. However these results were obtained at an inlet oxygen concentration of 0% and the NO_x removal dropped below 40% as the oxygen concentration was raised to 10%. Oxygen concentrations are higher than 10% under lean burn conditions in natural gas combustion. This study also observed that NO_x removal was increased at higher temperatures and at higher concentrations of water vapour. However there was the creation of N_2O, a greenhouse gas, as well as HNO_3 [48], which can cause acid rain. This study used low flow rates of only 1L/min; removal efficiency of NO_x would likely decrease at higher flow rates. Other studies show that NO_x removals of 70% can be achieved by the addition of ethene [29] and 37% NO_x removal can be achieved with the addition of propane and propene in addition to non-thermal plasma dielectric barrier discharge reactor [56].

The addition of hydrocarbons with non-thermal plasma followed by catalysts has been attempted to improve NO_x removal rates. One study focused on the application of a dielectric barrier discharge non-thermal plasma-catalyst system to simulated diesel exhaust. Diesel combustion is similar to MGT combustion as diesel occurs under lean burn operations and typically has between 4-15% oxygen content in the exhaust gas stream [43]. This research focused on three post-plasma catalysts: sodium zeolite Y (Na-Y), barium zeolite Y (Ba-Y) and alumina. The simulated exhaust gas was composed of 8% oxygen, 5% water vapour, 260ppm NO, 500ppm propene and 167ppm propane. The highest NO_x removal of 80% was observed to be the alumina catalyst after the NTP, however this occurred at a temperature of above 350°C. The Ba-Y plasma-catalyst

achieved a NO_x removal of approximately 75% at lower temperatures of 200°C [43].

This research also studied the effect of using two plasma-catalyst reactors in series of equal volume as a single plasma-catalyst reactor. Similar simulated exhaust gas was used in the experiment with a two stage plasma-catalyst. The results show that it was more effective then a single stage plasma catalyst. The single stage plasma-catalyst system reached NO_x removal efficiencies of 70%, while the two stage plasma-catalyst system achieved NO_x removal rates of nearly 90% [43]. The effect of different additives for NO_x transformation was studied without plasma over a Na-Y catalyst. The results show that the most effective NO_x conversion occurred with the addition of acetaldehyde, with a conversion of 64%. No conversion was observed with no additive added or with propane, propene or formaldehyde added [43]. This shows that the most effective additive tested for activating the Na-Y catalyst is acetaldehyde. This conclusion is important, as this study will use a sodium zeolite-Y catalyst.

The use of hydrocarbons as an additive for a plasma-catalyst system has also been investigated. Three catalysts were tested: copper-zeolite, vanadium pentoxide doped titanium oxide and a conventional three way catalyst (palladium and rhodium doped alumina) with a dielectric barrier discharge coaxial non-thermal plasma reactor [59]. Given that hydrocarbons are usually already present in natural gas combustion flue gases, this technique is promising for the removal of NO_x. In this experiment [59] simulated exhaust gas was used with the following composition: 400ppm NO, 10% oxygen, 10% carbon dioxide and 0.5% C_2H_4. The results show that without the use of a catalyst the combination of NTP and C_2H_4 could reach NO_x removals of approximately 40% at elevated temperatures (above 100°C) and just under 60% at room

temperature. The study showed that the copper zeolite catalyst combined with NTP and C_2H_4 was the most effective system for NO_x removal, reaching 80-90% removal at temperatures above 300°C [59]. However this study was also conducted at a relatively low flow rate of 2L/min.

Shimizu *et al* [42] has also studied the potential for NO_x removal by plasma-catalysts without the addition of hydrocarbons using a sodium zeolite catalyst, copper zeolite catalyst and a three way catalyst. Similar simulated exhaust gas compositions were used with 400ppm NO, 10% O_2, 10% CO_2 and no hydrocarbons. The research determined that the sodium zeolite catalyst could reach NO_x removals of close to 100% between temperatures of room temperature and 300°C, whereas the copper zeolite catalyst achieved a maximum NO_x removal of 60% at room temperature and the three way catalyst achieved a maximum NO_x removal of 80% at room temperature [42]. The limitation to this research is that the NO_x removal may have simply been by a process of absorption by the catalyst and therefore any NO_x removed would simply be released from the catalyst at a later time.

Miessner *et al* [64] have further examined additional types of catalysts in plasma-catalyst systems in an excess oxygen environment. A total of six catalysts were studied with a non-thermal plasma reactor. The catalysts were: lead-alumina, titanium oxide, alumosilicate, silver-mordernite, alumina and zirconium oxide. This experiment used simulated exhaust gas with the following composition: 500ppm NO, 13% O_2, 1000ppm propene with a flow rate of 2L/min. The results show that only the alumina and zirconium oxide catalyst in combinational with NTP attained NO_x removals of above 50%. The alumina plasma-catalyst had a NO_x removal rate of 60% at 300°C, while the zirconium oxide plasma-catalyst was just under 60% removal at 300°C [64]. The results for the alumina catalyst are supported by previous research [63]. It was also

determined that the catalysts caused the formation of N_2O. The lead-alumina plasma-catalyst had the highest N_2O formation with 36ppm, but the highest hydrocarbon removal with only 14ppm of propene being emitted. The alumina-silicate plasma-catalyst had the opposite effect producing only 7ppm of N_2O, while having an emission of 68ppm of hydrocarbons. As well with only the plasma and no catalyst there was observed to be 3ppm of N_2O and 67ppm of propene [64], suggesting the catalysts cause some production of N_2O.

Kwak *et al* [60] have studied the use of a combination of barium-zeolite and sodium zeolite catalysts for a plasma-catalyst system. This experiment used simulated exhaust gas with a composition of 8% O_2, 2% water vapour, 245ppm NO and 520 ppm C_3H_6 (propene). The researched studied the effect of catalyst composition on NO_x removal in a plasma-catalyst system. The combinations of sodium zeolite and barium zeolite included 100% barium, 80% barium, 60% barium, 40% barium, 20% barium and 2-1 barium-sodium, and 100% sodium. The research determined that the 100% barium catalyst was the most effective with a NO_x removal rate of 75% at a temperature of 200°C [60].

Kim *et al* [58] studied the effect of using an oxidizing agent, hydrogen peroxide, with a discharge plasma reactor and a photo-catalyst. In this study the photo-catalyst used was titanium dioxide (TiO_2). The plasma reactor was a cylindrical reactor with the spherical photo-catalyst pellets packed inside the reactor. This study also used a reactor with spherical alumina catalyst pellets packed inside a reactor to compare the results of alumina with titanium oxide. Simulated combustion gas was used with the following composition: O_2 10%, NO_x 400ppm and N_2 balance. This study was conducted at a temperature of 100°C and a flow rate of 2L/min. The results show that the photo-catalyst was most effective for NO_x removal with an injection of 1000ppm of hydrogen peroxide,

reaching a removal of approximately 95%. However the results also show that the photo-catalyst was also effective with no hydrogen peroxide injection, achieving a NO_x removal efficiency of approximately 87%. The results also indicate the alumina catalyst was not nearly as effective as the photo-catalyst with hydrogen peroxide injection, obtaining a NO_x removal of just over 50% [58]. This study was conducted at a low flow rate of only 2L/min and removal efficiencies might decrease with increased flow rates. Kim *et al* [58] also used spherical pellet catalysts, whereas the research undertaken in this experiment will use a honeycomb type catalyst and results would likely vary.

Given that hydrocarbons are present in the exhaust of MGTs the use of a plasma-catalyst system for the removal of NO_x appears to be a promising technology for this application.

2.3.2 Hydrocarbon-VOC Conversion and Removal by Non-Thermal Plasmas and Plasma-Catalysts

Non-thermal plasma and plasma-catalyst have been shown to be effective for removing some types of volatile organic compounds form air streams. Recent studies have observed that non-thermal plasma and plasma-catalysts can effectively remove VOCs such as toluene [67-72], acetaldehyde [73], trichloroethylene [74, 75] and 1,1,1 - trichloroethane [33]. Although the removal of VOCs from the exhaust of MGTs is important, the main objective of this present research is to remove the hydrocarbon-VOCs in natural gas combustion exhaust by converting the VOCs to aldehydes. The aldehydes then may activate the sodium zeolite-Y and in the process are removed. Therefore the overall mechanism of the plasma-catalyst system removes the VOCs in a two stage process. One study has shown that VOCs or hydrocarbons can be converted by non-thermal plasma to aldehydes [43]. This study used a simulated exhaust

gas containing 535ppmC propene, 260ppm NO, 8% O_2 with a specific energy density of 30J/L (~8.4wh/m^3) for the non-thermal plasma reactor. The study observed that at 180°C 110.8ppm of acetaldehyde were formed and 30.7ppm of acetaldehyde were formed at 30°C [43]. As mentioned in the previous section Hoard and Tonkyn [43] also observed that acetaldehyde was the most effective at activating a sodium zeolite catalyst for NO_x removal, which will be the same catalyst used in this research. However more research needs to be conducted to verify the capability of non-thermal plasma for the creation of aldehydes using natural gas combustion exhaust.

Chapter 3: Experimental Facilities and Procedure

3.1 Micro-Gas Turbine Test Cells

Two types of micro-gas turbines (MGT) were characterized in this research: a single stage combustion type MGT (Elliott TA-80R 80kW MGT) and a dual stage combustion type MGT (Ingersoll-Rand PowerWorks 70kW MGT). Both MGTs operate on a lean burn basis, meaning that there is excess air during combustion. However the dual stage combustion type MGT operates on a much leaner basis than the single stage combustion type MGT. The operating conditions of both MGTs are presented in Table 3-1.

Table 3-1: Operating parameters of tested single and dual stage combustion type micro-gas turbines

Parameter/Type	Single Stage (Elliott 80kW)	Dual Stage (Ingersoll-Rand 70kW)
Exhaust Temperature	279°C	232°C
Efficiency	28%	28%
Exhaust Mass Flow	0.77kg/s	0.73kg/s
Exhaust Flow Rate [a]	0.642m³/s	0.608m³/s
Natural Gas Inlet Flow Rate	10.4L/min	5.80L/min [b]
Normalized Air-to-Fuel Ratio (λ)	6.1	10.2
Electrical Output	480 VAC, 50 or 60Hz	480 VAC, 60Hz
Noise @ 1m	75dBa	75dBa
Heat Rate	12,200 BTU/hr	13,080 BTU/hr
Input Pressure	78psia	75psia

[a] Based on STP condition for ideal gas = 22.4L/mol of gas
[b] Based on HHV for methane = 41.2MJ/m³

3.1.1 Single Stage Combustion Type Micro-Gas Turbine Test Facilities and Procedures

The emissions of an 80kW single combustion type micro-gas turbine (Elliot TA-80R) were characterized as shown in Figure 3-1. The exhaust mass flow rate was 0.77kg/s and the average velocity in the exhaust tube was estimated to be approximately 10m/s and therefore a sampling tube with a 6.4mm diameter was used to ensure iso-kinetic sampling the micro-gas turbine's exit. The sampling tube was placed

Micro-Gas Turbine
Elliott 10kW

Exhaust   254mm (10") diameter

To Outdoors

6.4mm (1/4") diameter

Particulate Sampling (CPC, HAZDUST)
9.5mmm (3/8")

Air Pump

Sampling Chamber
102mm (4") diameter   VOC meter
305mm (12")   Eurotron Greenline (NOx, COx)

Figure 3-1: Experimental facilities for single stage combustion type micro-gas turbine

approximately 60cm downstream from the micro-gas turbine's exhaust exit. The sampling tube was approximately 120cm long, which was attached to a static gas-sampling chamber. The gas-sampling chamber was 30.5cm long with a diameter of 10.2cm. An air-sampling pump with a flow of 5L/min was connected to the gas-sampling chamber to draw the micro-gas turbine's exhaust through the sampling tube into the chamber. The micro-gas turbine's exhaust was then characterized using the instrumentation as summarized in Table 3-2.

Table 3-2: Instrumentation used in MGT exhaust gas analysis

Instrument	Parameter	Range	Resolution	Accuracy
Eurotron Greenline™ Combustion Gas Analyzer (ppm)	NO	0-1999ppm	1ppm	±4%
	NO_2	0-99ppm	1ppm	±4%
	CO	0-4000ppm	1ppm	±4%
	SO_2	0-1999ppm	1ppm	±4%
	CO_2	0-99.9%	0.1%	--
	O_2	0-25%	0.1%	<±1%
HazDust™ Optical Particle Counter	PM	0.01-200 mg/m^3	0.02 mg/m^3	±10%
TSI™ Condensation Particle Counter	PM	0.001-10,000 part/cm^3	0.01μm	<10% @10,000 part/cm^3
TLV Hydrocarbon Sniffer (ppm hexane)	VOC	0-10,000ppm	2ppm	---
Gastec™ Measurement System (ppm)	Ozone	0.025-3ppm	0.01ppm	10%
	Hydrocarbons	0.02-0.8%	0.002%	10%
	Acetaldehyde	2.5-100ppm	0.1ppm	10%

The characterization of the single stage combustion type micro-gas turbine was conducted using both methane and propane as combustion fuels. The power output of the micro-gas turbine was varied between 0kW (idle) to 80kW at intervals of 10kW. In one of the methane tests the power output of the micro-gas turbine was raised to full power at 100kW. At each 10kW interval the concentration of NO, NO_2, CO, SO_2, VOCs and PM in the exhaust gas were measured. The Eurotron Greenline Combustion Analyzer measured NO, NO_2, CO, and SO_2 at a rate of one sample per

minute. The particulate matter was recorded at a rate of one sample per minute by the HazDust Optical Particle Counter (OPC) and was recorded manually from the display of the TSI Condensation Particle Counter (CPC). The VOC measurements were also recorded manually at a rate of one sample per minute from the display of the TLV sniffer. The measurements were first taken at idle during the initial start up of the micro-gas turbine to characterize cold start emissions. The measurements were then repeated at start up after the micro-gas turbine had been running for a few hours to characterize warm start emissions.

The MGT's exhaust was also collected in stainless steel sampling containers, which were under a vacuum. The exhaust gas was collected at 0kW, 60kW and 80kW during the methane test and at 60kW and 80kW for the propane test. The collected gases were then analyzed by FTIR adsorption spectroscopy (BioRad FTS 40). The exhaust gas was also collected through filter paper in order to characterize the particulate matter by ESEM (Electroscan 2020 ESEM).

3.1.2 Dual Stage Combustion Type Micro-Gas Turbine Test Facilities and Procedures

The experiment was conducted at the Canadian Mining and Energy Technologies (CANMET) Center in Ottawa, Ontario, Canada. The emissions of a 70kW dual stage combustion type micro-gas turbine (Ingersoll-Rand PowerWorks 70L) were characterized as shown in Figure 3-2.
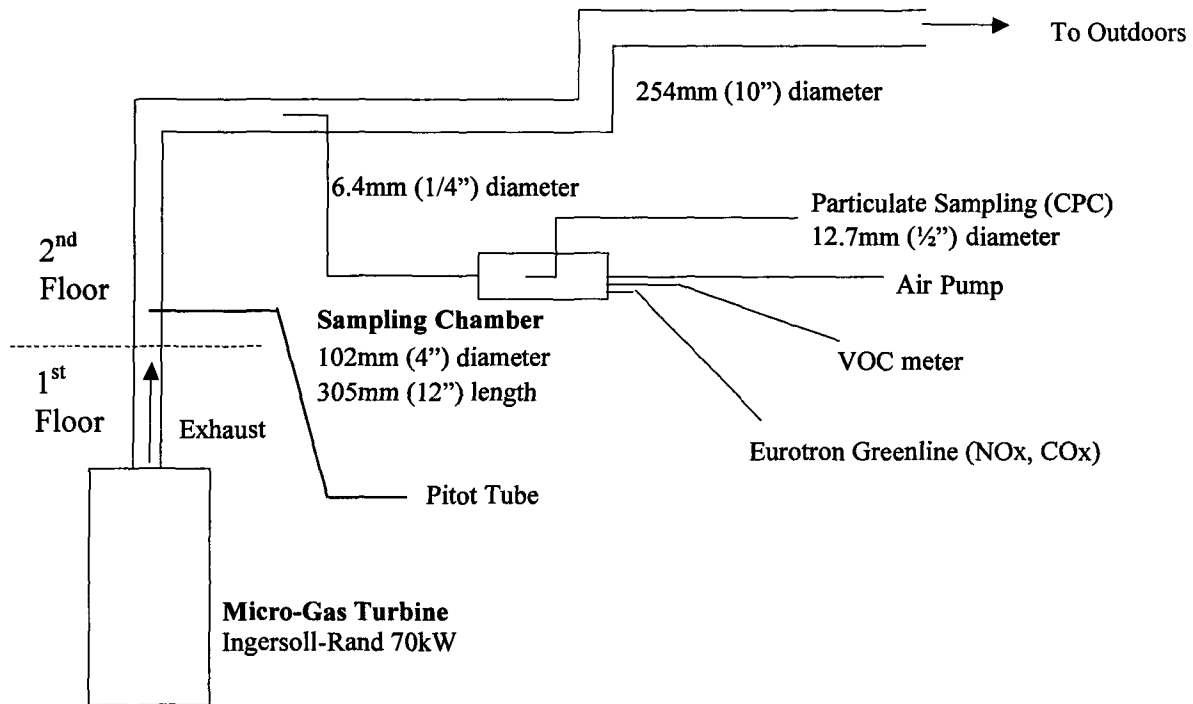
Figure 3-2: Experimental facilities for dual stage combustion type micro-gas turbine

The exhaust gas mass flow rate was 0.73kg/s and the velocity was measured using a pitot tube that was located approximately 1m downstream from the exhaust exit of the micro-gas turbine. The exhaust gas velocity was measured to be 10m/s and therefore a sampling tube with a 6.4mm diameter was used t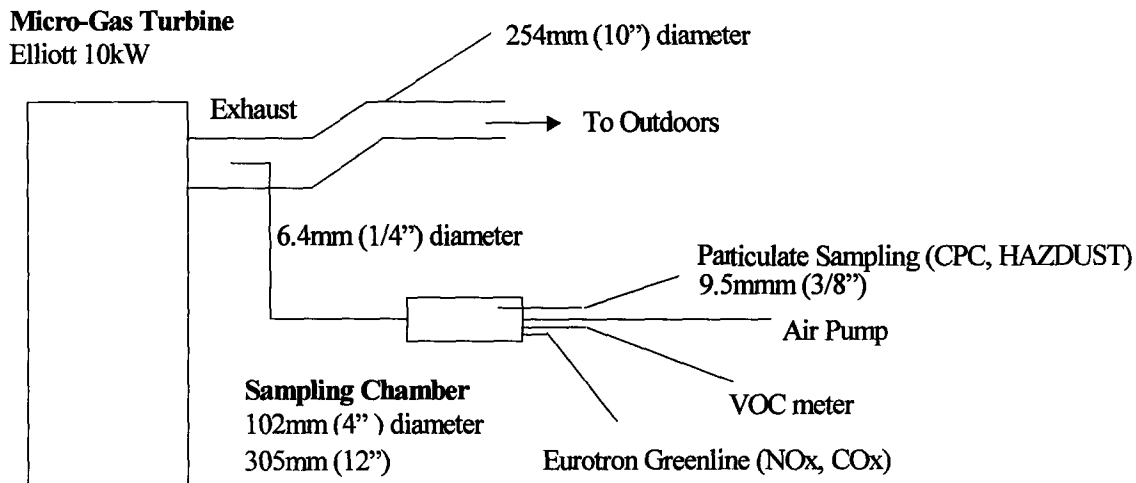o ensure iso-kinetic sampling. The sampling tube was located on the second floor of the facility about 3 to 4 meters downstream from the exit of the micro-gas turbine. The sampling tube was approximately 200cm long, which was attached to a static gas-sampling chamber. The gas-sampling chamber was 30.5cm long with a diameter of 10.2cm. An air-sampling pump with a flow of 5L/min was connected to the gas-sampling chamber to draw the micro-gas turbine's exhaust through the sampling tube into the chamber. The micro-gas turbine's exhaust was then characterized by the instrumentation as summarized in Table 3-1.

The characterization of the dual stage combustion type micro-gas turbine was conducted using methane as the fuel. The emissions from the micro-gas turbine were measured at start up and at full load (70kW) only. The measurements were taken both at initial start up for cold start characterization and at start up after the micro-gas turbine had been running for at least half an hour for warm start up characterization. At each instance the concentration of NO, NO_2, CO, SO_2, VOCs and PM in the exhaust gas were measured. The Eurotron Greenline Combustion Analyzer measured NO, NO_2, CO, and SO_2 at a rate of one sample per minute. The particulate matter was recorded at a rate of one sample per 30 seconds initially and then at one sample per minute manually from the display of the TSI CPC. Particle size distribution was measured by changing screen sizes in CPC from $0.017\mu m$ to $0.162\mu m$. The VOC measurements were also recorded manually at a rate of one sample per minute from the display of the TLV sniffer. All the instruments were observed during start up periods and maximum values were recorded.

The MGT's exhaust was also collected in stainless steel sampling containers, which were under a vacuum. The exhaust gas was collected at cold start up, warm start up and a full load. The collected gases were then analyzed by FTIR adsorption spectroscopy.

3.2 Non-Thermal Plasma Discharge Characteristics Test Loop

Discharge characteristics of the trench type barrier discharge non-thermal plasma reactor, as shown in Figure 3-3, were obtained for an AC sinusoidal wave applied voltage supplied by a neon transformer. The trench reactor is a dielectric barrier discharge reactor. The upper electrode has 5 triangular shaped channels, which are 20mm in width and 10mm in height. As shown in Figure 3-3 the trench reactor is 120mm wide. The bottom electrode is a flat plate 11.6mm in height with a lip 1.6mm high and

5mm wide to contain the dielectric barrier. The dielectric barrier consists of two alumina plates 1.36mm thick, 109mm wide and 139mm in length. The overall length of the trench reactor is 280mm. In order to determine the power across the reactor, a 2 channel oscilloscope was used to plot the voltage across the reactor and a known capacitor. The experimental set up is illustrated in Figure 3-4. The resulting voltages were plotted on an x-y plot to form Lissajous diagrams [30, 35-37], where the area of the Lissajous figure corresponds to the power across the reactor.
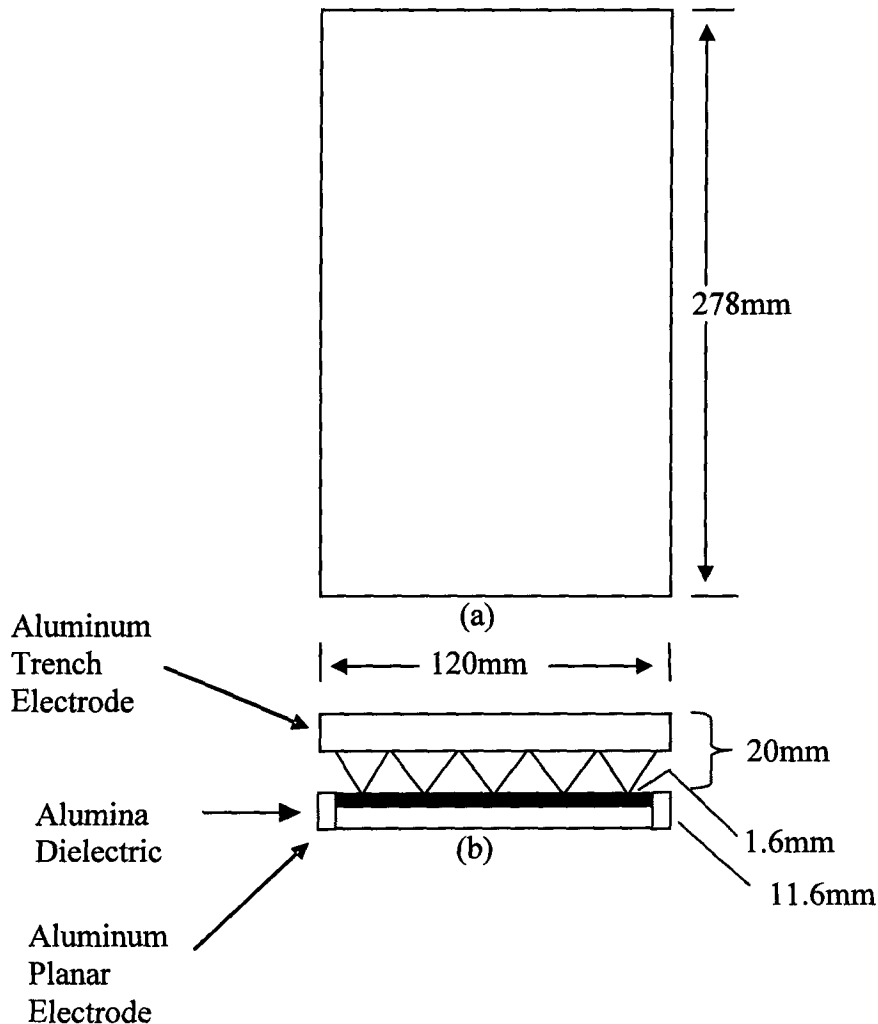
Figure 3-3: Trench type barrier discharge reactor (a) top view and (b) side view

54
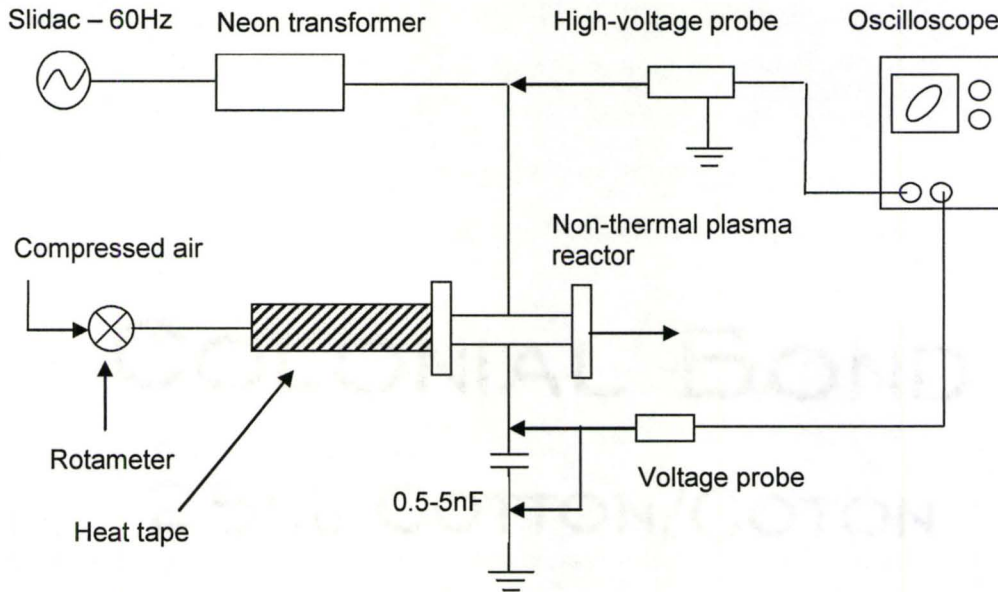
Figure 3-4: Experimental set up for barrier discharge reactor power measurements

To obtain an optimized Lissajous diagram the capacitor had to be varied as the applied voltage across the non-thermal plasma reactor varied. Table 3-3 shows the capacitance change according to the applied voltage across the non-thermal plasma reactor. A typical Lissajous figure is shown in Figure 1-3 in Chapter 1.

Table 3-3: Applied voltage versus capacitance used in Lissajous power determinations

Applied Voltage (kV)	Capacitance (nF)	Applied Voltage (kV)	Capacitance (nF)
2	0.5	12	5
4	1	14	5
6	1	16	5
8	2.2	18	5
10	2.2	20	5

The power distribution across the reactor was determined under three conditions: no flow, room temperature air flow and heated air flow. Under the no flow condition the power distribution was simply taken at room temperature with no air flow through the reactor. The last two tests were preformed by forcing air through the reactor at room temperature and at 50°C. The air was set to rates between 28 – 200 L/min and the flow was measured by a rotameter.

3.3 Natural Gas Combustion Test Loop Facilities and Experimental Procedure

The natural gas combustion facilities are comprised of an integrated pollution control system for controlling flue gas emissions. The system is consists of a natural gas combustor, a dust flow separator type electrostatic precipitator (DFS-ESP), a trench type barrier discharge non-thermal plasma reactor (NTP), a sodium zeolite Na-Y catalyst reactor, a large main ESP and five sampling ports. Each sampling port is equipped with interchangeable sampling tubes as well as T-type thermocouples. An overall dimensioned schematic of the natural gas test loop is presented in Figure 3-4. The total length of the entire integrated loop is approximately 4.9m.

Figure 3-5 shows the experimental set-up of the pressure drop test. The pressure drop was measured for the non-thermal plasma reactor, the catalyst and the plasma-catalyst together. All three tests were conducted using a Validyne DP103 Ultra-Low pressure transducer connected to a Baker Instruments demodulator (model CDC-23). Air flow was introduced to the natural gas test loop as shown in Figure 3-5 via a rotameter with flows rates ranging from 0-10 Nm^3/hr. The pressure drop across the plasma reactor was measured from sampling ports 2 to 3. The pressure

drop measurement of the catalyst was measured from sampling ports 3 to 4 and for the plasma-catalyst system the pressure drop was measured between sampling ports 2 to 4.
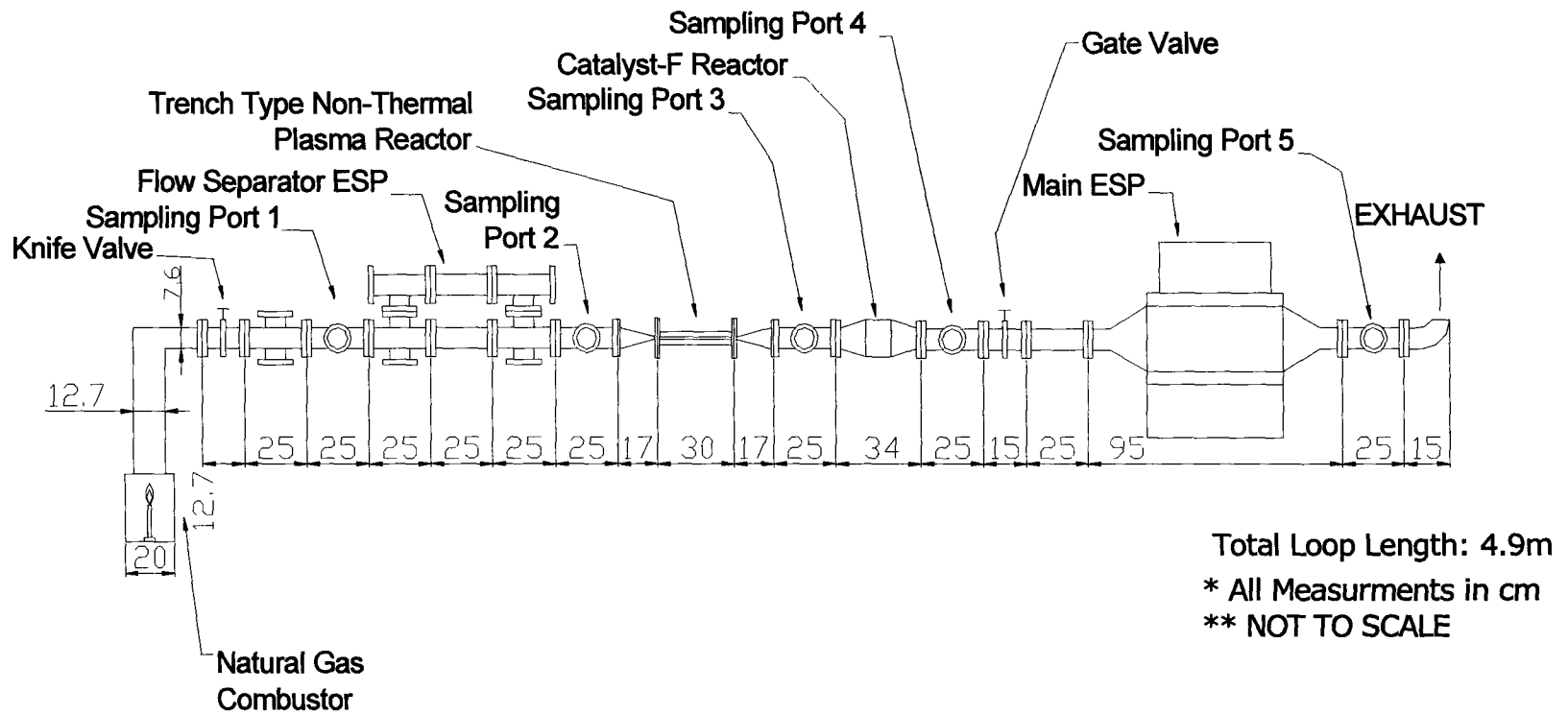
Figure 3-4: Overall schematic of natural gas combustion loop
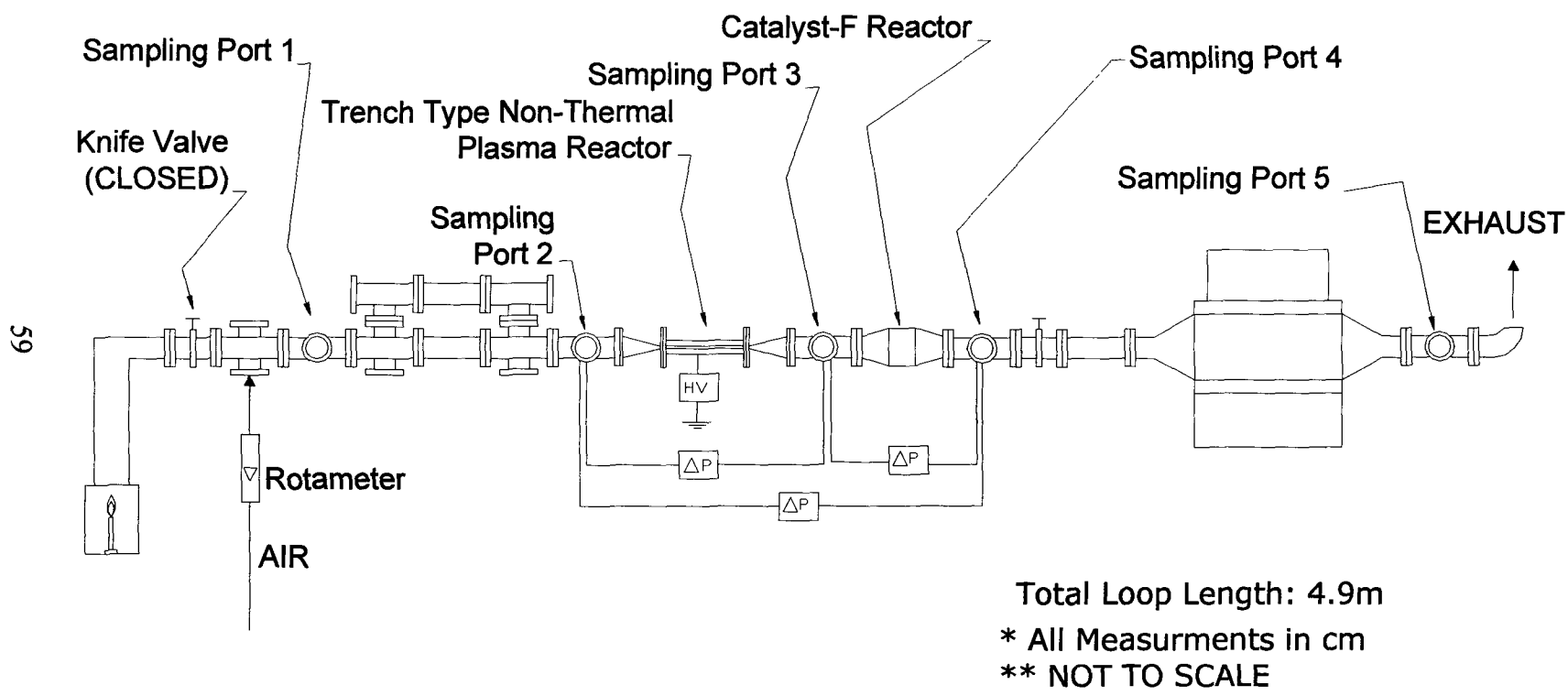
Figure 3-5: Overall schematic of pressure drop experiment in natural gas loop
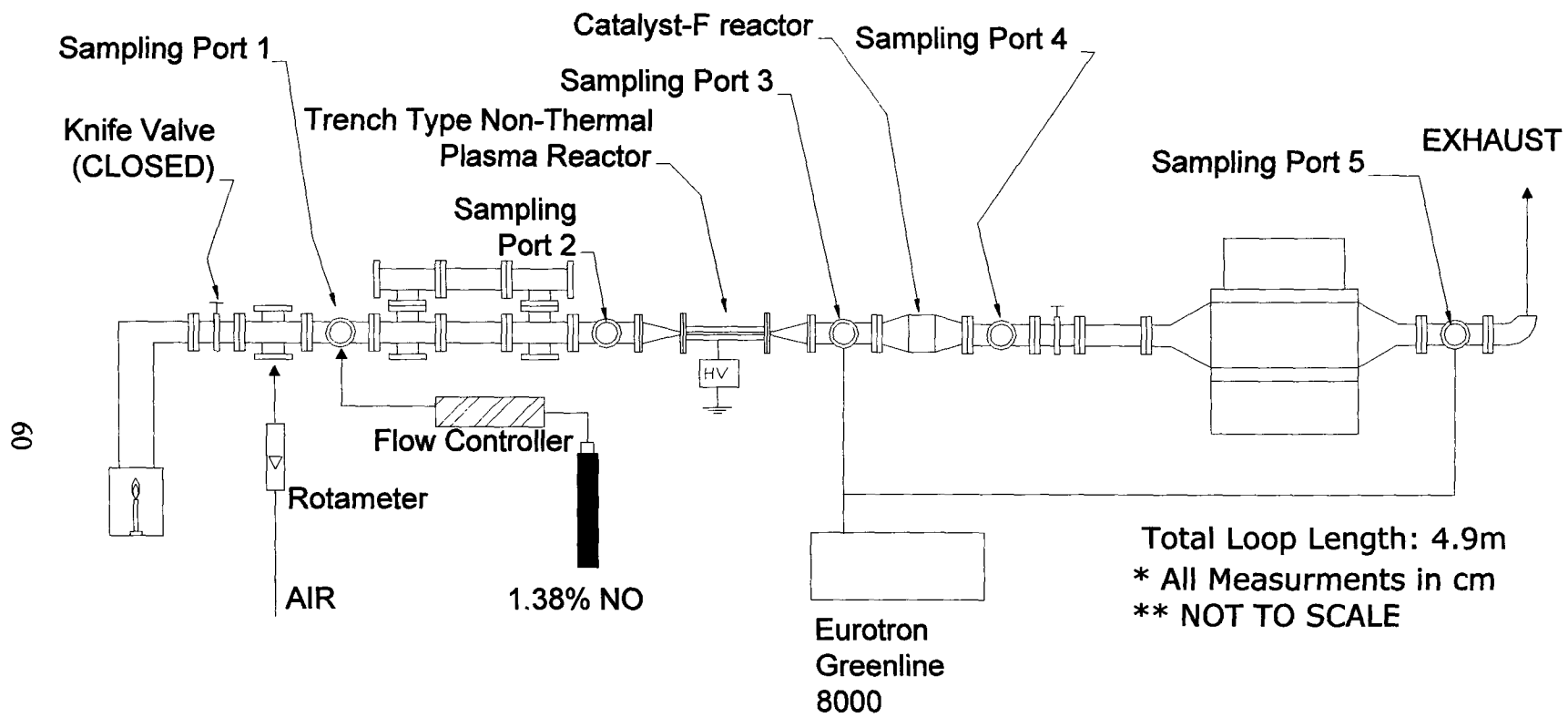
Figure 3-6: Experimental set up for plasma-catalyst NO test
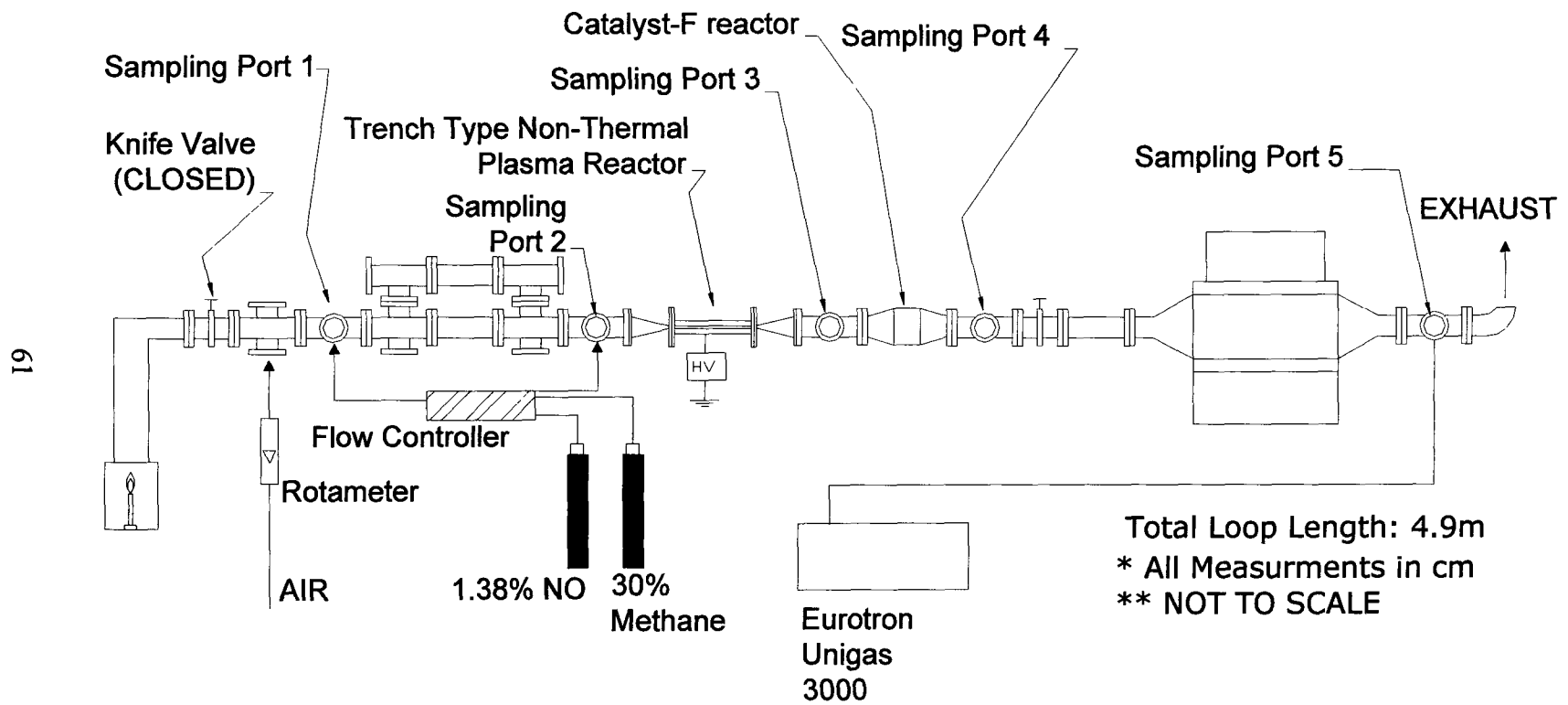
Figure 3-7: Experimental set up for plasma-catalyst NO with CH_4 test

Sampling Port 3

Catalyst-R reactor

Sampling Port 1

Trench Type Non-Thermal
Plasma Reactor

Sampling Port 4

Sampling Port 5

EXHAUST

Knife Valve
(OPEN)

Sampling
Port 2

$\frac{3}{8}$" Stainless Steel
Sampling Tube

Greenline 3000

Rotameter

180° Ball Valve

Sampling
Pump

$\frac{3}{8}$" Teflon Tubing

AIR

Natural Gas

Total Loop Length: 4.9m
* All Measurments in cm
** NOT TO SCALE

FTIR
Chamber

HV
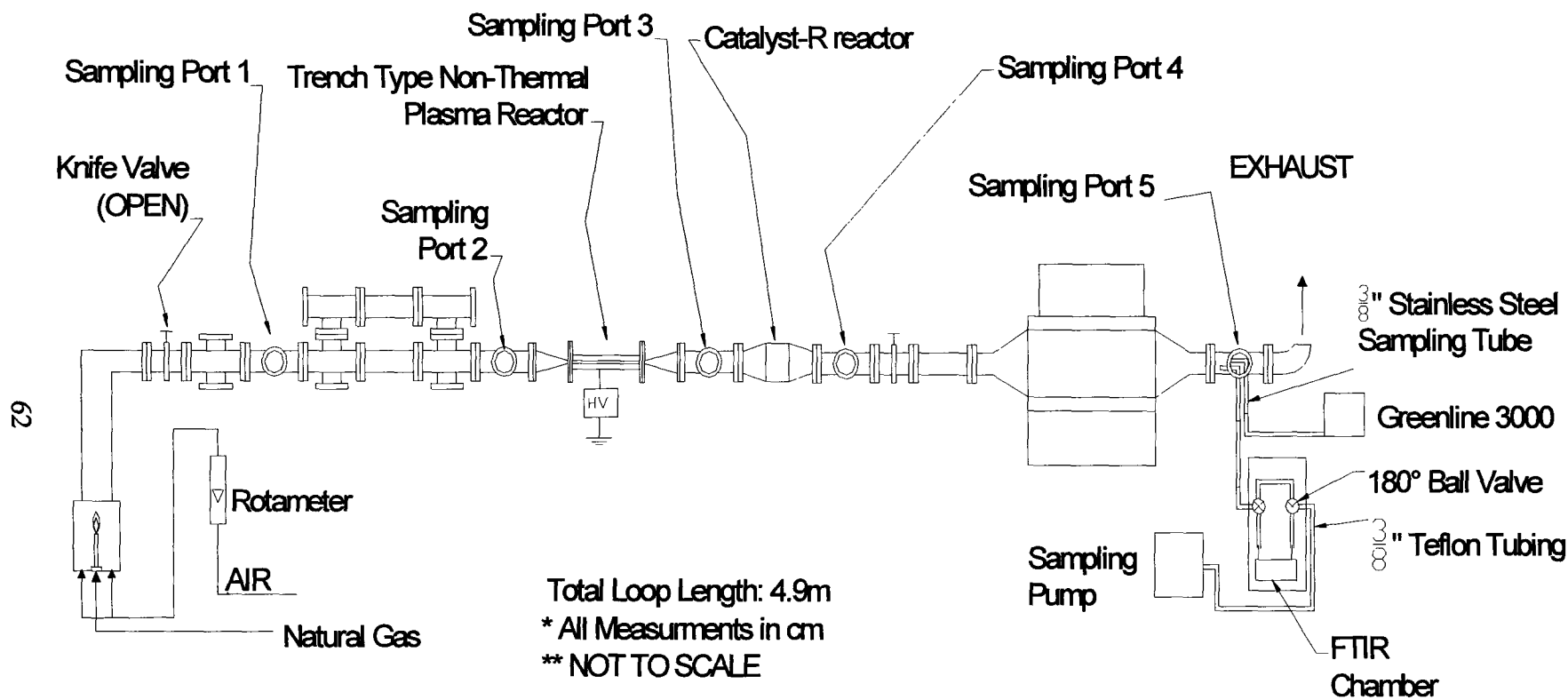
Figure 3-8: Experimental set up for natural gas combustion loop characterization

Figure 3-6 illustrates the experimental set-up for the simulated gas test. In this experiment N_2-NO 1.38% was introduced into the natural gas combustion test loop, with the combustor off, through an Edwards Datametrics 6100 flow controller. The air flow rate was controlled by a rotameter and introduced to the natural gas test loop. In the first test the air flow rate was set to five flow rates between 0-9.5 Nm^3/hr. The flow rate of the NO gas was then adjusted to dilute the NO in the loop to approximately 20ppm. The non-thermal plasma reactor was then adjusted to applied voltages between 10kV and 20kV, in steps of 2.5kV. At each applied voltage setting the concentration of NO and NO_2 was measured at sampling port 5 by the Greenline 8000. The specifications of the Greenline 8000 are given in Table 3-4. This test was then performed again without the catalyst. In the second test the NO and NO_2 were measured before the catalyst by the Greenline 8000 at sampling port 3. The test was then conducted a third time, with the catalyst removed from the loop, and the concentration of NO and NO_2 were measured at sampling port 5.

Table 3-4: Eurotron Greenline 8000 & Eurotron Unigas 3000 specifications

Instrument	Parameter	Range	Resolution	Accuracy
Eurotron Greenline™ 8000 Combustion Gas Analyzer (ppm)	NO	0-4000ppm	1ppm	±5ppm<125ppm ±4% >125ppm
	NO_2	0-1000ppm	1ppm	±5ppm<125ppm ±4% >125ppm
	CO	0-20000ppm	1ppm	±10ppm<300ppm ±4% up to 2000ppm ±4% > 2000ppm
	CO_2	0-100%	0.1%	---
	O_2	0-25%	0.1%	±0.1%

For the next experiment the sodium zeolite Na-Y catalyst coated on 400cpsi cordierite monolith reactor was placed back into the natural gas loop and the initial NO remained set to 20ppm. The sodium zeolite-Y reactor was then heated for a period of 2 hours by wrapping the catalyst chamber (steel) in standard electrical heating tape with an output of 300°C. The first test was repeated with a heated catalyst at five flow rates between 0-9.5 Nm^3/hr.

In the next test the same experimental setup was used as the previous test with the addition of CH_4 into the loop via the flow controller, as shown in Figure 3-7. Once again in this test the air flow rate was set to five flow rates between 0-9.5 Nm^3/hr and the flow rate of the NO was accordingly adjusted to dilute the NO in the loop to approximately 20ppm. 30% compressed CH_4 (balance N_2) was set to flow rates via the flow controller to allow concentrations of 20ppm (CH_4/NO = 1), 30ppm (CH_4/NO = 1.5), 40ppm (CH_4/NO = 2) and 50ppm (CH_4/NO = 2.5) of CH_4 to be introduced to the loop at sampling port 2, just before the NTP trench reactor. At each flow setting the concentrations of NO, NO_2 and CO were recorded using the Eurotron Unigas 3000 handheld combustion analyzer at sampling port 5, as shown in Figure 3-7. The specifications of the Unigas 3000 are given in Table 3-4.

In the next stage of experiments the natural gas combustion loop was characterized for emissions and the experimental set-up for the characterization is shown in Figure 3-8. The natural gas loop was characterized using a Unigas 3000 handheld combustion analyzer and the specifications of the Unigas 3000 are shown in Table 3-3. The natural gas loop was characterized under two conditions: cold start and hot steady state conditions. Before the start of the experiments the loop was preheated by wrapping the loop with heat tape. The heat tape was turned on for half an hour before the experiment to reduce condensation on the

walls of the loop.   Cold start conditions were measured at the initial start up of the natural gas combustion loop at a flow rate of 5.1Nm^3/hr. Once the readings were stable the flow rate was increased to 6.8Nm3/hr, 8.5 Nm^3/hr, 10.2 Nm^3/hr, 11.4 Nm^3/hr and then down to 5.1 Nm^3/hr and 3.4 Nm^3/hr. The hot steady state conditions were characterized after the natural gas loop had been running for four hours to ensure the loop was fully heated.   Measurements were initially taken at 3.4Nm^3/hr and then increased to 5.1Nm^3/hr 6.8Nm^3/hr, 8.5 Nm^3/hr, 10.2 Nm^3/hr, and 11.4 Nm^3/hr for intervals of 10 minutes.

Chapter 4: Characterization of Micro-Gas Turbine Flue Gas Emissions

4.1 Single Stage Combustion Type Micro-Gas Turbine Emission Characteristics

Experiments were conducted at the micro-gas turbine test cell (Chapter 3) to characterize the flue gas emissions of the MGT. The testing was conducted at varied loads with both methane and propane as the fuel. The results for this testing are presented in the following sections.

4.1.1 Volatile Organic Compounds and Hydrocarbons

Figure 4-1 shows the concentrations of VOCs in both the methane test and propane test of the single stage combustion type micro-gas turbine. In both the propane and methane tests the concentrations of VOCs decreased with increasing micro-gas turbine load. The results show that the VOC concentration for natural gas combustions was between 100-120 ppm (C_6H_{14} equivalent) and the VOC concentration for propane combustion ranged from 150-170 ppm (C_6H_{14} equivalent). The higher VOC concentration for propane was expected because propane has a longer carbon chain. Thus when propane is broken down there is a higher number of volatile hydrocarbons that could be formed from the breakdown of propane and subsequent reactions. In addition Figure 4-1 shows a significant difference between the VOC concentrations for cold and hot start conditions with natural gas. The initial VOC concentration for the hot natural gas start was observed to be 120 ppm (C_6H_{14} equivalent), while the cold start was observed to be 280 ppm (C_6H_{14} equivalent), approximately twice the concentration. This result was also expected, as

Figure 4-1: VOC concentration versus load for single combustion type micro-gas turbine for propane and natural gas combustion

Figure 4-2: Hydrocarbon concentration versus load for single combustion type micro-gas turbine for propane and natural gas combustion

when the micro-gas turbine is cold the combustion process may initially be quenched along the micro-gas turbine's walls resulting in portions of uncombusted or partially combusted fuel. Figure 4-2 shows the concentration of hydrocarbons versus power for the natural gas and propane combustion tests. As expected the concentration of hydrocarbons decreased with increasing power, as was the case for VOCs. As VOCs represent a portion of the total hydrocarbons in the exhaust gas this result was anticipated.

4.1.2 Oxygen and Carbon Dioxide

Figure 4-3 shows the oxygen concentration with power for both the natural gas and propane tests. For the natural gas test the oxygen level varied between 18.5-19.7%, whereas the oxygen level ranged between 18.2-19.4% for the propane test. The carbon dioxide for the natural gas test ranged between 0.8-1.9% and between 1.0-1.8% for the propane test. Figure 4-4 presents a time plot of the concentrations of O_2 and CO_2 for the natural gas test. In the first part of the Figure 4-4 the cold start test to a full load of 101.2kW can be seen and in the second half of Figure 4-4 a hot start to a full load of 80kW can be seen. The first test yielded slightly higher concentrations of CO_2 because of the higher load.

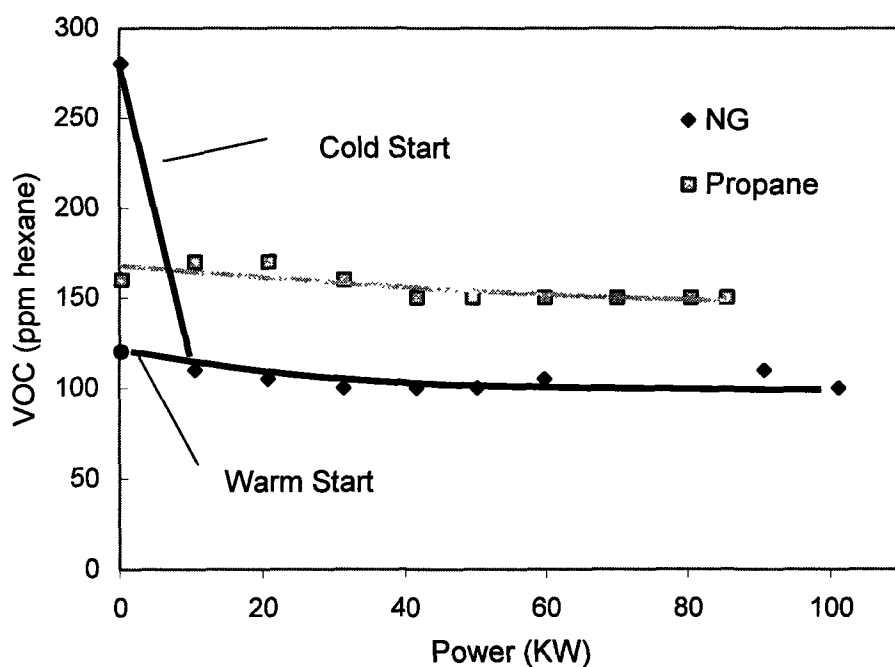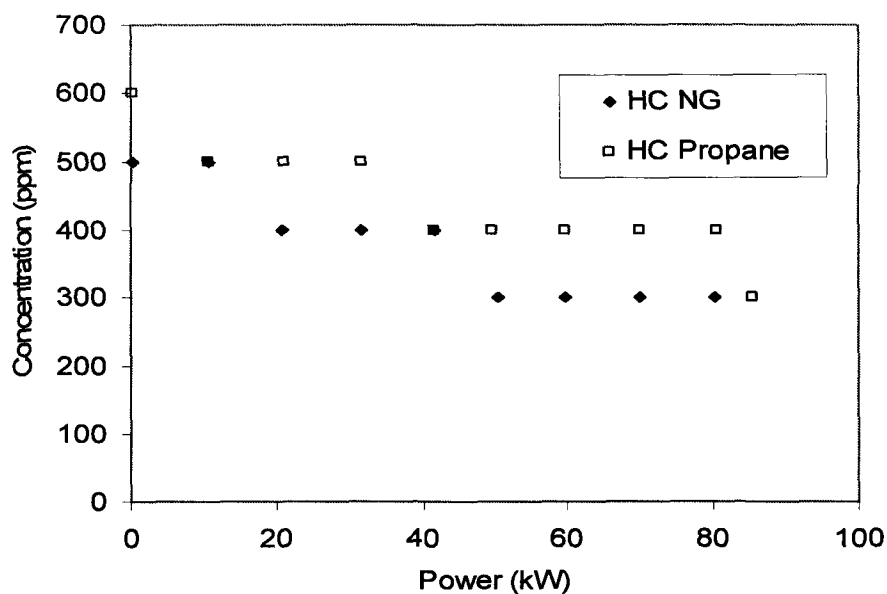**Figure 4-3:** Oxygen and carbon dioxide concentration versus load for single combustion type micro-gas turbine for propane and natural gas combustion

Figure 4-4: Oxygen and carbon dioxide concentration versus time for the natural gas combustion test

4.1.3 Carbon Monoxide

Figure 4-5 shows the CO concentration in ppm and in mg/m^3 for both the propane and natural gas tests. The CO concentration for both natural gas and propane decrease significantly with increasing power. Propane combustion yielded a much larger concentration of CO than methane combustion. CO formation occurs from incomplete combustion and is toxic to humans. The propane test resulted in a CO range from 387ppm upon start up to 35ppm at 85.6kW. The methane test has a smaller range from 252ppm at start up to 3ppm at 101.2kW. Comparing the power range which both fuels were tested, from idle to 80kW, reveals that the propane produces 30-40% more CO than when methane is used. As can be observed from Figure 4-5, this difference is greater than the uncertainty of the measurements.

Figure 4-6 shows the concentration of CO for the propane and natural gas test with the mass of CO related to the power produced by the micro-gas turbine. As with Figure 4-5 the amount of CO produced during low power is high. The mass of CO per MWh formed during start up is much greater for propane at approximately 70kg/MWh, whereas for natural gas it is approximately 50kg/MWh. However in both the propane and methane combustion tests the CO mass concentration per unit energy becomes very low at full power, when combustion is most complete and therefore efficient.

Figure 4-7 shows the concentration of CO in ppm versus time for the natural gas combustion test. The difference between the initial cold start and hot start of the single stage combustion type MGT can clearly be seen as the cold start produces CO concentrations close to 1150ppm, while the hot start produces concentration of 120ppm. It can also be observed from Figure 4-7 that the shut down of the MGT produce a spike in CO emissions perhaps due to slightly fuel rich conditions during

shutdown. As well it can be observed that the full power emissions at 101.2kW are lower than the emissions at 80kW.

Figure 4-5: Carbon monoxide (CO) concentration versus load for the single stage combustion type micro-gas turbine for propane and natural gas combustion
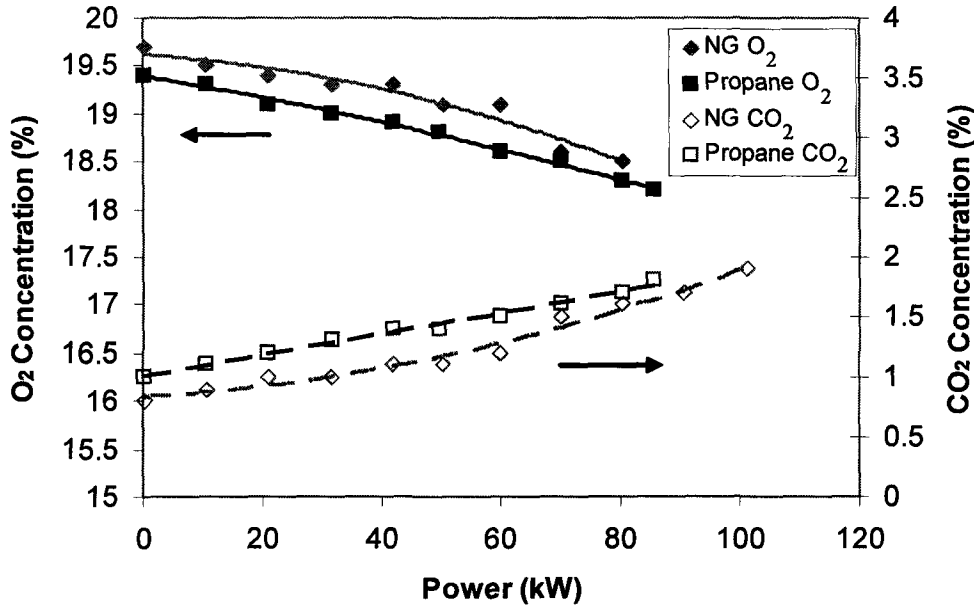
Figure 4-6: Carbon monoxide (CO) concentration versus load for single stage combustion type micro-gas turbine for propane and natural gas combustion
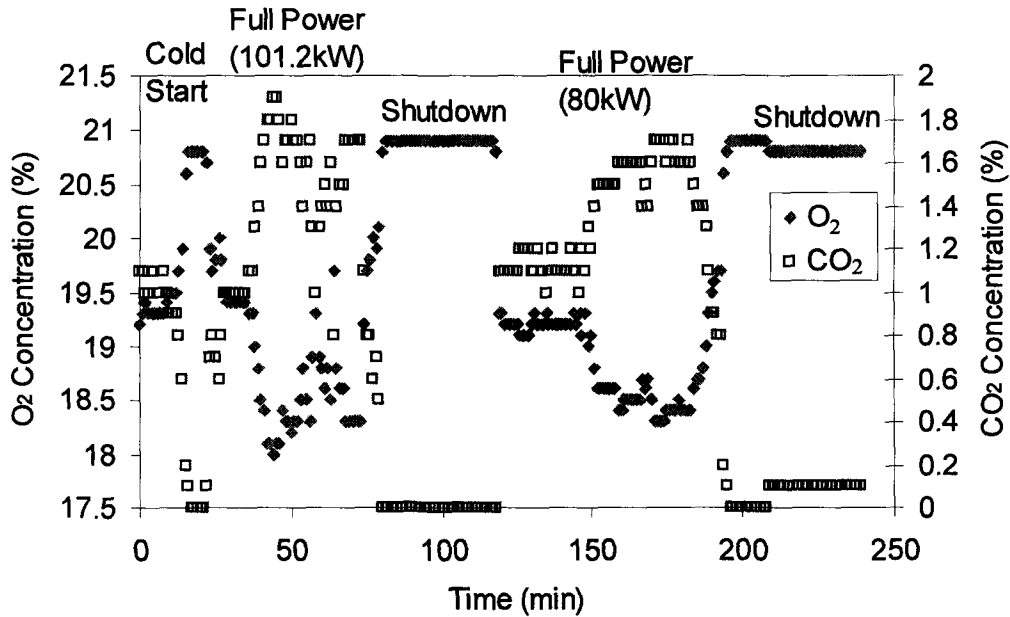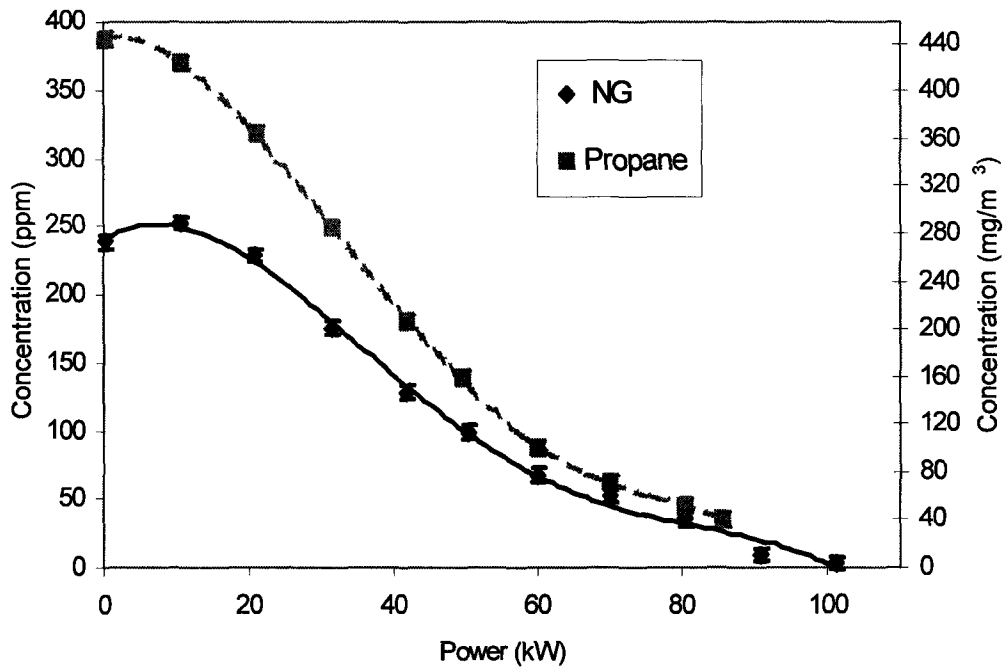

Figure 4-7: Carbon monoxide (CO) concentration versus time for single stage combustion type micro-gas turbine natural gas combustion test

4.1.4 Nitrogen Oxides (NO$_x$)

The concentration of NO, NO$_2$ and NO$_x$ (NO + NO$_2$) for the natural gas test and the propane test are displayed in Figure 4-8 and Figure 4-9, respectively. The NO and NO$_2$ was also measured with an Ecophys NO$_x$ meter provided by the onsite facilities. The Greenline's NO and NO$_2$ measurements were observed to be in good agreement with the Ecophys NO$_x$ monitor, being within 2ppm of the Ecophys' NO$_x$ measurements at each reading. The concentration of NO$_x$ increased with increasing power in both cases. The amount of NO$_2$ in the natural gas test was almost constant at 1ppm (the detection limit of the instrument), with the amount of NO increasing significantly to 10ppm at 80.4kW and further to 14ppm at 101.2kW. Similar findings were recorded in the propane test as the NO$_2$ concentration was close to constant at 2ppm and the NO rose to 13ppm at 80.5kW. The concentration of NO$_x$ at 80kW was observed to be 12ppm or 22.6mg/m^3 (as NO$_2$) for the natural gas case and 16ppm or 30.1mg/m^3 (as NO$_2$) for the propane test. The concentration of NO$_x$ increasing with increasing power might be attributed to a higher combustion temperature within the micro-gas turbine at higher loads. The increased temperature would then create the formation of more thermal NO$_x$.

Figure 4-10 shows the concentration of NO, NO$_2$ and NO$_x$ for the natural gas test with the mass of NO$_x$ related to the power produced by the micro-gas turbine. These results assume a constant exit flow rate of 0.5m^3/s at all loads. NO, NO$_2$ and NO$_x$ are all reported in terms of the equivalent weight of NO$_2$, as NO and NO$_2$ have different molecular mass and are difficult to directly compare. Figure 4-8 shows mass concentration of NO, NO$_2$ and NO$_x$ related to the power produced by the micro-gas turbine. The results for both tests at idle are omitted as no useful power is being generated at idle. Figure 4-11 shows an initial drop in NO$_x$ mass

concentration for natural gas followed by an almost constant level of NO_x until 60kW. After 60kW there is another jump in NO_x mass concentration followed by a constant level until full power is reached. For the propane test a similar trend to the previous figures is remarked, with the concentration of NO_x decreasing with increasing power.

Figure 4-12 shows the results for NO_x concentration versus time for the second natural gas combustion test. As seen in Figure 4-8 the concentration of NO_x increases with increasing power for the single stage combustion type MGT.

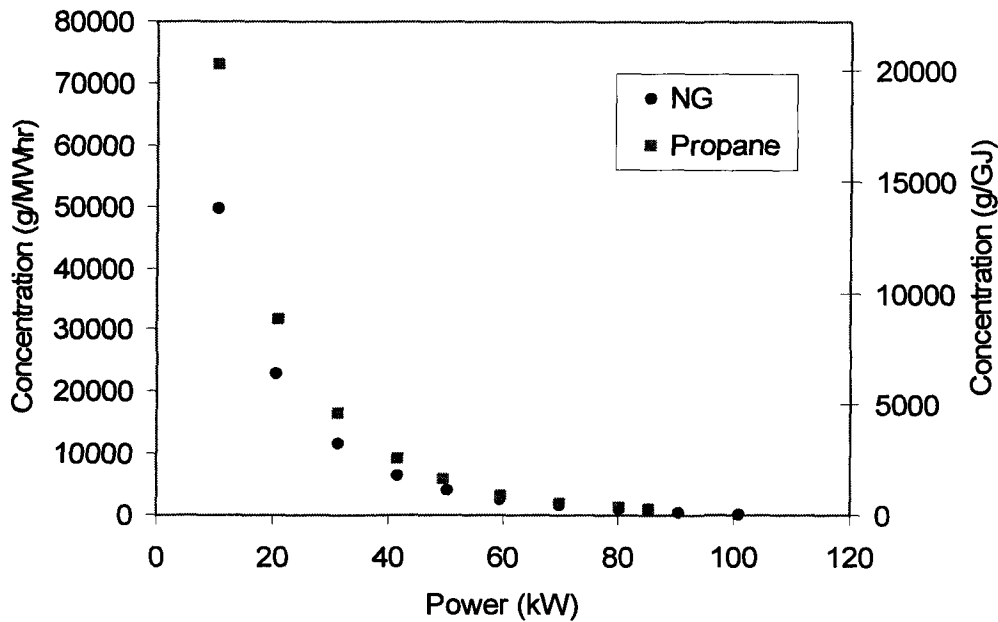**Figure 4-8:** NO, NO_2 and NOx concentration versus load for single stage combustion type micro-gas turbine for natural gas combustion
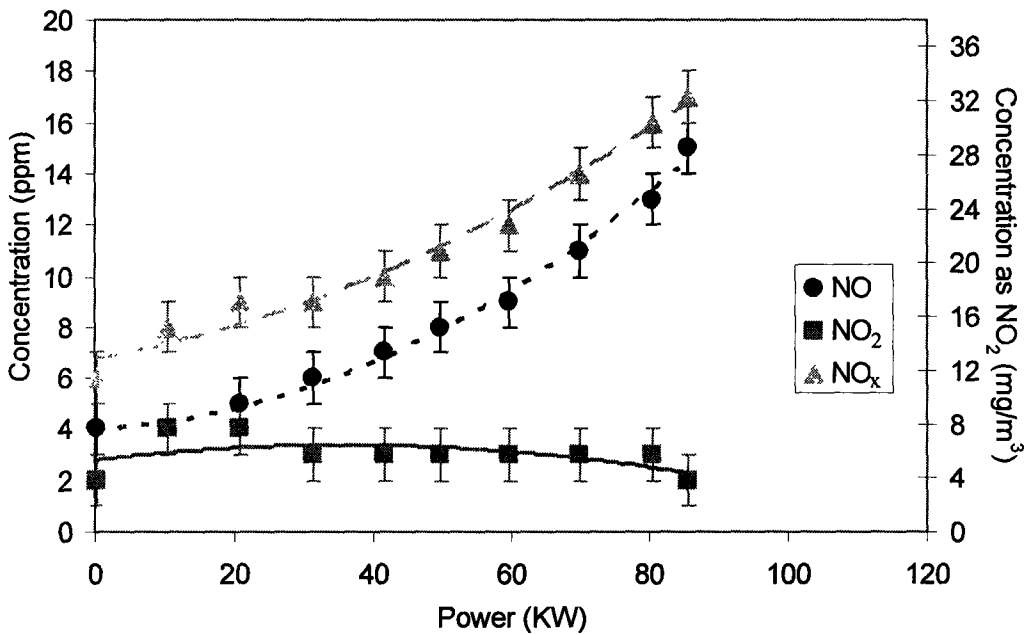
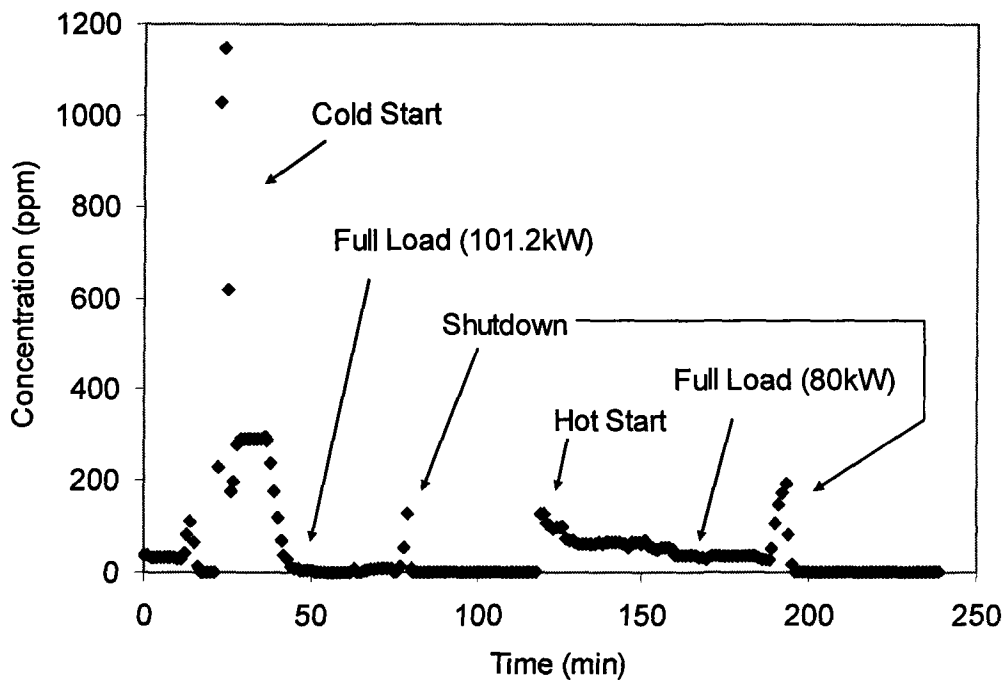**Figure 4-9:** NO, NO_2 and NO_x concentration versus load for single stage combustion type micro-gas turbine for propane combustion
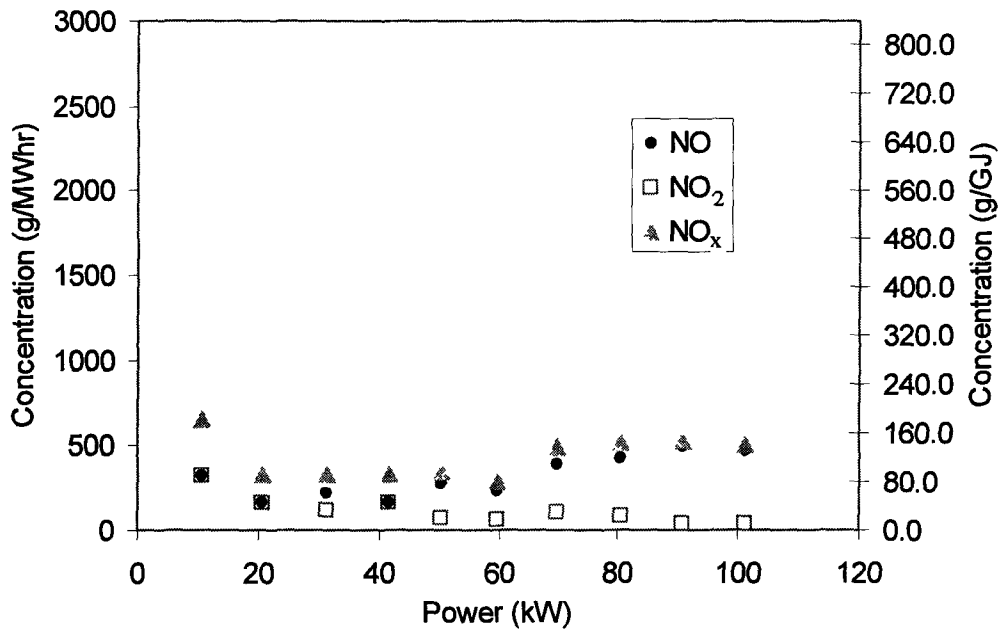
Figure 4-10: NO, NO_2 and NO_x mass concentration versus load for single stage combustion type micro-gas turbine natural gas combustion
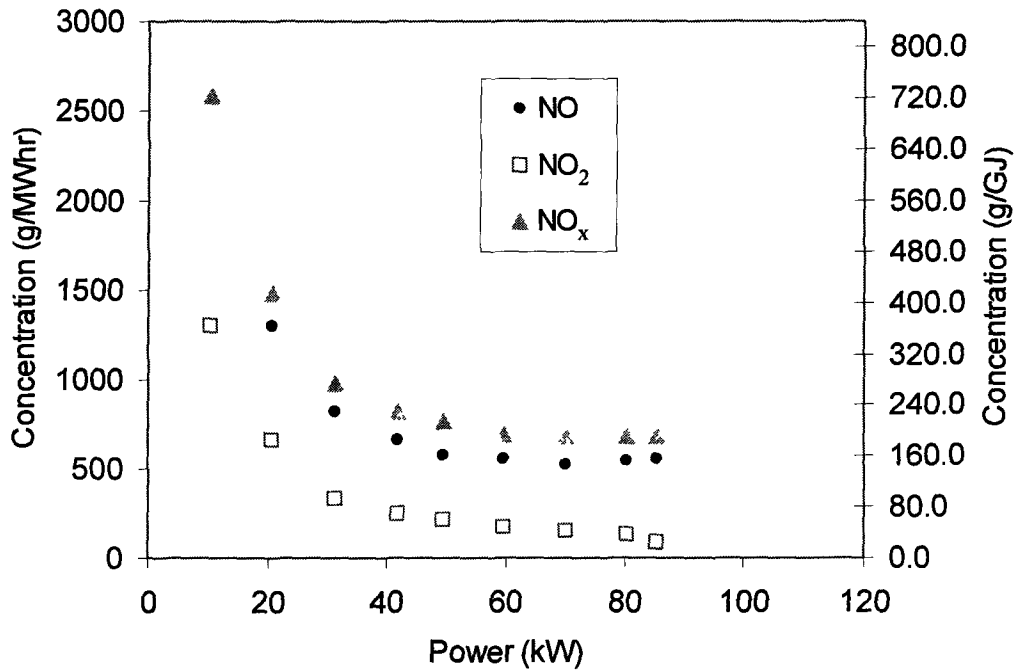
Figure 4-11: NO, NO_2 and NO_x mass concentration versus load for single stage combustion type micro-gas turbine for propane combustion
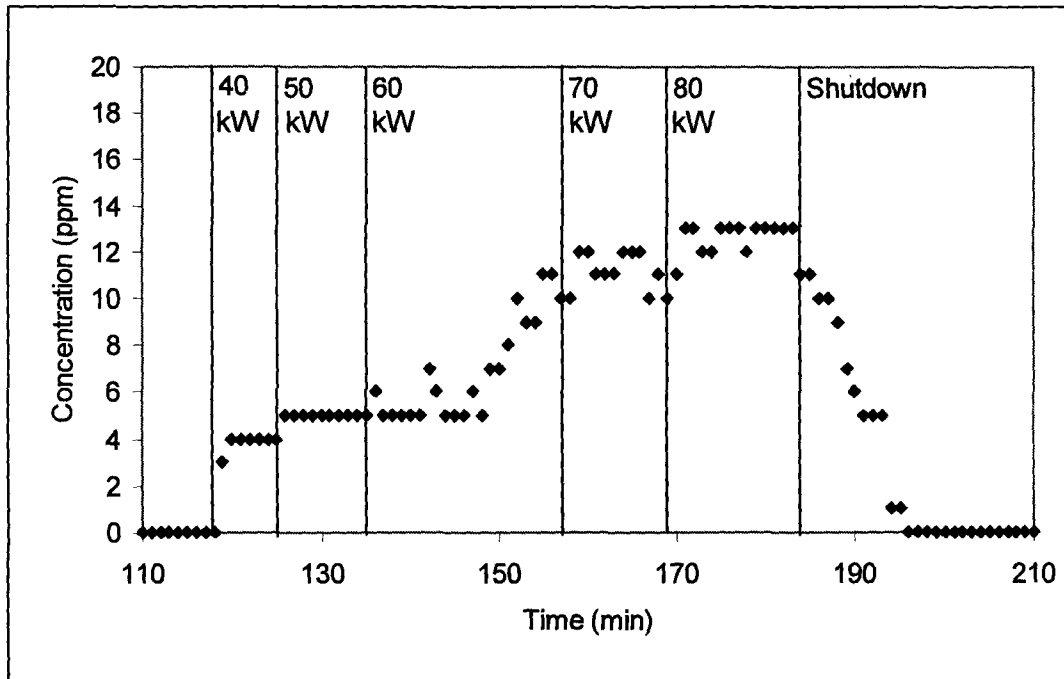
Figure 4-12: NO_x concentration versus time for the second natural gas combustion test

4.1.5 Particulate Matter (PM)

Figure 4-13 shows the mass concentration of particulate matter for both the propane and natural gas tests. For the propane case particulate matter augments with increasing load on the micro-gas turbine. For the natural gas test the opposite seems to be true, the particulate matter measured by mass goes down with increasing load. By mass, it can be observed that natural gas exhaust from the micro-gas turbine contains between 25-50% less particulate matter than propane exhaust. This may be due to partial incomplete combustion of the propane causing a small amount of soot to form. As well the mass concentration is not indicative of the number of particles released in the emissions. It is therefore possible that the natural gas exhaust contains as many particles as the propane exhaust, however the particles may simply be smaller. The number

density of the natural gas was measured, however it was not recorded for the propane case, so no direct conclusion can be made.

The mass concentration and the number concentration of the PM from the natural gas test are shown in Figure 4-14. As expected, the particle mass concentration for natural gas combustion is highest at start up and decreases with increasing load. The propane combustion test shows that propane generates a higher number of particles than methane due to the higher C_{x-} combustions. The particle mass concentration was is still much lower, two to three orders of magnitude lower when compared to with a diesel power generator ($10\text{-}10^3 \text{mg/m}^3$). The order of magnitude of particle concentration is 10^8 to 10^9 [pt/m^3] for natural gas combustion.

Particulate samples were also collected through the use of a filter paper media. The resulting particulate matter size distribution for particles larger than 1 micron as measured by ESEM is shown in Figure 4-15. As shown in Figure 4-15 the majority of the particles for both natural gas and propane lie between 1 to 7 μm. There are also a number of particles that were recorded to be larger than 20 microns. ESEM imaging also shows that the shape of the particles is roughly spherical. This bimodal particle size distribution most likely represents that ash content of the particulate matter or is due to agglomeration of smaller soot particles from the micro-gas turbine. Since natural gas consists of more than 95% methane, the micron-sized particles are concentrated in the 2 to 6μm range and the propane particles show a large number above 20μm due to the longer carbon chain of propane.

4.1.6 Ozone and Aldehydes

Ozone and aldehydes were also measured at steady state, but were observed to be below the detection limit of the instrument, 0.025ppm and 4ppm, respectively.
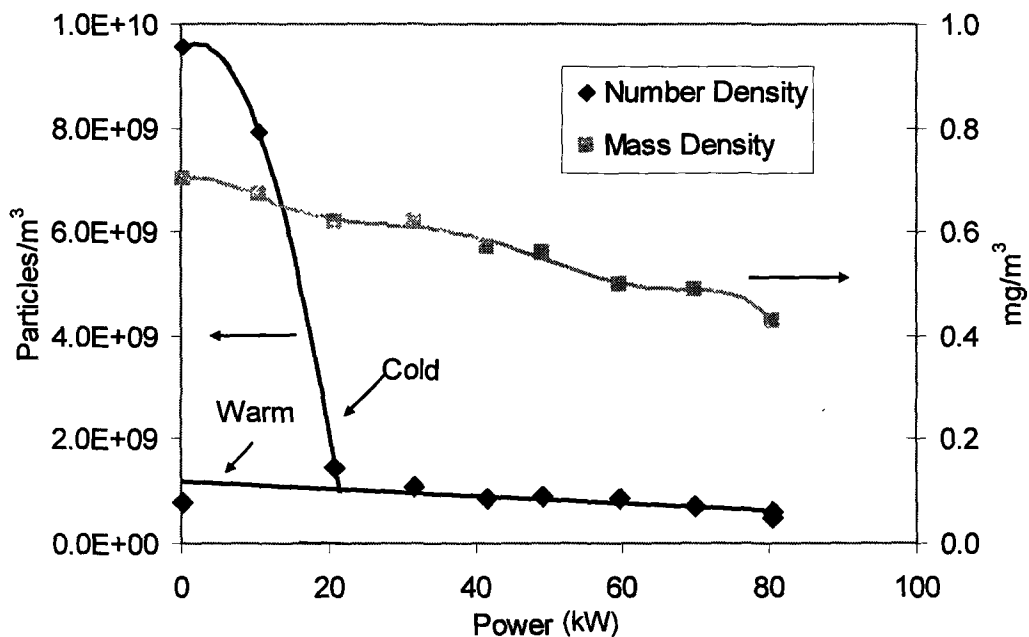
Figure 4-13: PM mass concentration versus load for the single stage combustion type micro-gas turbine for natural gas and propane combustion
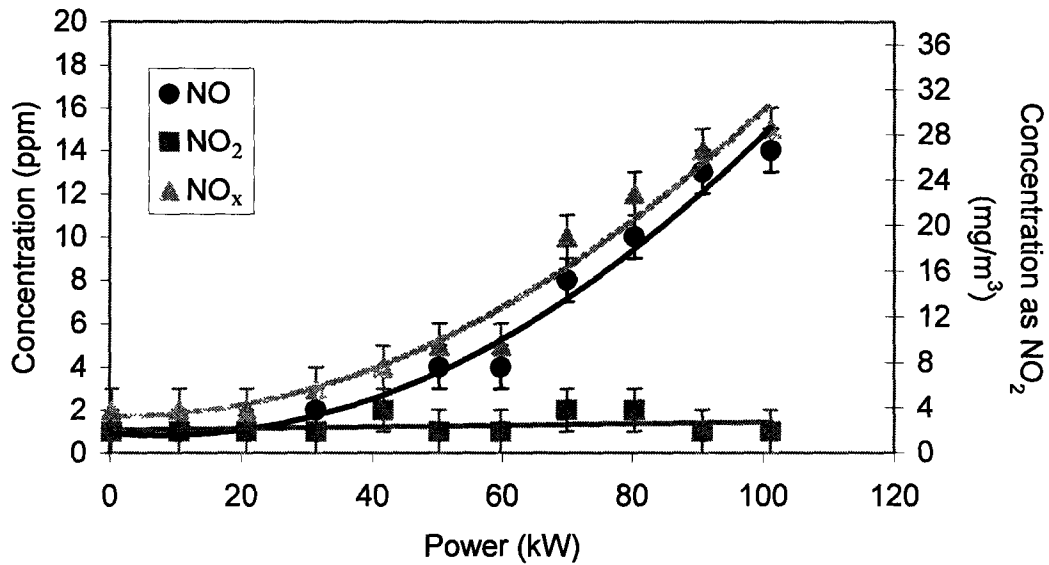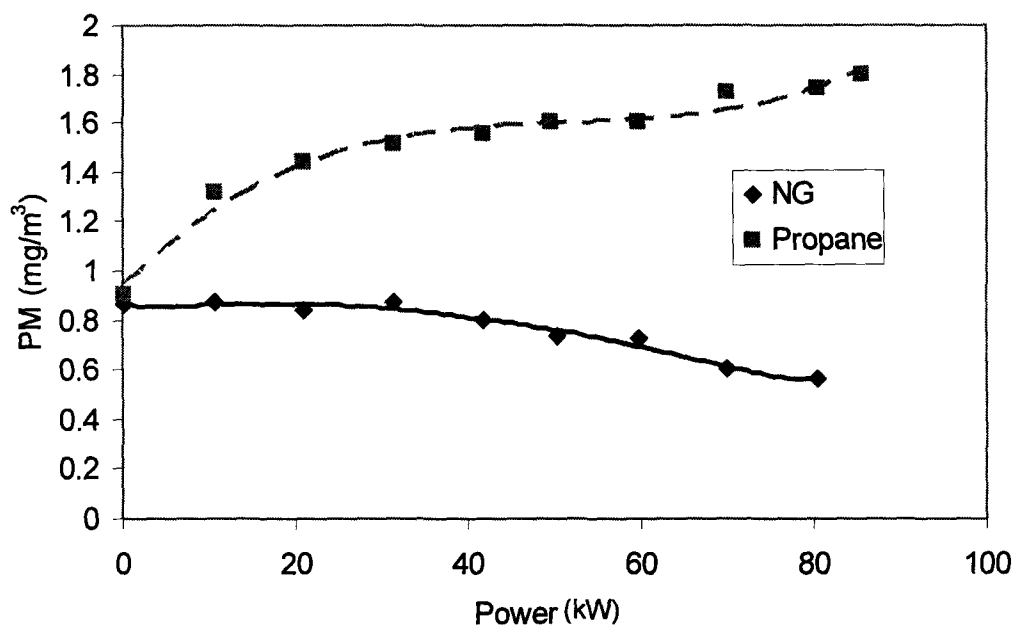
Figure 4-14: PM mass concentration and number concentration versus load for single stage combustion type micro-gas turbine for natural gas combustion
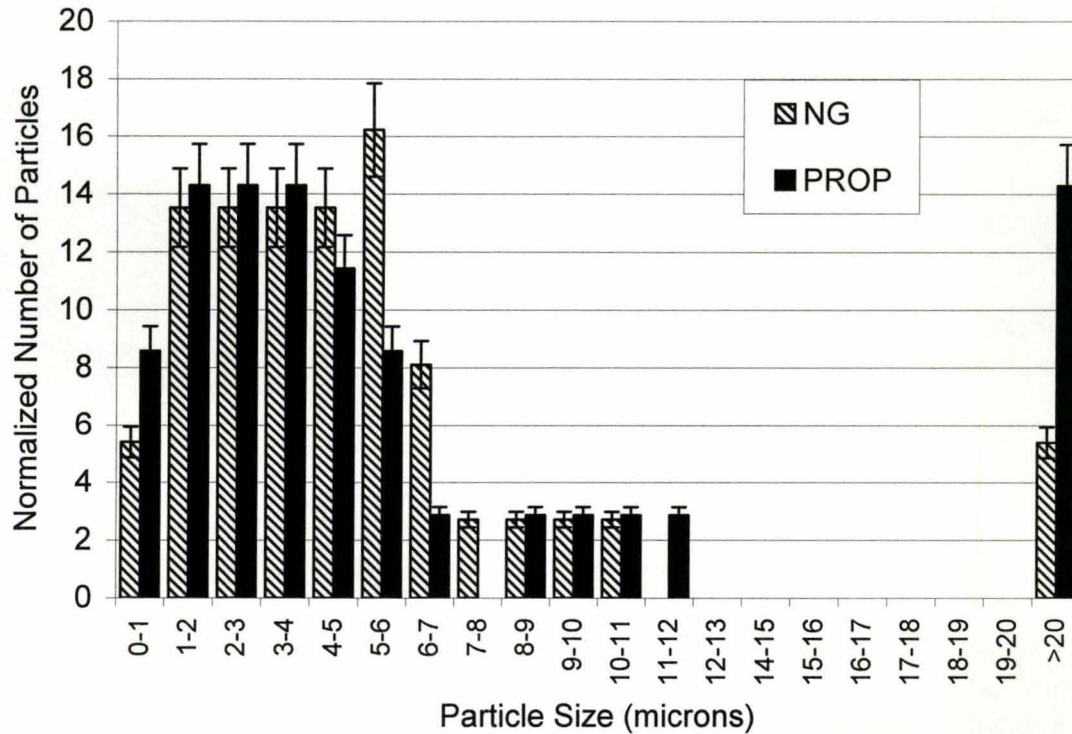
**Figure 4-15**: PM number density from ESEM analysis for the single stage combustion type micro-gas turbine for natural gas and propane combustion for micron range particles

4.1.7 Fournier Transformed Infrared (FTIR)Trace By-Product Analysis

The gas samples collected at 0kW, 60kW and 80kW for natural gas test, as well as the gas samples collected at 60kW and 80kW for the propane test were analyzed by FTIR. The overall FTIR spectra for 0kW, 60kW and 80kW natural gas test are presented in Figures 4-12, 4-14 and 4-16, respectively. At all three loads, the full spectras reveals both water and CO_2 present in the samples. Water is seen at wave numbers between 3630-3855cm^{-1} and between 1600-1540cm^{-1}. CO_2 is noted at wave numbers between 2340-2360cm^{-1} and at 668cm^{-1}. The detailed spectra for the 0kW, 60kW and 80kW natural gas tests are presented in Figures 4-

80

13, 4-15 and 4-17, respectively. For the 0kW case in Figure 4-13, a large amount of hydrocarbons can be seen between wave numbers of $3100cm^{-1}$ and $2115\ cm^{-1}$. These peaks most likely correspond to CH_4, C_2H_4 or C_2H_6, as well what is likely C_2H_4 can be seen around $889\ cm^{-1}$. Furthermore, C_3H_8 can be noted at $2826cm^{-1}$ and $1172cm^{-1}$. Carbon monoxide is also shown, with peaks at $2168cm^{-1}$ and $2109cm^{-1}$. The greenhouse gas and NO_x compound N_2O is evident with a peak at $1194cm^{-1}$.

The 60kW and 80kW analyses have similar results. Both results reveal N_2O peaks at between $2528cm^{-1}$ and $2542cm^{-1}$. However, the 80kW test also shows N_2O at a wave number of $1188\ cm^{-1}$ and NO at $1315\ cm^{-1}$. Both tests show evidence of C_2H_2 at a peak of approximately $731cm^{-1}$ and show C_2H_4 at a peak of about $1011cm^{-1}$ to $1014cm^{-1}$. However the 60kW spectra shows CH_4 at $1270cm^{-1}$ and C_3H_8 at $1068cm^{-1}$, unlike the 80kW case.

Figures 4-18 and 4-20 show the overall FTIR spectra for the 60kW and 80kW propane test, respectively. The results are the same as natural gas with water at wave numbers between $3630-3855cm^{-1}$ and $1600-1540cm^{-1}$. CO_2 is noted at wave numbers between $2340-2360cm^{-1}$ and at $668cm^{-1}$. Figures 4-19 and 4-21 show the detailed FTIR spectra for the 60kW and 80kW propane test, respectively. Both cases show compounds that probably correspond to CH_4, C_2H_4 or C_2H_6 between $2849cm^{-1}$ and $3100cm^{-1}$. Both spectra reveal C_2H_4 with peaks at $1014cm^{-1}$, $925cm^{-1}$ and $895cm^{-1}$. The 60kW case showed N_2O with peaks at $2542cm^{-1}$ and $1188cm^{-1}$, whereas the 80kW case showed N_2O with a peak at $564cm^{-1}$.

The results for both natural gas and propane show that the hydrocarbon emissions for both tests were primarily CH_4, C_2H_2, C_2H_4 and C_2H_6. These hydrocarbons probably represent the observed VOC emissions. As well most cases showed the presence of N_2O a greenhouse gas.

Figure 4-16: The overall FTIR absorption spectra for emissions gas sampled from the single stage combustion type turbine at 0 kW for natural gas

Figure 4-17: The detailed FTIR absorption spectra for emissions gas sampled from the single stage combustion type turbine at 0 kW for natural gas

Figure 4-18: The overall FTIR absorption spectra for emissions gas sampled from the single stage combustion type turbine at 60 kW for natural gas
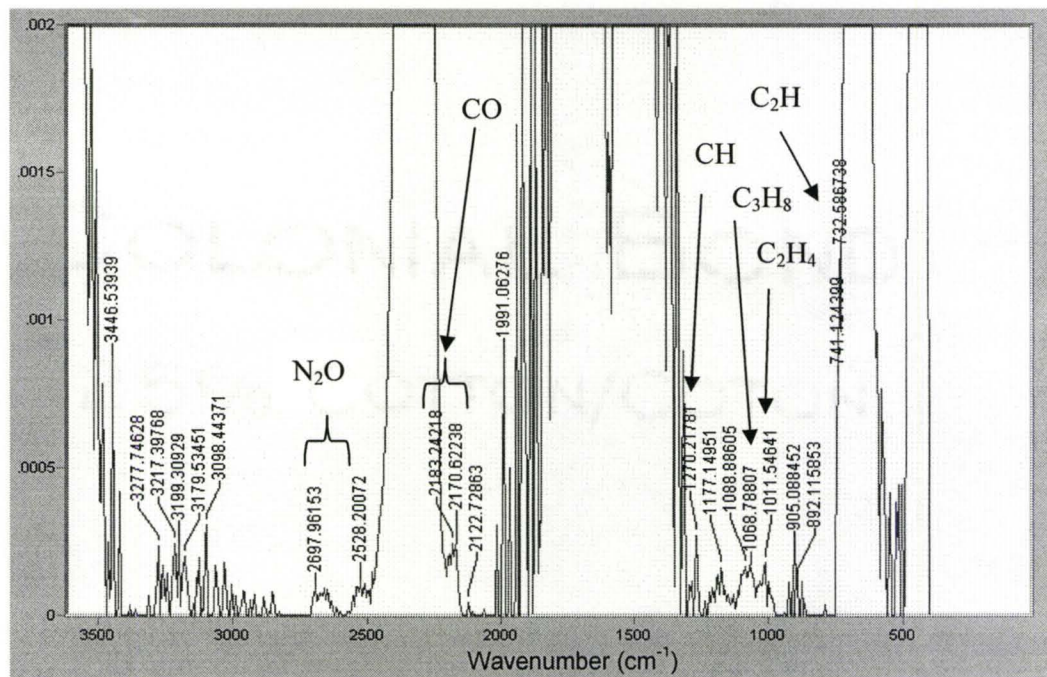
Figure 4-19: The detailed FTIR absorption spectra for emissions gas sampled from the single stage combustion type turbine at 60 kW for natural gas
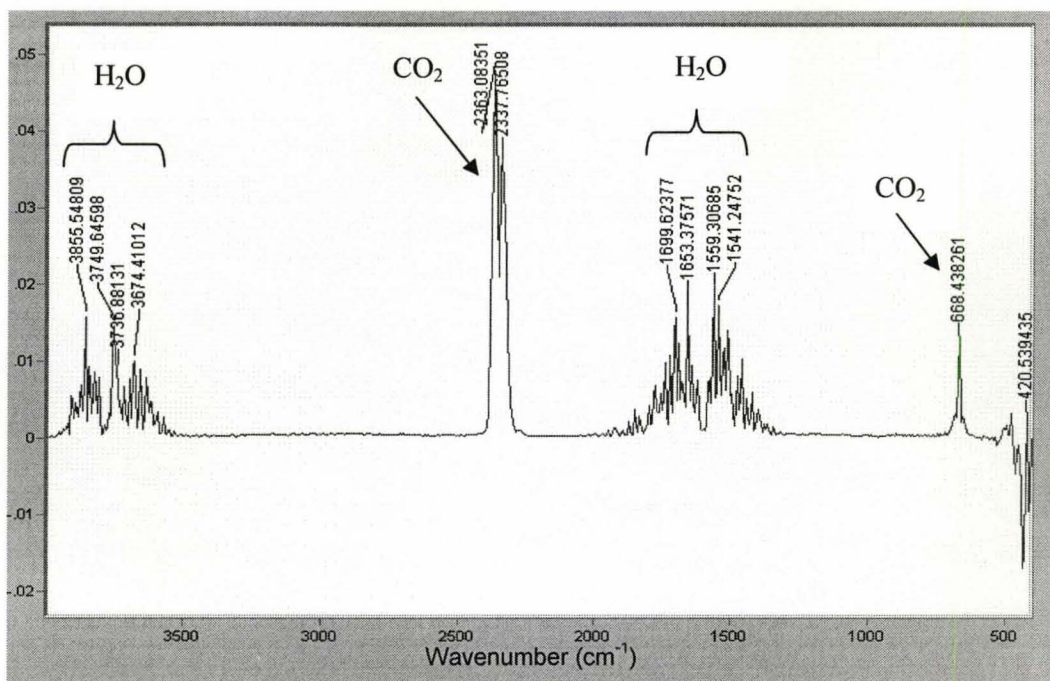
Figure 4-20: The overall FTIR absorption spectra for emissions gas sampled from the single stage combustion type turbine at 80 kW for natural gas
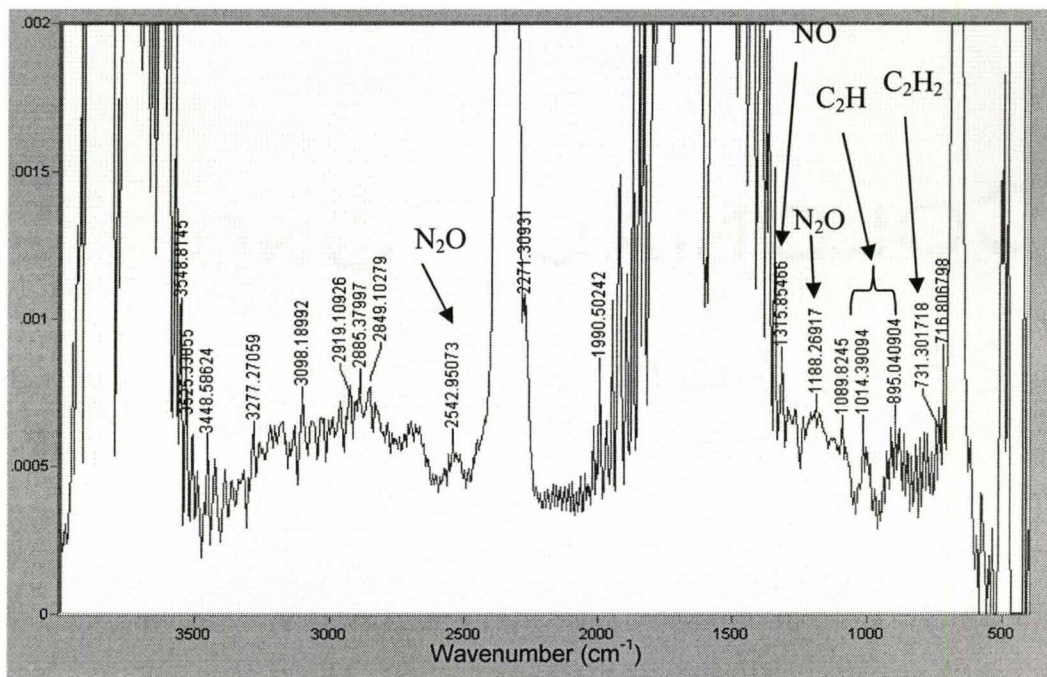
Figure 4-21: The detailed FTIR absorption spectra for emissions gas sampled from the single stage combustion type turbine at 80 kW for natural gas
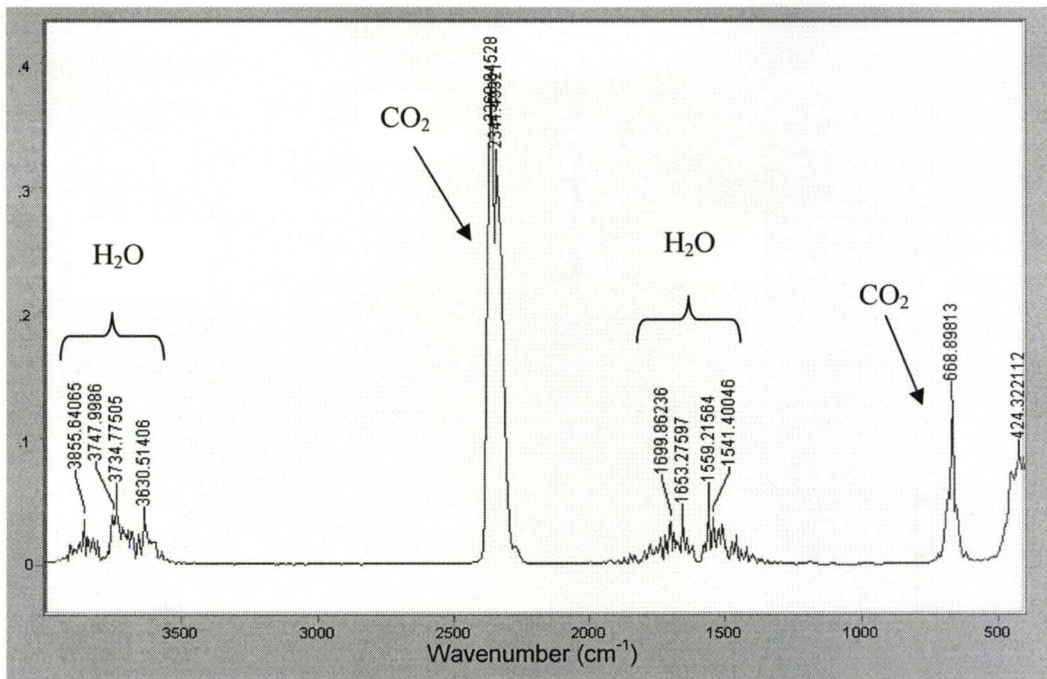
Figure 4-22: The overall FTIR absorption spectra for emissions gas sampled from the single stage combustion type turbine at 0 kW for propane
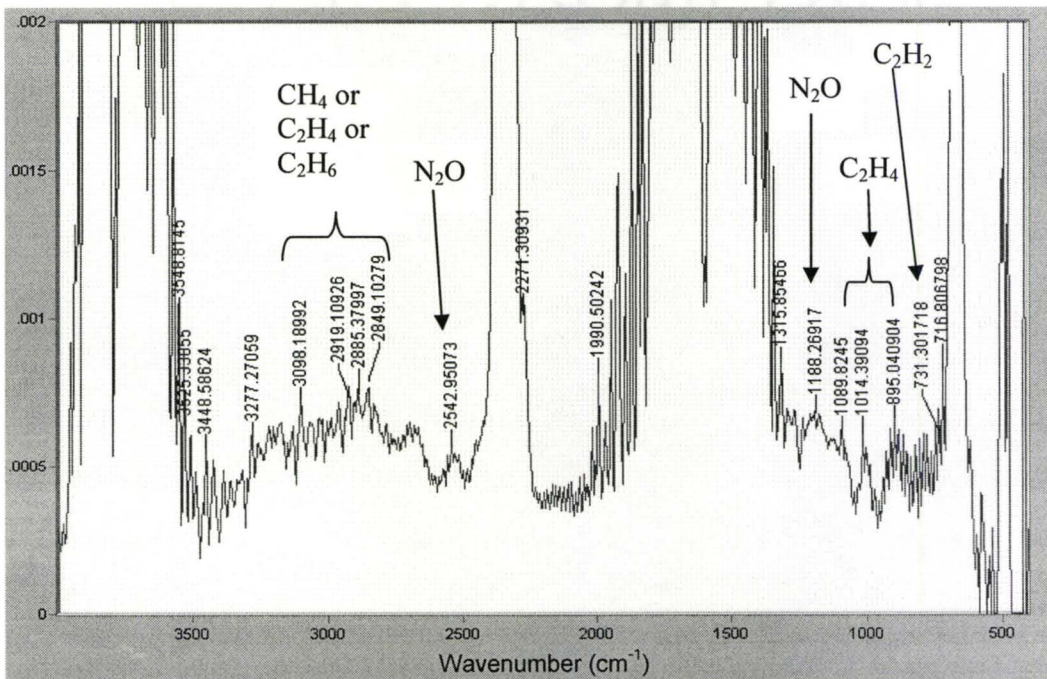
Figure 4-23: The detailed FTIR absorption spectra for emissions gas sampled from the single stage combustion type turbine at 0 kW for propane
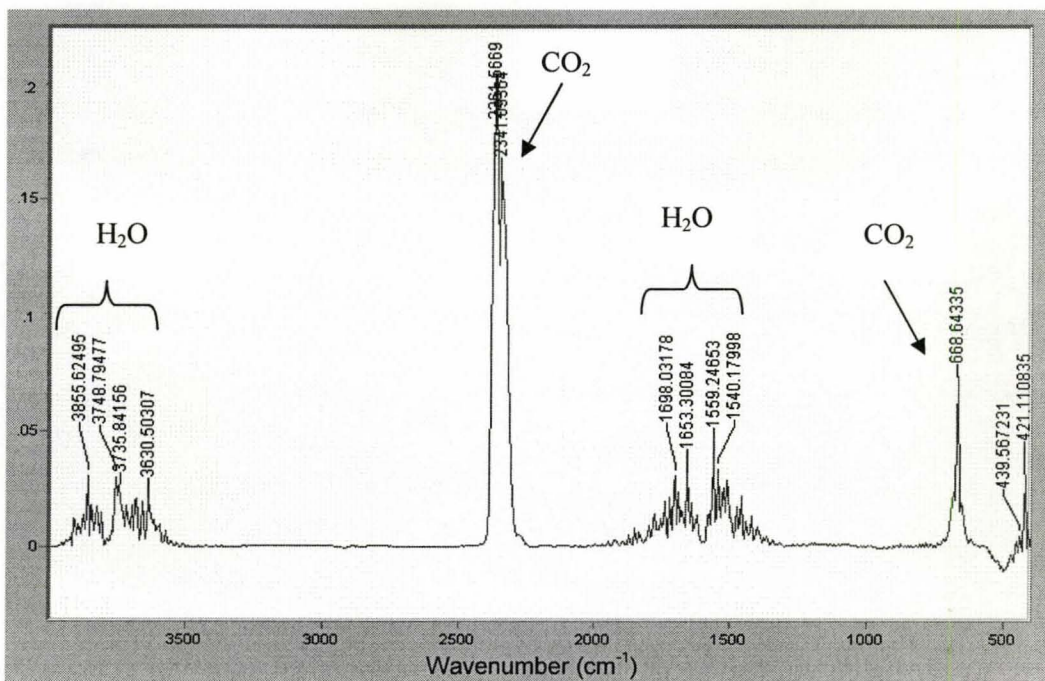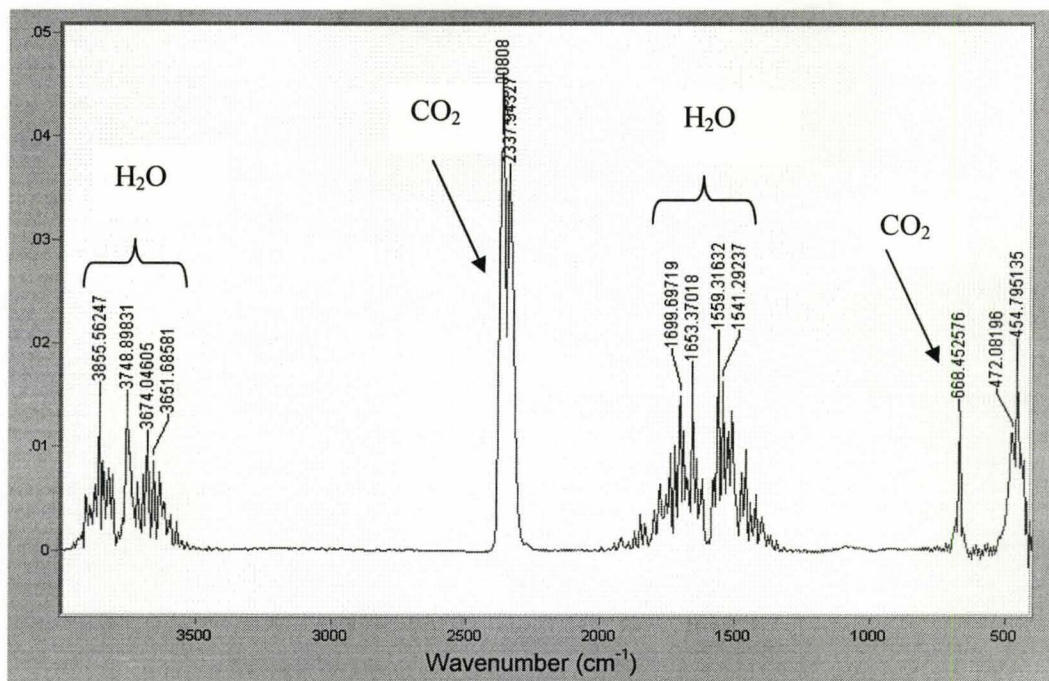
Figure 4-24: The overall FTIR absorption spectra for emissions gas sampled from the single stage combustion type turbine at 60 kW for propane
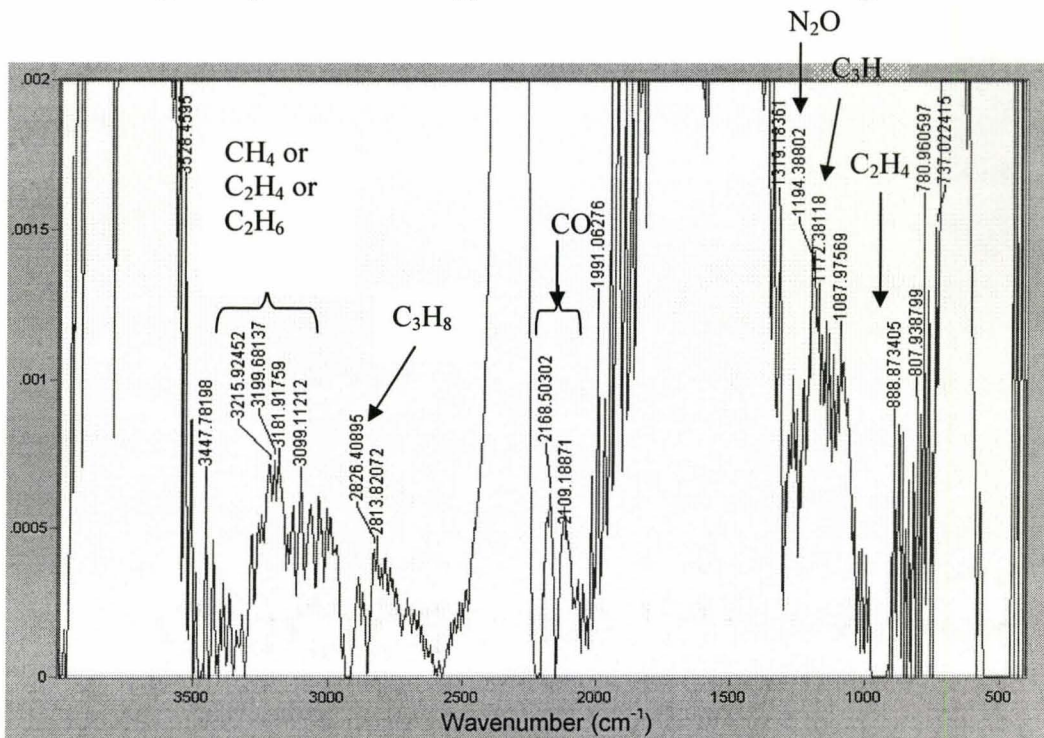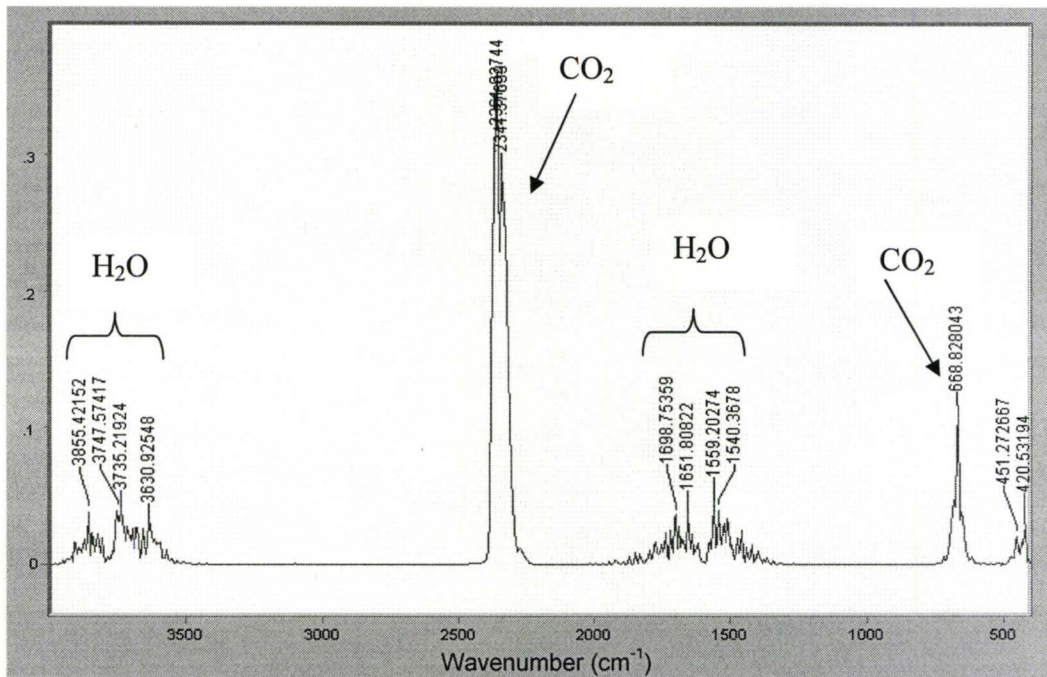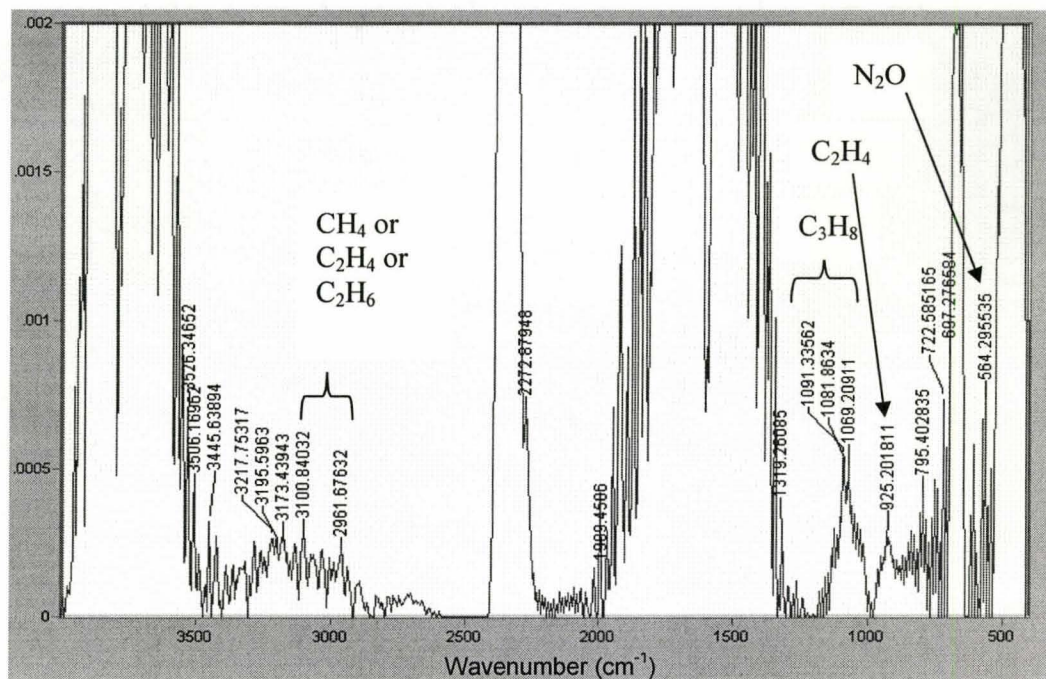
Figure 4-25: The detailed FTIR absorption spectra for emissions gas sampled from the single stage combustion type turbine at 60 kW for propane

4.2 Dual Stage Combustion Type Micro-Gas Turbine Emission Characteristics

Experiments were conducted to characterize the flue gas emissions of a 70kW dual stage combustion type micro-gas turbine. This dual stage combustion type micro-gas turbine cannot operate at varied loads and as a result testing focused primarily on cold start up, warm start up and full load (70kW) emission characteristics. As seen in Table 4-1 the dual stage combustion type MGT operates on a leaner basis than the single stage combustion type MGT.

4.2.1 Emission Characteristics from Cold Start to Steady State

The emission characteristics for the cold start up of the dual stage combustion type micro-gas turbine are presented in Figure 4-26. It should be noted that during the initial start the two combustion stages were observed. The first combustion stage lasted for only approximately 30 seconds and had higher emissions than the second combustion stage. Only the maximum emission values were recorded during the first stage of combustion. The second combustion stage is presented in Figure 4-26. Figure 4-26(a) shows the oxygen and carbon dioxide concentrations versus time for cold start up. The oxygen level increases with time during the cold start up. The oxygen levels are initially at 17.0% and increase to 18.9% after approximately ten minutes when steady state is reached. The CO_2 levels decrease with increasing time as expected. The CO_2 levels ranged from 2.6% at the initial start up to 1.3% at steady state.

Figure 4-26(b) shows the emission changes in CO, NO, NO_2 and NO_x for cold start conditions. It is apparent that the majority of the changes in emissions occur in the first ten to thirty minutes, with emissions decreasing dramatically. The CO concentration was initially 4ppm and
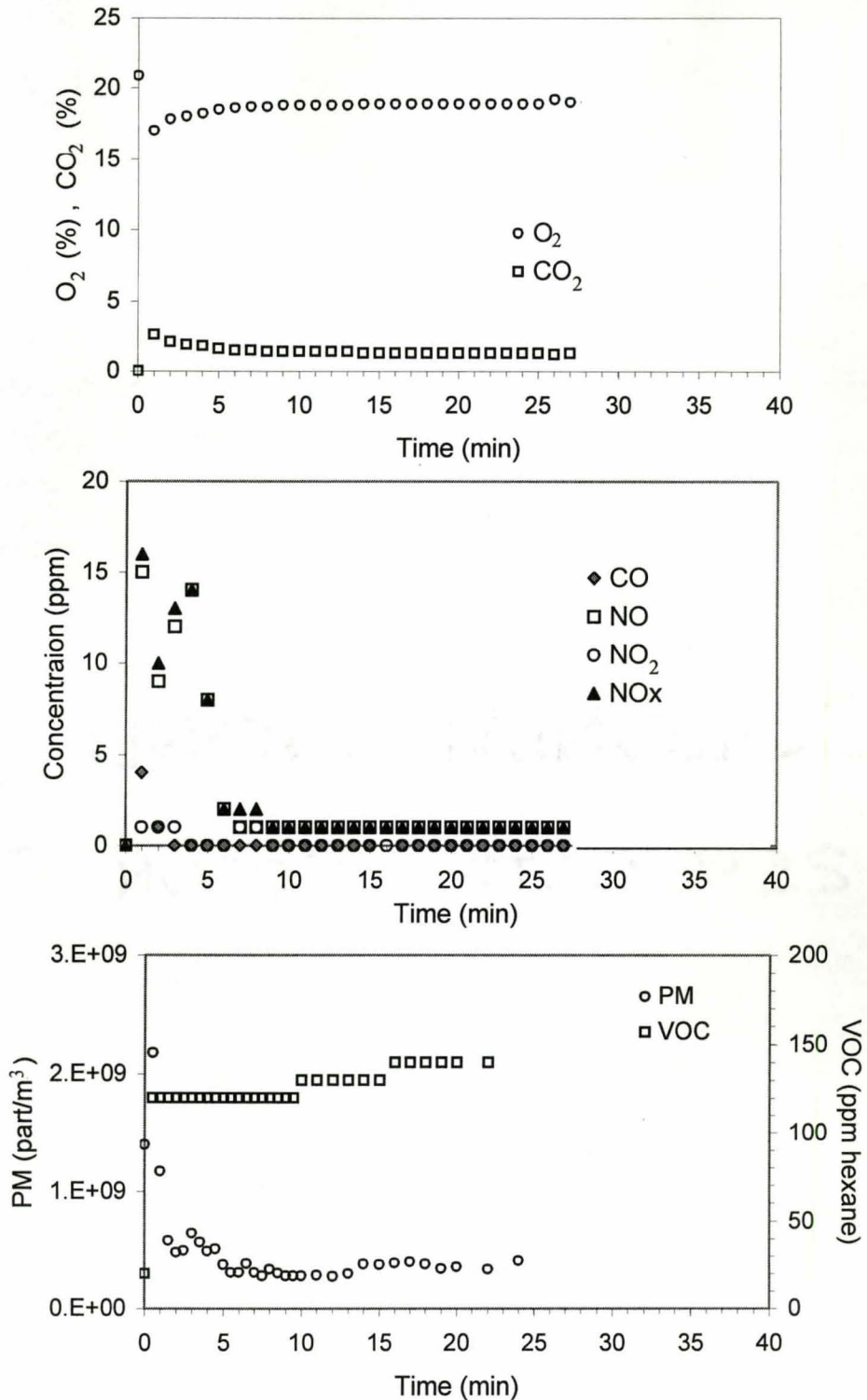
Figure 4-26: Change in the emissions of (a) O_2 and CO_2 (b) CO, NO, NO_2, and NO_x and (c) PM and VOC from the cold start of the dual stage combustion type 70 kW micro-gas turbine

then after three minutes drop to 0ppm or below the detection limit of the instrument. NO_2 was also observed to be very small, starting at 2ppm and then dropping to 1ppm at steady state. The NO accounted for most of the NO_x and was initially high at 15ppm, then decreasing to 2ppm after about six minutes.

The concentration of VOCs and the particulate matter concentration are presented in Figure 4-26(c). The VOC concentration is seen to increase with increasing time until steady state is reached. The VOC concentration ranges from 120ppm to 140ppm at steady state. The particulate concentration is initially high and then decreases with time. This is expected as until the micro-gas turbine is at steady state there is most likely some incomplete combustion producing particulate matter, as can also be observed from the VOC concentrations.

4.2.2 Comparison of Cold Start, Warm Start and Steady State Emissions Characteristics

A comparison of the warm start and cold start emission results for a second test of the dual stage combustion type micro-gas turbine are shown in Figure 4-27. Figure 4-27(a) shows the oxygen and carbon dioxide concentrations versus time for cold start and warm start. For the warm start case the emissions of both the carbon dioxide and oxygen leveled off quickly to steady state concentrations of 1.3% and 18.9%, respectively. The cold start case, as seen previously, took about five minutes to reach steady state concentrations. The concentration of NO and CO for cold start and warm start tests are presented in Figure 4-27(b). A similar trend for NO is observed, as the warm start emissions are initially lower than the cold start and drop very quickly from 6ppm to 1ppm. The CO concentration for the warm start is almost not observed at 0-1ppm. The cold start up had a CO concentration of 4ppm decreasing to 0ppm at

three minutes. Ozone and aldehydes were also measured at steady state, but were observed to be below the detection limit of the instrument, 0.025ppm and 4ppm, respectively.

A summary of the emissions at cold start up, warm start up and steady state are presented in Table 4-1. The emissions were also converted to mass concentrations with respect to useful power produced by the micro-turbine. The conversion was done by using the measured flow velocity and calculating the flow rate of the exhaust. The flow rate was found to be $0.5m^3/s$, which agreed well with the mass flow of 0.7kg/s given by the micro-gas turbines specifications. As can be observed in Table 4-1 the maximum concentration of CO of 25ppm during cold start was significantly higher then at warm start up of 15ppm. The particulate matter was an order of magnitude higher during cold start up then at steady state operation.

4.2.3 Particulate Matter Emissions

A particle size distribution was measured for the steady state operation of the micro-gas turbine and is shown in Figure 4-28. Figure 4-29 shows the normalized particulate versus the relative size of the particles. From Figure 4-28 it can be seen that the size distribution is bimodal and that there is a significant portion of particles smaller than 29nm. As well, Figure 4-29 shows that the mean diameter can be observed to be on the order of 35nm.
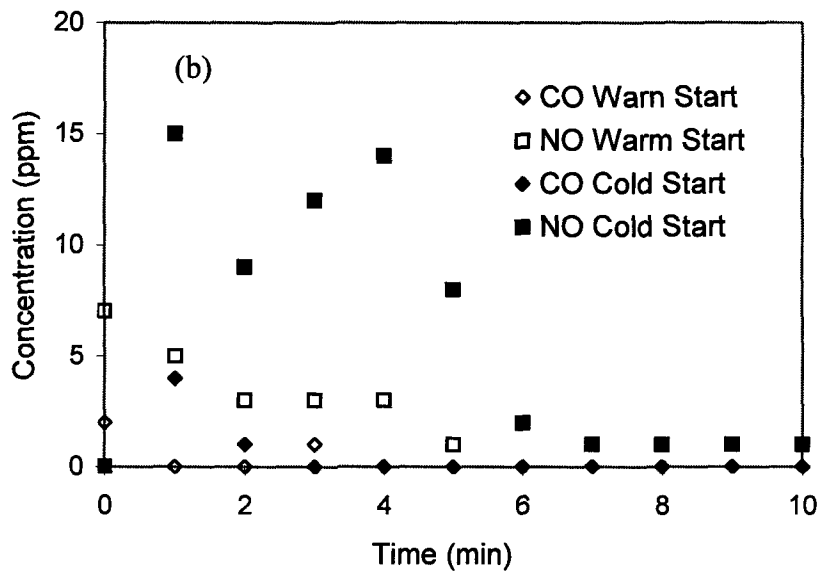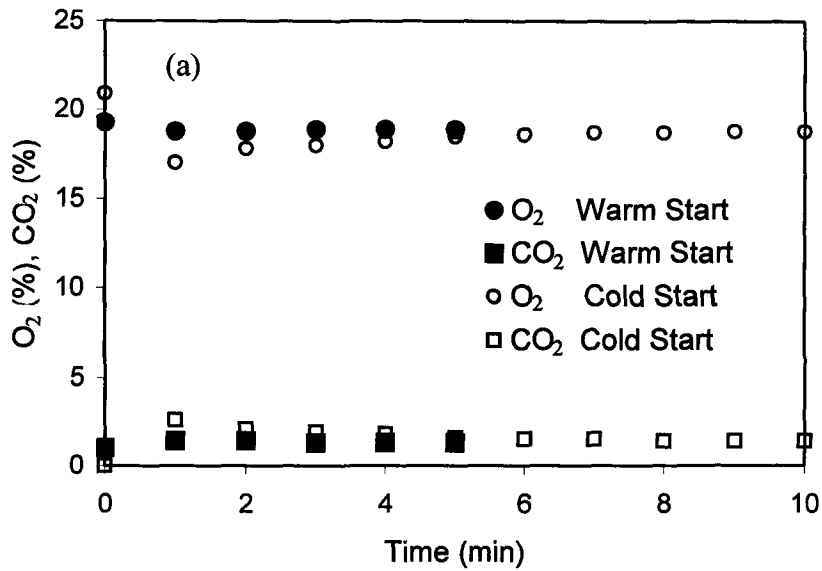
Figure 4-27: Comparison of the change in the emissions of (a) O_2 and CO_2 and (b) CO, NO, NO_2, and NO_x and during the first 10 minutes from the warm start and the cold start of the dual stage combustion type micro-gas turbine.

Table 4-1: Summary of the   dual stage combustion type micro-gas turbine emissions

Emission		Max (Min) Cold Start	Max (Min) Warm Start	Range at Full Power	Estimate Start up g/MWh	Estimate Full Power g/MWh
O_2	%	(17)	(18.8)	18.9-19.2		
CO_2	%	2.6	1.4	1.1-1.4		
NO	ppm	15	9	1-2	40-500	40-70
NO_2	ppm	1	1	0-1	0-60	0-60
CO	ppm	25	15	0-1	0-800	0-30
SO_2	ppm	1	1	0-1	0-40	0-40
PM	part/m^3	2.5×10^9	-	$1\text{-}5 \times 10^8$		
VOC	ppm	200	150	80-140	400-10000	400-7000
O_3	ppm	-	-	<0.025		
Aldehydes	ppm	-	-	<4		
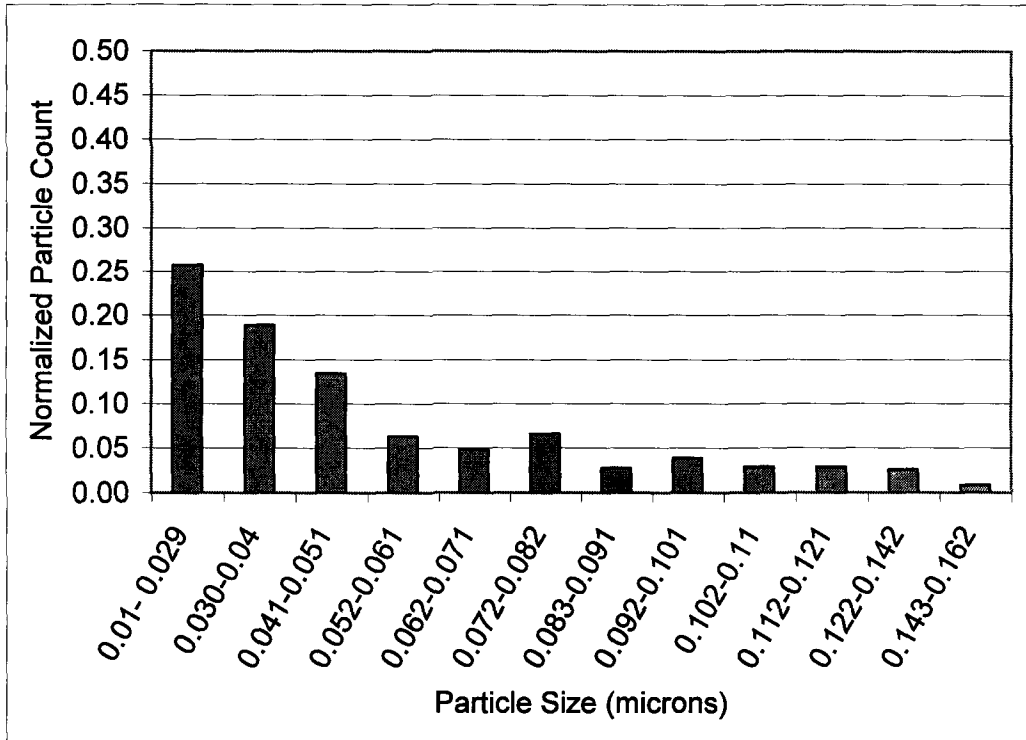
Figure 4-28: Particle size distribution for dual stage combustion type micro-gas turbine at full load for nanometer range particles
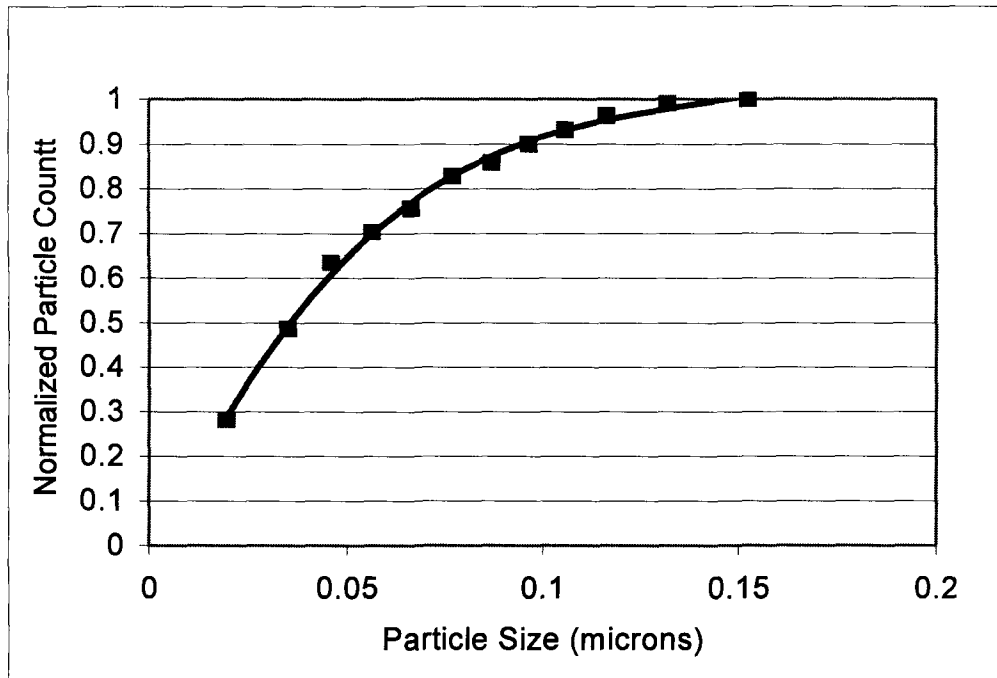
Figure 4-29: Particle number versus size for dual stage combustion type micro-gas turbine at full load for nanometer range particles

4.2.4 FTIR Trace By-Product Analysis for Cold Start , Warm Start and Steady State

Figure 4-30 show the overall FTIR spectra for the cold start up of the micro-gas turbine. As expected the full spectra reveals both water and CO_2 present in the samples. Water is seen at wave numbers between 3630-3855cm^{-1} and between 1450-1720cm^{-1}. CO_2 is noted at wave numbers between 2340-2360cm^{-1} and at 668cm^{-1}. However, two large peaks are also seen 930cm^{-1} and 966cm^{-1}. These peaks seem to correspond very well to ammonia (NH_3), mostly likely from the conversion of hydrocarbons with nitrogen present in the exhaust, which has been noted by Kilpinen et al [65] in a modeling study of CH_4 reburning. The detailed FTIR spectra are presented in Figure 4-31. The detailed spectra reveals numerous hydrocarbons present during cold start. At 2963cm^{-1} C_2H_4 is probably present and at 2899cm^{-1} C_2H_6 is also most likely seen. CH_4 can also be observed at a wave number of 2369cm^{-1}, with what is likely C_3H_6 at a peak of 1045cm^{-1}.

Figure 4-32 displays the overall FTIR spectra for the warm start of the micro-gas turbine. As in the case for the cold start water is observed at wave numbers between 1550-3855cm^{-1} and between 1450-1720cm^{-1}. CO_2 is noted at wave numbers between 2340-2360cm^{-1} and at 668cm^{-1}. Furthermore, the same peaks are once again observed at 930cm^{-1} and 966cm^{-1}. Once again these peaks seem to by NH_3. A large peak of C_2H_4 is also seen 2963cm^{-1} as it was in the cold start case. In both cases the formation of methene is most likely due to the incomplete combustion of methane upon initial start up. Figure 4-33 shows the detailed FTIR spectra for the warm start of the micro-gas turbine. This spectra reveals a peak at 1270cm^{-1}, which is probably methane, caused by fuel slip during start up. As in the cold start case C_2H_6 is observed with a peak at 2899cm^{-1}. A peak at 3334cm^{-1} seems to confirm to the potential for NH_3 in the exhaust.

The overall FTIR spectra for steady state operation of the micro-gas turbine is presented in Figure 4-34. Once more water is observed at wave numbers between 1550-3855cm^{-1} and between 1450-1720cm^{-1}. CO_2 is noted at wave numbers of 2363cm^{-1} and 667cm^{-1}. Furthermore smaller peaks are noted at 930cm^{-1} and 964cm^{-1}. The detailed FTIR spectra is for steady state operation is presented in Figure 4-35. The detailed spectra does not reveal any peaks consisted with hydrocarbons as in the warm and cold start cases, suggesting a more efficient combustion at steady state. There is a peak at 518cm^{-1}, which most likely corresponds to SO_2. The SO_2 in this case would be created from a slight impurity in the fuel used.
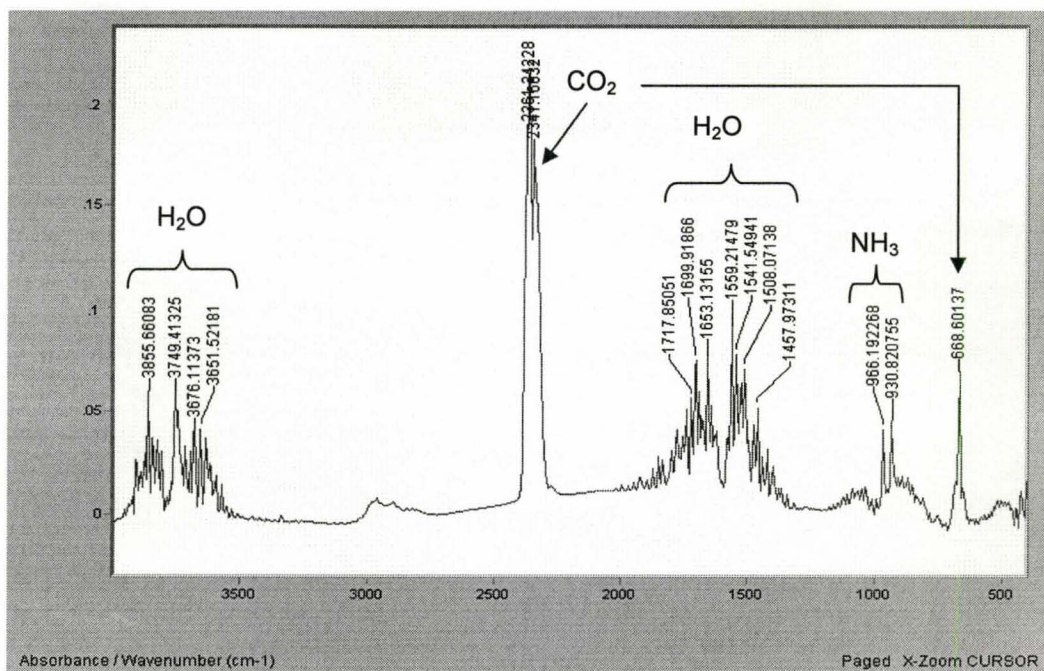
Figure 4-30: The overall FTIR absorption spectra for emissions gas sampled from the dual stage combustion type micro-gas turbine at cold start
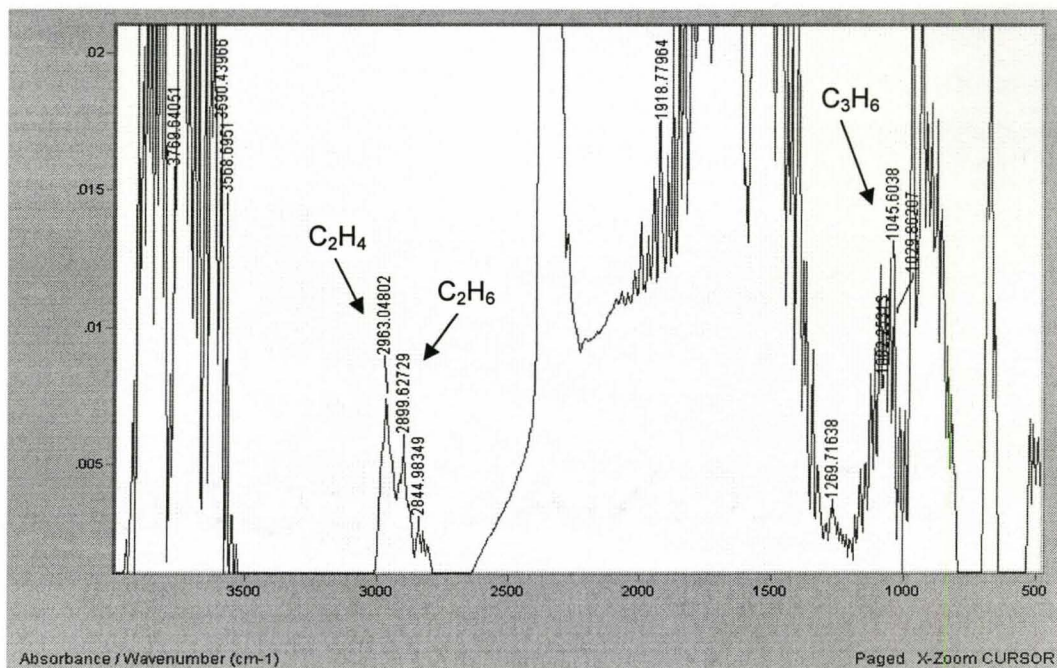
Figure 4-31: The detailed FTIR absorption spectra for emissions gas sampled from the dual stage combustion type micro-gas turbine at cold start
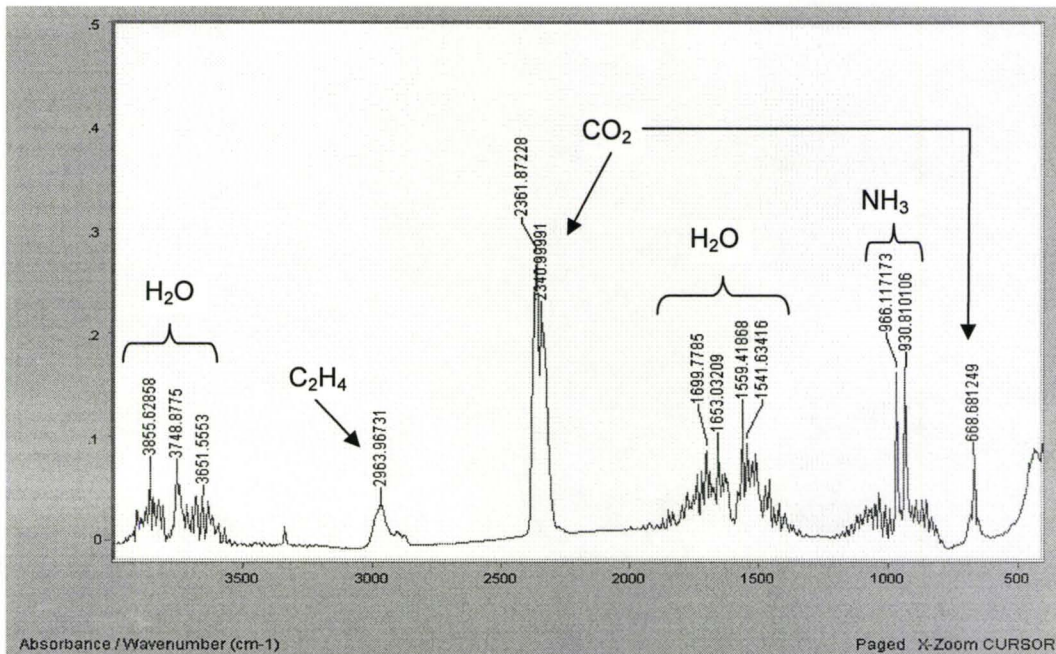
Figure 4-32: The overall FTIR absorption spectra for emissions gas sampled from the dual stage combustion type turbine at warm start
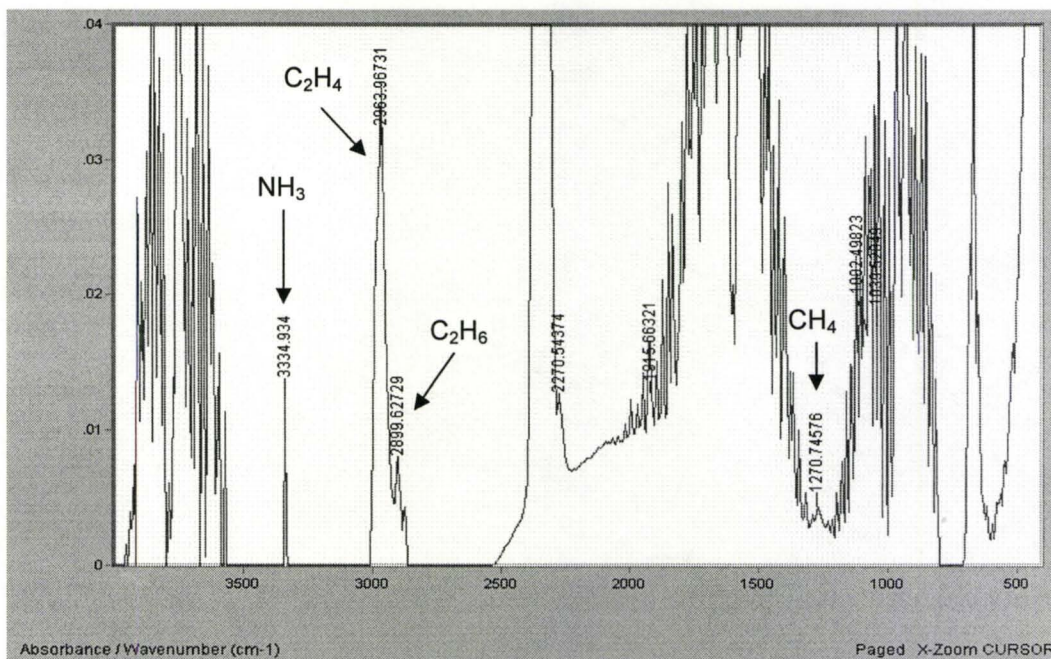
Figure 4-33: The detailed FTIR absorption spectra for emissions gas sampled from the dual stage combustion type turbine at warm start
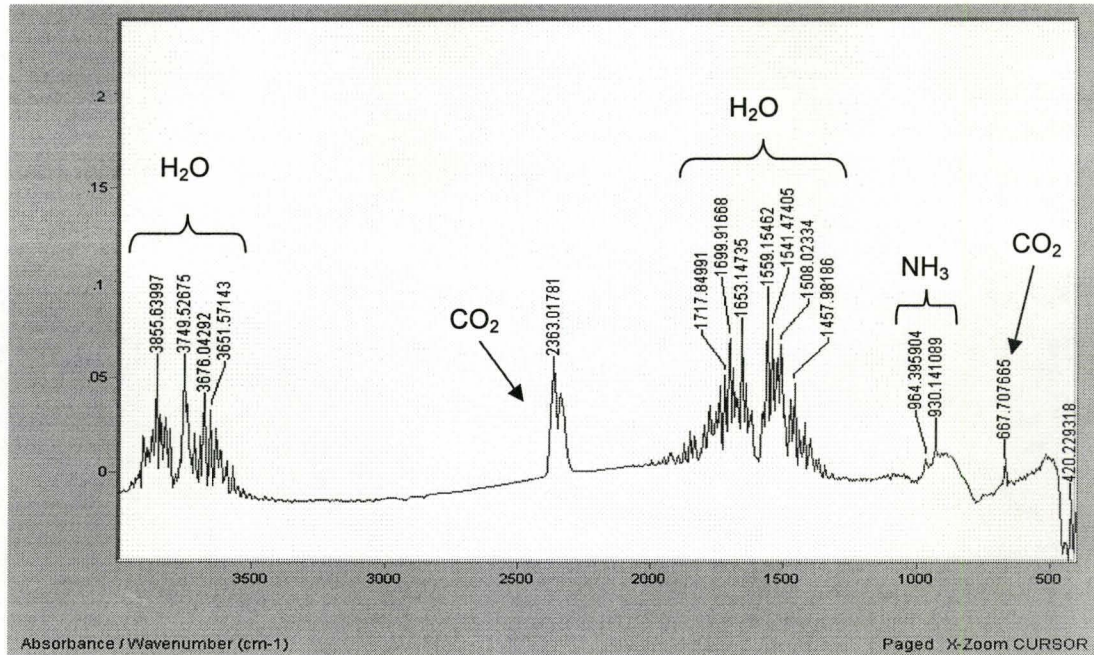
Figure 4-34: The overall FTIR absorption spectra for emissions gas sampled from the dual stage combustion type turbine at steady state
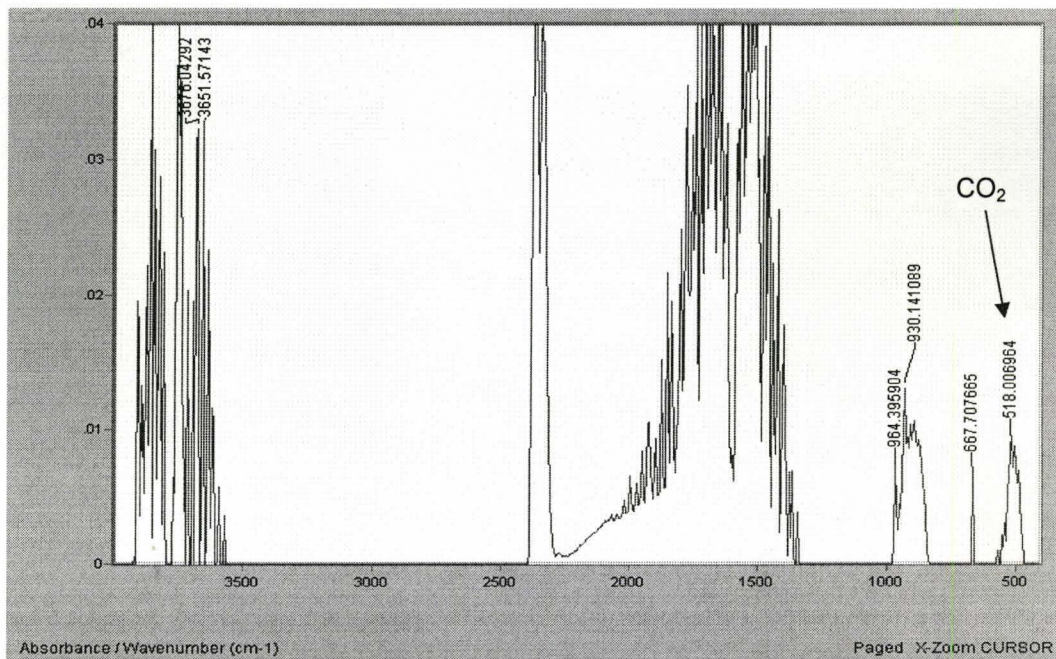
Figure 4-35: The detailed FTIR absorption spectra for emissions gas sampled from the dual stage combustion type turbine at steady state

4.3 Comparison of Single Stage Combustion Type Micro-Gas Turbine, Dual Stage Micro-Gas Turbine and Previous Micro-Gas Turbine Characterizations

The single stage combustion type MGT and the dual stage combustion type MGT are compared to previous MGT characterizations of the Honeywell Parallon 75kW MGT, the Capstone 60kW MGT and the Ingersoll-Rand 70kW MGT in Table 4-2.

Table 4-2: Comparison of the emissions from natural gas fired single stage combustion type MGT, dual stage combustion type MGT, Honeywell 75kW MGT, Ingersoll-Rand 70kW MGT and Capstone 60kW MGT [39-41]

MGT	Air-to Fuel Ratio	Load	NO_x	CO	THC/ VOCs	CO_2	PM
			kg/yr/kWh$_e$			t/yr/kWh$_e$	Part/yr/kWh$_e$
Honeywell 75kW	6.6	100%	8.96	0.52	<4.7[a]	6.05	---
Capstone 60kW	7.1	100%	1.29	1.04	0.57[a]	7.34	---
Ingersoll-Rand 70kW	10.2	100%	0.58	0.22	0.57[a]	6.97	---
Dual Stage (Ingersoll-Rand 70kW)	10.2	100%	0.56	0.34	84-147[a]	6.96	1.4×10^{14}
Single Stage (Elliott 80kW)	6.1	100%	6.14	0.74	86[a]	7.43	1.1×10^{14}

[a] THC and VOCs calculated as hexane (C_6H_{14})

Table 4-2 shows that the results for the present dual stage combustion type MGT (Ingersoll-Rand) and the Ingersoll-Rand MGT measured by the ETV [41] are in good agreement with very close emissions in all categories. This is expected, as the MGTs are the same

make and model, and it confirms the validity of both sets of measurements. It can also be observed form Table 4-2 that the richer burning Honeywell MGT and the single stage combustion type MGT have much higher NO_x emissions as compared to the leaner burning MGTs. The CO emissions for all MGTs are very similar, the Ingersoll-Rand MGT having the lowest emission at 0.22 kg/yr/kWh and the Capstone MGT having the highest emissions at 1.04 kg/yr/kWh. The CO_2 emissions are also fairly similar between all the MGTs characterized. The Honeywell MGT has the lowest emission of this greenhouse gas at 6.06 t/yr/kWh, whereas the Elliott single stage MGT has the highest CO_2 emission at 7.43 t/yr/kWh.

Both the Capstone and the Ingersoll-Rand MGTs had identical emissions of total hydrocarbons when the THC was converted to mass per year per kilowatt. The measurements for the Honeywell MGT were below the detection limit of the instrument used during that experiment; therefore it can only be observed that the THC is less than 4.7kg/yr/kw. The emissions of THC from the Elliott single stage combustion type MGT and the Ingersoll-Rand dual stage MGT appear to be high when compared to the other MGTs, however this is because the measurements are for VOCs and not just total hydrocarbons. As VOCs include hydrocarbons as well as other non-hydrocarbon compounds, it is expected that the measurements of VOCs would be higher then measurements of THC. The emissions of PM for the Elliott single stage combustion type MGT are on the same order of magnitude as the Ingersoll-Rand dual stage combustion type MGT. The ETV characterizations did not measure PM.

4.4 Natural Gas Combustion Test Loop Flue Gas Emission Characteristics

In order to determine the operating conditions of the natural gas combustion loop, the loop was characterized under cold start conditions and steady state conditions after the loop had be running for a given period of time. Figure 4-36 and Figure 4-37 show the concentration of oxygen and carbon dioxide with time for the cold start and steady state conditions, respectively. In both cases as the air flow rate is increase the oxygen content increases and the CO_2 concentration decreases. This is expected as the natural gas fuel rate remains constant and the increase in air flow rate dilutes the combustion exhaust. Steady state oxygen concentrations are lower and CO_2 are higher than cold start conditions. This is most likely due to the natural gas test loop being at a more elevated temperature and more complete combustion occurring, thus causing more oxygen to be consumed and more CO_2 to be produced.

Figure 4-38 and Figure 4-39 show the concentration of NO, NO_2 and CO with time for the cold start and steady state conditions, respectively. In both tests the NO concentration decreases with increasing air flow rate, while the CO concentration increases with increasing air flow rate. In both cases the NO_2 concentration was between 0-1ppm, the detection limit of the instrument. The NO concentration most likely decreases with increasing flow rate due to the cooling effect of the introduction of more room temperature air. The more air that is introduced to the combustion chamber cools the flame temperature, thus decreasing the amount of thermal NO_x produced. Under cold start conditions the maximum NO concentration is 14ppm, whereas under steady state conditions the maximum NO concentration is 44ppm. Again this is probably due to the temperature effect. Under cold start conditions the

chamber begins at room temperature and is heated by the flame. At steady state conditions the natural gas combustion loop had been running for four hours, thus the chamber would presumably be at a more elevated temperature than during cold start. This fact would increase the overall flame temperature, hence increasing thermal NO_x production.

The CO concentrations for the cold start condition and for the steady state condition are similar. In both cases CO concentrations were zero until a flow rate of $6.8Nm^3/hr$ and increased dramatically up to a flow rate of $11.9Nm^3/hr$, where CO concentrations were observed to be unstable. Although an increase in air flow rate should decrease the amount of CO produced by combustion, in this case and increased was noted. This is probably due to the instability of the flame that was observed. At low flow rates the flame was observed to be very stable and conical in shape. As the flow rate increased the flame was highly unstable, even momentarily extinguishing at a flow rate of $11.9Nm^3/hr$. The instability of the flame probably caused zones of incomplete combustion, thus increasing the CO concentrations.

Table 4-3 shows a comparison of the emissions from the natural gas combustion test loop and typical MGT exhaust.

Table 4-3: Comparison of natural gas combustion loop at cold start, steady state and typical MGT emissions

Emission/ Source	Natural Gas Test Loop Range (Cold Start)	Natural Gas Test Loop Range (Steady State)	Typical MGT Range (Full Power)
O_2 (%)	16.0-20.3	11.6-20.3	17.7-18.7
CO_2 (%)	1.5-2.8	0-5.2	1.26-1.75
CO (ppm)	0-135	0-146	0-5
NO (ppm)	0-16	0-42	0-18.6 (NO_x)
NO_2 (ppm)	0-2	0-3	

As can be seen from Table 4-3 the emissions from the natural gas test loop have large ranges. As mentioned before the emissions from the natural gas combustion test loop vary greatly with flow rate. Therefore lower flow rates would be more suitable for NO_x after-treatment testing and higher flow rates for CO after-treatment experiments. The concentrations of both CO_2 and O_2 correspond to MGT exhaust conditions.
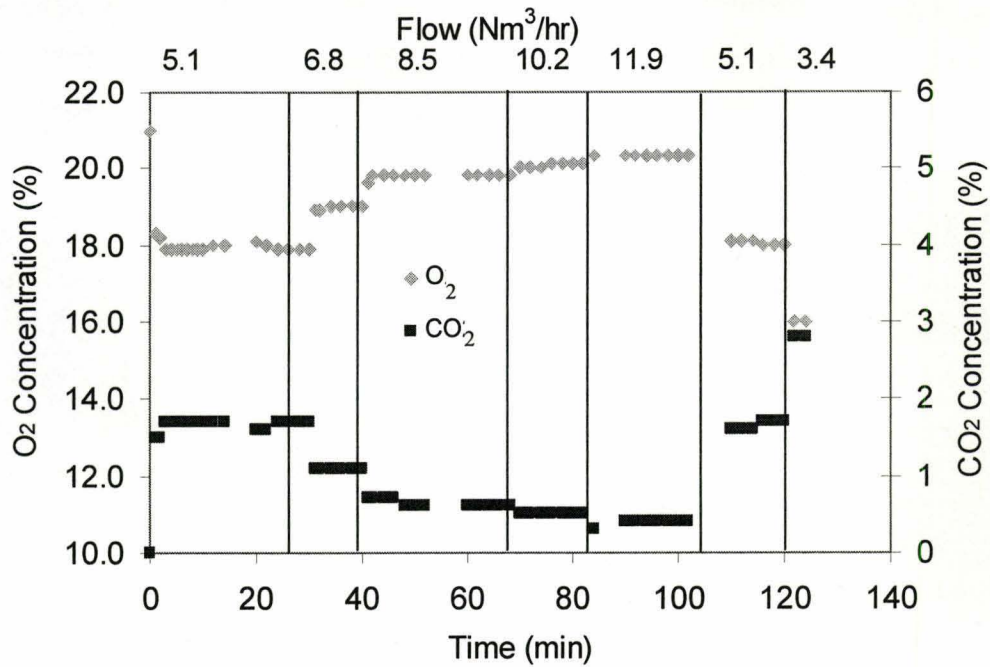
Figure 4-36: Cold start O_2 and CO_2 concentrations versus time and flow characteristics of natural gas combustion test loop
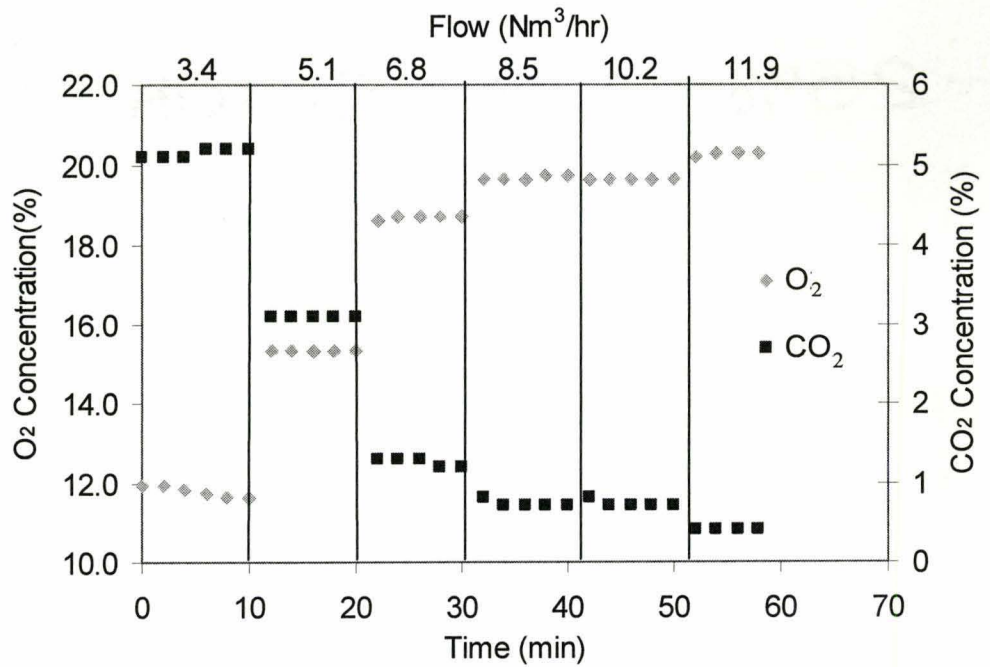
Figure 4-37: Steady state O_2 and CO_2 dioxide concentrations versus time and flow characteristics of natural gas combustion test loop
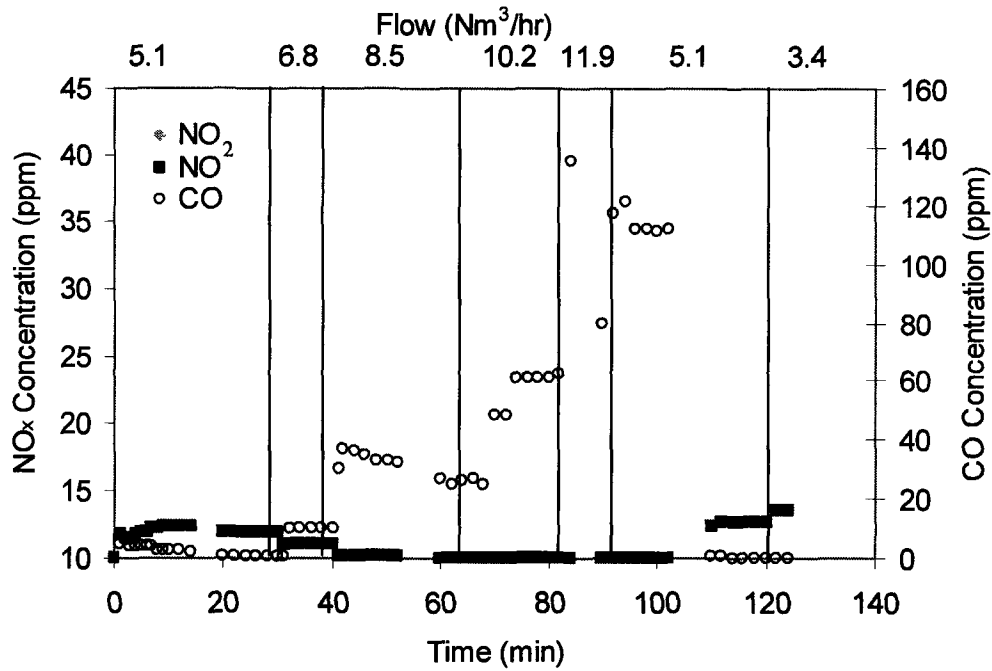
Figure 4-38: Cold start NO, NO_2 and CO concentrations versus time and flow characteristics of natural gas combustion test loop
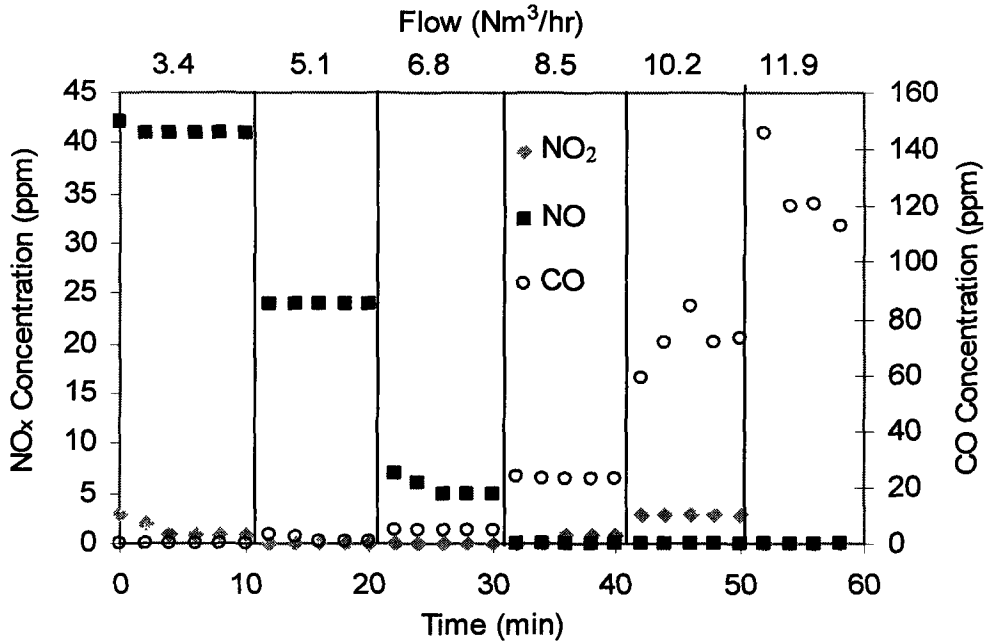
Figure 4-39: Steady state NO, NO_2 and CO concentrations versus time and flow characteristics of natural gas combustion test loop

Chapter 5 – Experimental Results of Simulated Natural Gas Micro-Gas Turbine Combustion Treatment by Plasma-Catalyst

5.1 Pressure Drop of Plasma-Catalyst System

An important property of any combustion after treatment system is the pressure drop inherent with the system. High pressure drops can adversely affect the combustion process by reducing the efficiency of combustion. Both the theoretical and experimental pressure drops were determined for the trench type plasma reactor. The pressure drop was also determined for the catalyst and the plasma-catalyst system. Figure 5-1 shows the experimental and theoretical pressure drops for the plasma-catalyst system. Figure 5-1 shows that the pressure drop increases with increasing gas flow rate. The reported pressure drop at 10 Nm^3/hr (~0.6m/s) is 220 Pa. This value seems to be on the same order of magnitude per meter to literature values of ceramic foam catalysts [76]. A theoretical pressure drop for the trench-type non-thermal plasma reactor was also calculated using the modified Bernoulli equation as shown below.

$$\Delta P = k_{Total} \frac{v^2}{2g} + f\left(\frac{L}{D_H}\right)\left(\frac{v^2}{2g}\right) \times \#channels$$

Where v is the velocity in the reactor (assumed to be constant throughout the system), k is the loss coefficient (assumed to be a 45° contraction entrance [k=0.17] and expansion exit [k=0.6]), *f* is the friction factor (f ranged from 0.20198-0.04149m depending on Reynolds number), L is the length of the reactor, D_H is the hydraulic diameter of the reactor and the number of channels is five for the trench reactor. The theoretical value for the pressure drop of the trench NTP reactor also appears to correspond to the experimental values. The pressure drop was also measured with discharge in the NTP reactor and no effect was observed with the reactor

on. The pressure drop was also calculated for a 2mm parallel plate reactor and a 5mm parallel plate reactor with equivalent flow areas as the trench reactor. The trench reactor had a lower pressure drop than the 2mm parallel plate reactor, but a higher pressure drop than a 5mm parallel plate reactor.
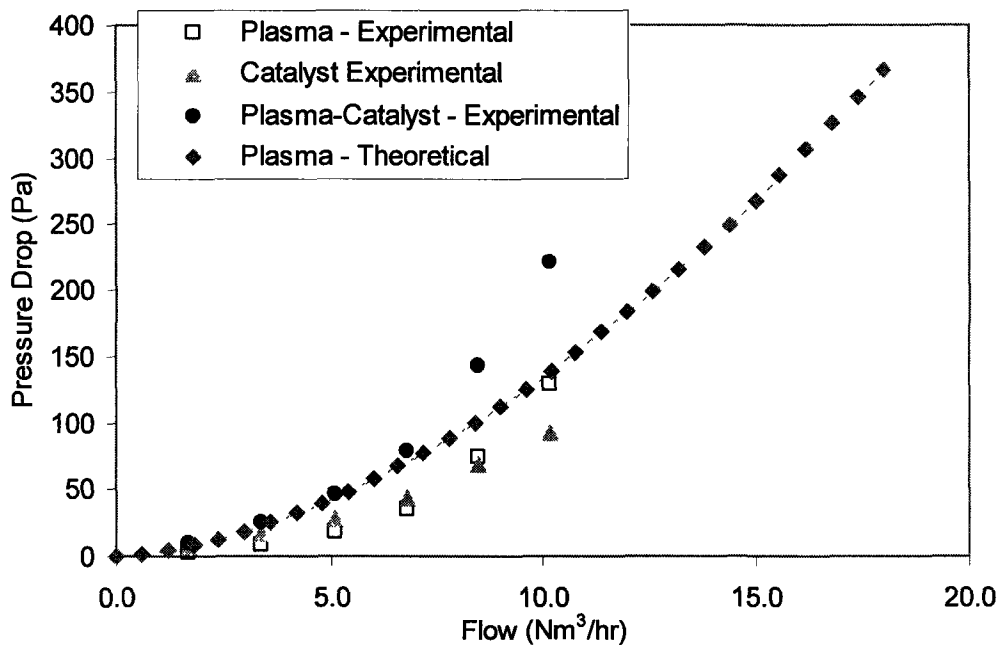
Figure 5-1: Theoretical and experimental pressure drop as a function of flow rate for trench type plasma-catalyst system

5.2 Discharge Characteristics of Trench Type Non-Thermal Plasma Reactor

Another important characteristic of non-thermal plasma reactors is the power across the reactor. The more power that is consumed to treat gaseous pollutants leads to reduced energy efficiency of the MGT power generation process. The combustion process becomes less energy efficient because more of the electrical power produced by combustion

must be diverted to power the NTP reactor. For example, an input of $4.2Wh/m^3$ can lead to an increase of approximately 3% in fuel consumption in an automobile [43]. In order to characterize the trench type NTP reactor a number of tests were performed to determine the power across the reactor versus the applied voltage. The power consumed by the reactor was measured using voltage-charge plots, otherwise known as Lissajous figures [36]. The trench type NTP reactor was tested under eight air flow rates from $0Nm^3/hr$ to $11.9Nm^3/hr$ for various applied voltages at room temperature. Many Lissajous figures were produced, so a typical Lissajous figure for an applied voltage of 12kV and a flow rate of $8.5Nm^3/hr$ is shown in Figure 5-2.
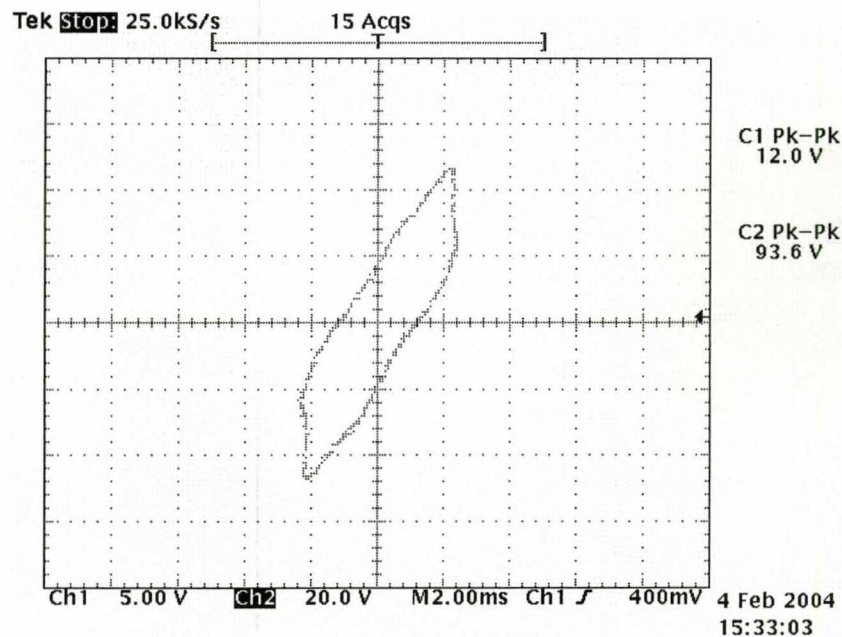
Figure 5-2: Voltage-charge characteristics (Lissajous figure) for an applied voltage of 12kV and an air flow rate $8.5Nm^3/hr$.

The injected discharge power to the reactor as a function of air flow rate for various applied voltages is shown in Figure 5-3. As can be observed in Figure 5-3, the power increases with increasing applied voltage, with the minimum power of approximately 2W at 12kV and a maximum power of 13W at 20kV for a flow rate of 11.9Nm^3/hr. Figure 5-4 further shows the effect of applied voltage on the power injected for air flow rates of 0Nm^3/hr and 11.9Nm^3/hr. Figure 5-3 also shows that from an initial air flow rate of 28L/min to and air flow rate of 11.9Nm^3/hr there is almost no significant effect for the power across the NTP reactor. However there is sudden increased in power across the NTP reactor for all applied voltages from no air flow to and air flow of 1.7Nm^3/hr. This may be caused by cooling effects of the air on the trench type NTP reactor, thus allowing for more power to build in the reactor before streamer corona onset occurs.

The effect of air temperature on the power injected to the trench reactor is shown in Figure 5-5. As can be observed in Figure 5-5, there appears to be no significant effect on the power injected to the NTP reactor with an air temperature from 22°C to 50°C at 8.5Nm^3/hr. The temperature difference in this experiment was relatively small, perhaps leading to no significant change in the power injected to the trench type reactor. The dielectric is also alumina and may not have had the same temperature change as observed in the air temperature.
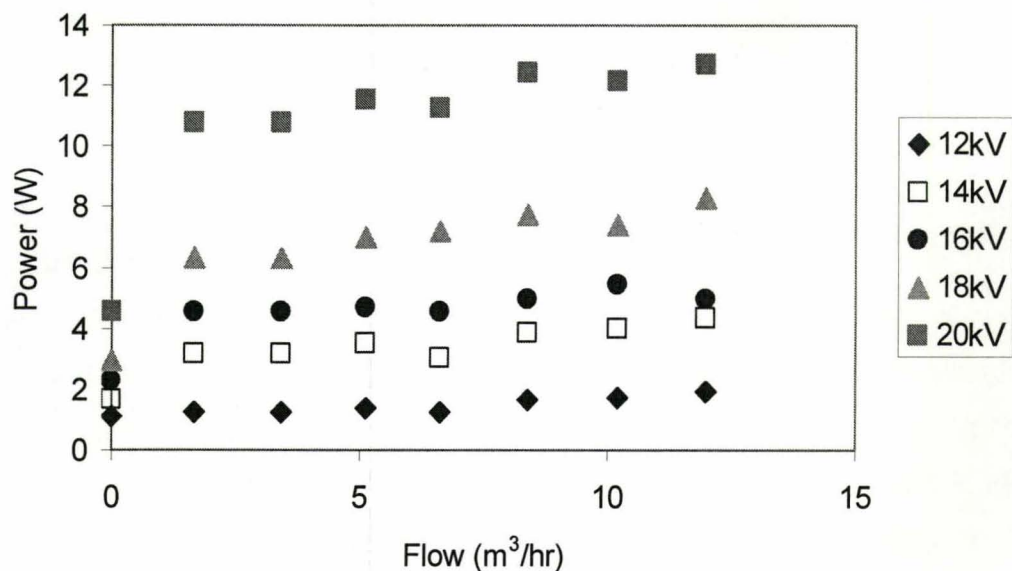
Figure 5-3: Power injected to the trench type NTP reactor as a function of gas flow rate for various applied voltages for air at 20°C
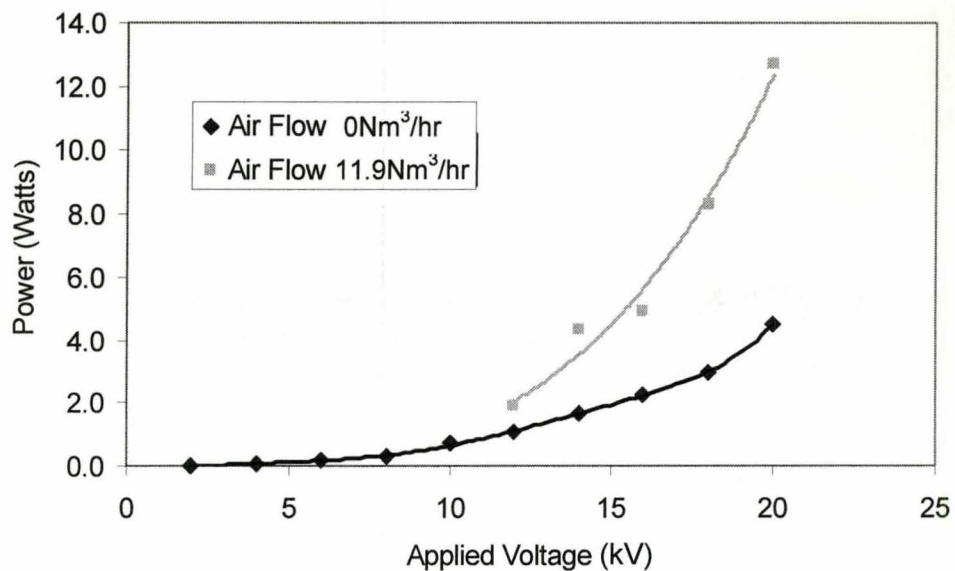
Figure 5-4: Power injected to the trench type NTP reactor as a function of gas applied voltage for a gas flow rate of $0Nm^3$/hr and $11.9Nm^3$/hr for air at 20°C
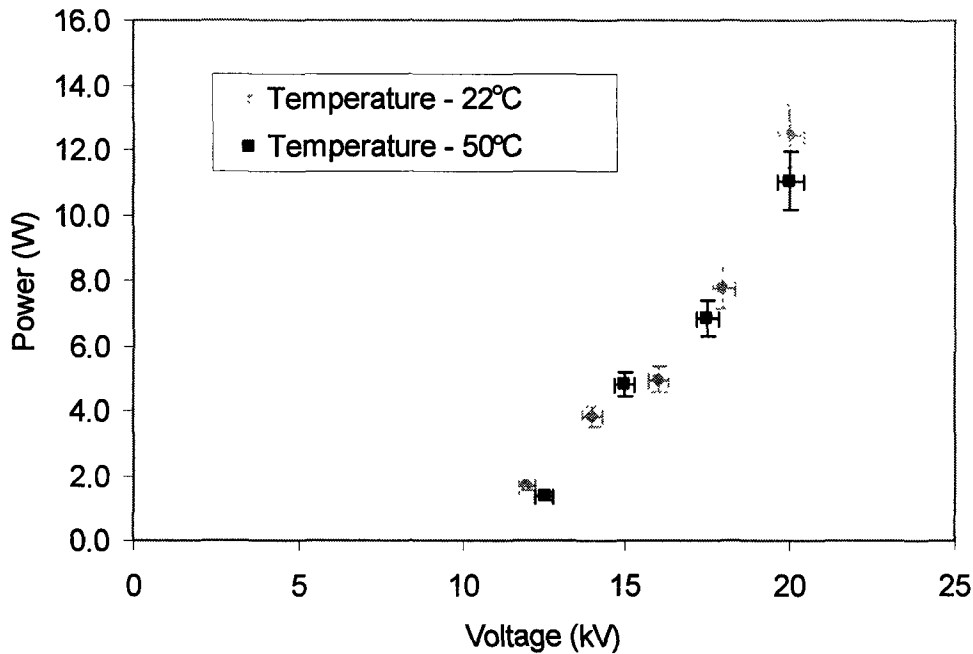
Figure 5-5: Power injected to the trench type NTP reactor as a function of gas applied voltage at a gas flow rate of 8.5Nm³/hr for gas temperatures of 22°C and 50°C

5.3 Simulated Natural Gas Combustion Emission Treatment by Non-Thermal Plasma and Plasma-Catalyst

The principal objectives of the trench type NTP reactor are to oxidize pollutants as well as reduce NO_x to harmless gas products. Specifically the NTP reactor is used to oxidize CO to CO_2, VOCs and NO to NO_2. In the first scenario the NTP reactor will oxidize a human toxin CO to a harmless gas CO_2. In the second case the NTP reactor will be used to oxidize VOCs to less harmful substances and to aldehydes, which will then be used to activate the sodium zeolite-Y catalyst used in the present plasma-catalyst system. In the third case NO will be oxidized to NO_2 by the NTP reactor, as NO_2 can readily be converted into N_2 and O_2 by the catalyst in the presence of aldehydes, whereas NO can not be easily handled by most catalysts. This section will discuss preliminary experimental results for the trench-type reactor plasma-catalyst system for

by using simulated natural gas combustion exhaust gases to demonstrate fundamental concepts and to examine NO_x removal in MGT exhaust gas.

5.3.1 NO to NO$_2$ conversion in a N$_2$-O$_2$-NO System by Non-Thermal Plasma

In order to determine the trench type NTP reactor's efficiency in converting NO to NO_2, the plasma reactor was tested using compressed NO sample gas.   As mentioned in Chapter 3, 20ppm of NO was introduced into the test loop and the NTP reactor was tested at different applied voltages using various flow rates of NO. The SED demonstrates the amount power required by the NTP reactor by the volume of gas treated. It is noted that NO to NO_2 conversion by NTP at this sampling port location is incomplete due to insufficient residence time for oxidizing reactions shown in Section 2.3.1.   Figure 5-6 shows the NO to NO_2 conversion efficiency is highest (75%) with a maximum SED at a flow rate of 3.4Nm^3/hr and lowest (35%) with a maximum SED at a flow rate of 8.5Nm^3/hr.

As expected the trench type NTP reactor works most efficiently at lower gas flow rates. The NTP process is more effective at lower flow rates due to an increase in the residence time in the reactor. Table 5-1 shows the residence time from the trench type NTP reactor entrance to the sampling point of the gas.

Table 5-1: Residence time for trench type NTP reactor to sampling point as a function of gas flow rate

Gas Flow Rate (Nm^3/hr)	Residence Time (s)
3.4	0.54
5.1	0.36
6.8	0.27
8.5	0.22
10.2	0.19

Increased residence time in the reactor increases the probability of gaseous pollutants (such as NO) interacting with oxygen radicals and ions (such as O^*, O_3, O_x^-, O_y^-, etc.) created by the non-thermal plasma. Free radicals and ions then combine to oxidize or reduce the gaseous pollutants to other compounds, in this case oxidize NO to NO_2 as demonstrated by some of the reactions listed in Section 2.3.1. An increase in residence time can also increase the NO to NO_2 conversion because of the rate of the reactions.

In all cases the conversion of NO to NO_2 increases with increasing electrical power. An increase electrical power increases the conversion efficiency of NO to NO_2 because of increased current in the NTP reactor, hence the electron density in the reactor. Thus an increase in electrons will increase the number of free radicals and therefore increasing the amount of NO oxidized to NO_2, as shown by many researchers [24, 35, 42-54].

Energy efficiency of NO to NO_2 conversion in terms of the energy yield (g [NO]/kWh = x[g] of [NO] conversion to [NO_2] per kWh of energy used) as a function of specific energy density (SED) for various gas flow rates is shown in Figure 5-7. Figure 5-7 shows the NO to NO_2 conversion is highest at 40 g[NO]/kWh at both the lowest and highest flow rates of $3.4Nm^3/hr$ and $8.5Nm^3/hr$, respectively. At higher SEDs the conversion efficiency of NO to NO_2 levels off for all flow rates at efficiencies of between 7-10 g[NO]/kWh. This demonstrates that although the conversion efficiency is highest at low flow rates, when energy efficiency is accounted for the trend is no longer observed. Therefore from an energy efficiency standpoint the trench type NTP reactor is as effective at higher flow rates as it is a lower flow rates as shown by Figure 5-7.
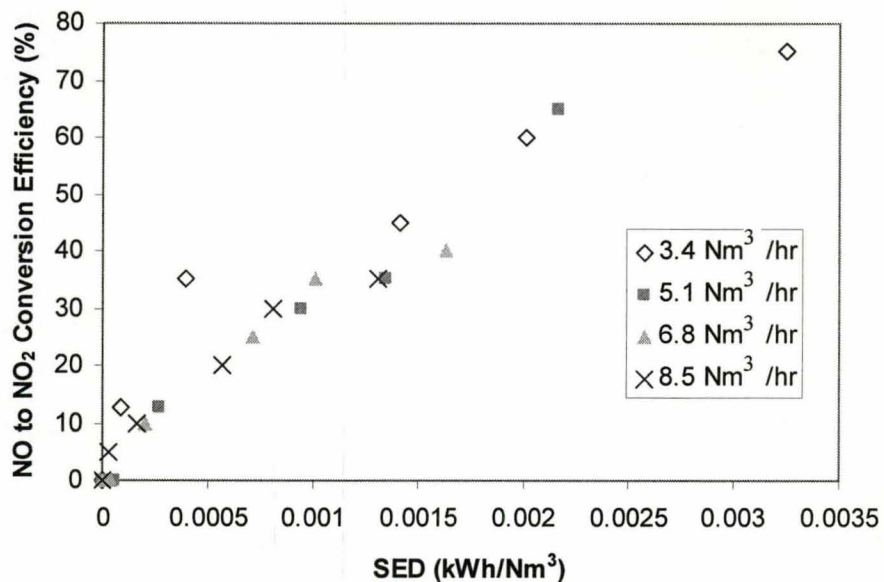
Figure 5-6: Conversion efficiency of NO to NO_2 conversion as a function of specific energy density for trench-type NTP reactor for various gas flow rates
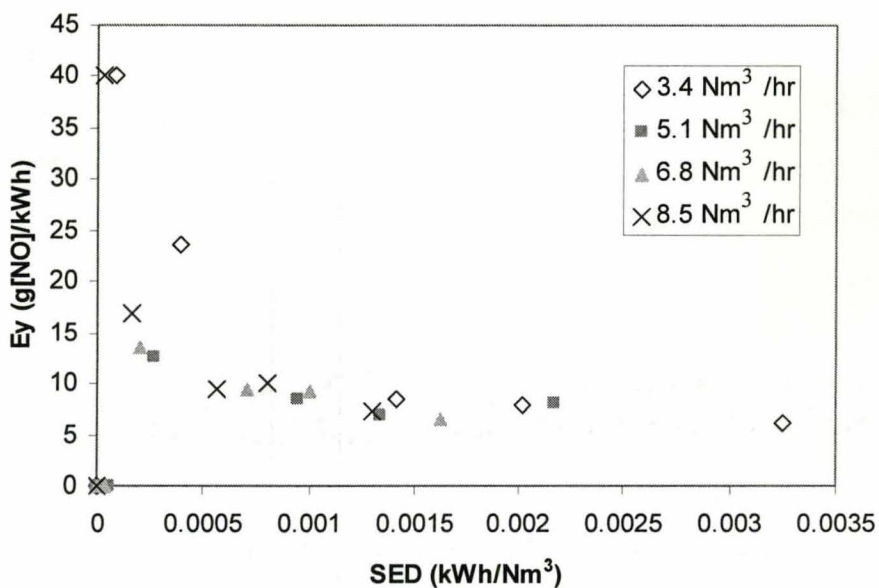
Figure 5-7: Energy efficiency of NO to NO_2 conversion as a function of specific energy density for trench-type NTP reactor for various gas flow rates

5.3.2 NO$_x$ Removal in a N$_2$-O$_2$-NO System by Non-Thermal Plasma-Catalyst System

The NO$_x$ removal efficiency of the trench type dielectric discharge non-thermal reactor followed by the sodium zeolite-Y catalyst coated on 400 cpsi cordierite monolith was also examined during this test. Figure 5-8 and Figure 5-9 show the NO$_x$ reduction versus the SED for gas flow rates between 3.4-9.5Nm^3/hr at 23°C and 65°C, respectively (note that in the following sections NO$_x$ removal will be based on the average molecular weights of NO and NO$_2$). Figure 5-8 shows that the NO$_x$ removal efficiency increases with increasing SED and decreasing gas flow rates. The removal of NO$_x$ increases with decreasing flow rates because the residence time is longer at lower flow rates. As mentioned previously in Section 5.3.1 this increase in removal efficiency (or conversion in the case of Section 5.3.1) of NO$_x$ occurs because there is a greater probability that the NO$_x$ will interact with electrochemically excited nitrogen by reduction reactions, as well as further oxidation of NO$_2$ to N$_2$O, NO$_3$ and HNO$_3$ (with trace water content absorbed in the catalyst) by free radicals as shown in Section 2.3.1, in the NTP reactor. Furthermore, the increase in residence time also increases the probability that the NO$_2$ formed by the NTP reactor will be absorbed in the catalyst surface and thus be removed by free radical reactions.

Figure 5-8 shows that the maximum removal efficiency of NO$_x$ at flow rates 3.4Nm^3/hr and 5.1Nm^3/hr were the same at 65%, however the removal efficiency at 5.1Nm^3/hr was achieved at a lower SED. This means that more gas was treated with the same electrical power injected into the plasma reactor, therefore the process was more effective at 5.1Nm^3/hr than at 3.4Nm^3/hr. It can also be observed from Figure 5-11 that between SEDs of 0 - 0.0010kWh/m^3 all flow rates show similar NO$_x$ removal efficiencies of approximately 30%. This means that the plasma-catalyst

system is as effective for NO_x removal at higher flow rates as it is for lower flow rates, when at lower SEDs.

By comparing Figure 5-8 to Figure 5-9 it can be observed that the NO_x conversion was greater at 23°C then at 65°C. The maximum NO_x removal at 23°C was 65%, whereas it was only 50% at 65°C. This is the opposite trend that was expected, as catalysts generally require elevated temperatures to operate effectively, however 65°C is still below minimum values for catalyst operation reported in literature. The test at 23°C may have been more effective for NO_x removal for two reasons. First the cordierite monolith would have had a greater capacity to absorb at lower temperatures, thus resulting in more NO_x being absorbed at 23°C then at 65°C. Secondly, reaction (1) mentioned in Section 2.3.1 occurs more readily at room temperature then at elevated temperatures. This would result in more NO being removed at 23°C then at 65°C via reaction (1).

Figure 5-8: NO_x removal efficiency versus SED for trench-type non-thermal plasma-catalyst for gas flow rates between 3.4-9.5Nm^3/hr at 23°C

Figure 5-9: NO_x removal efficiency versus SED for trench-type non-thermal plasma-catalyst for gas flow rates between 3.4-9.5Nm^3/hr at 65°C

It has been observed by Hoard *et al* [43] that sodium cordierite catalysts require aldehydes in order to be activated and remove NO_x from air streams. As no aldehydes or hydrocarbons were used during these tests it is unlikely that the catalyst was properly activated. Therefore it is probable that the results from this test represent the absorption of NO_2 to the catalyst, rather than the aldehydes reaction of NO_2 to N_2 and O_2 through a catalytic reaction.

Figures 5-10 and 5-11 show the energy efficiency of NO_x removed as a function of SED for various gas flow rates for gas temperatures of 23°C and 65°C, respectively. As can be observed from comparing Figure 5-9 to Figure 5-10 the NO_x removed is greater for the test at 23°C then for 65°C at low SEDs. The maximum NO_x removal at 23°C was 114g/kWh, whereas at 65°C the maximum NO_x removal was 15g/kWh. Again, this large difference could be due to the effective mass of NO_2 being absorbed more readily by the catalyst at 23°C then at 65°C and NO removal by reaction (1). It can also be observed that at higher SEDs of about 0.001kWh/m^3 that the NO_x removal is similar for both experiments. This trend can also be seen in Figures 5-8 and 5-9. This suggests that at higher SEDs there is not a significant difference between the NO_x removal efficiencies for 23°C and 65°C of the plasma-catalyst system.
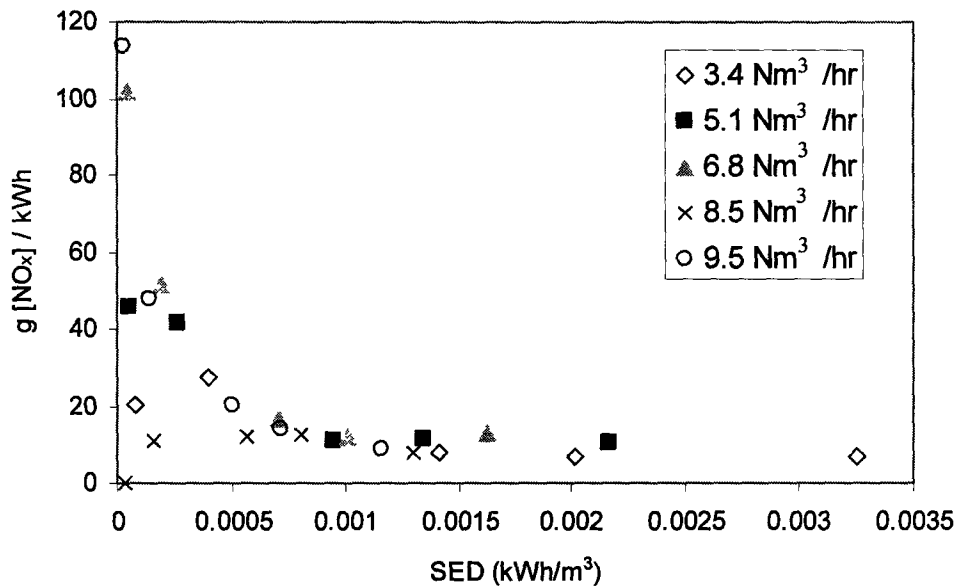
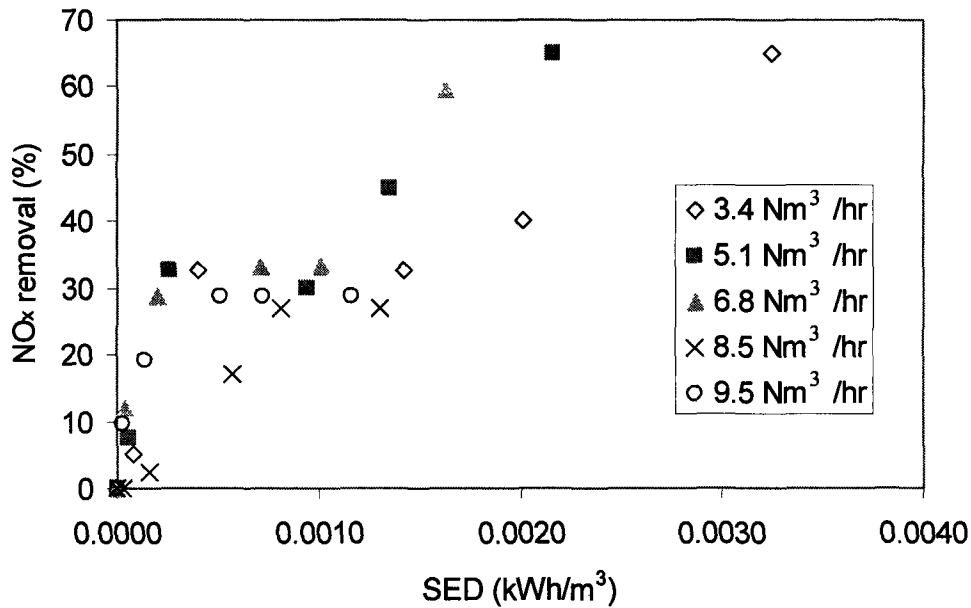**Figure 5-10:** Energy efficiency of NO_x removal by mass versus SED for trench-type non-thermal plasma-catalyst for gas flow rates between 3.4-9.5Nm^3/hr at 23°C

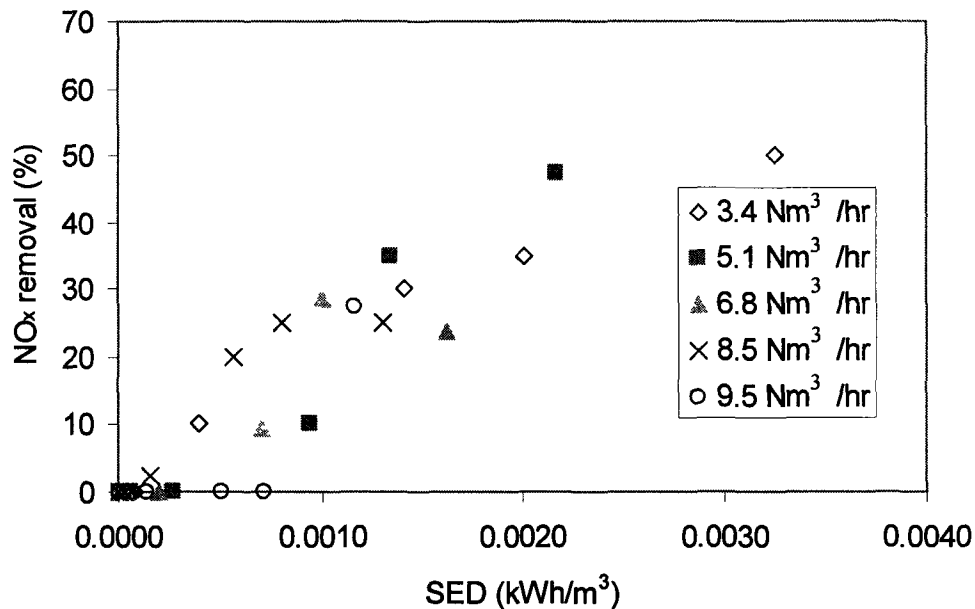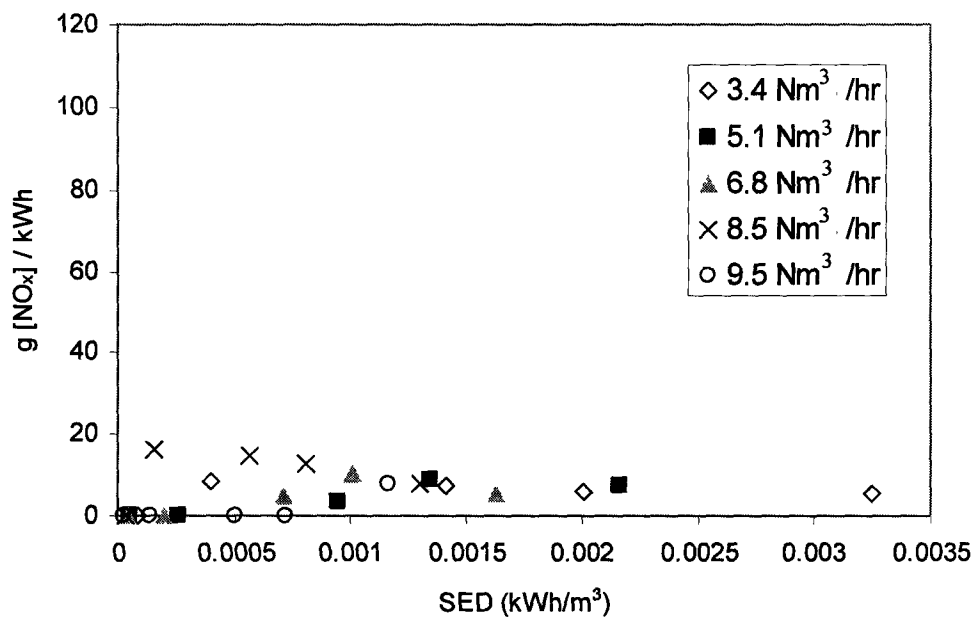**Figure 5-11:** Energy efficiency of NO_x removal by mass versus SED for trench-type non-thermal plasma-catalyst for gas flow rates between 3.4-9.5Nm^3/hr at 65°C

119

5.3.3 NO_x Removal in a N_2-O_2-NO-CH_4 System by Non-Thermal Plasma-Catalyst System

The NO_x removal efficiency of the plasma-catalyst system was examined during this test for various NO to CH_4 ratios at 23°C. Methane was injected into the system in order to create aldehydes by its decomposition in the NTP reactor. The first large difference that was observed when compared to the previous test without CH_4, was the power injected into the NTP reactor. The power injected into the NTP reactor was approximately four times higher than the previous test. This change in the injected power may be due to the presence of CH_4, which would require more power to decompose the CH_4 and as has been observed by other investigations [51, 55, 56].

Figures 5-12 to 5-15 show the NO_x removal efficiency of the plasma-catalyst system for the addition of CH_4 for flow rates of 3.4 Nm^3/hr, 5.1 Nm^3/hr, 6.8 Nm^3/hr, and 8.5Nm^3/hr, respectively. As can be observed from Figures 5-12 to 5-15, the NO_x removal efficiency increases with increases SED, as expected. As previously mentioned in Section 5.3.2 this trend occurs both due to an increase in residence time in the plasma-catalyst system and because more power is being injected into the NTP reactor compared to the flow rate. Figure 5-12 to 5-15 also show that in most cases there is not a large difference in NO_x removal efficiency based on the concentration of CH_4 injected into the system, with the exception of the maximum SEDs at flow rates of 3.4Nm^3/hr and 8.5Nm^3/hr. The maximum NO_x removal of 52% occurred at a flow rate of 3.4 Nm^3/hr with a CH_4 to NO ratio of 1.5. In all cases except at 8.5Nm^3/hr, the maximum NO_x removal occurred with CH_4 to NO ratio of 1.5; at 8.5Nm^3/hr the maximum NO_x removal occurred at a CH_4 to NO ratio of 1.0. It can also be observed

that the maximum NO_x removal efficiencies between the flow rates of $5.1Nm^3/hr$ to $8.5Nm^3/hr$ are very similar, only varying from 33% at a flow rate 8.5 Nm^3/hr to 38% at a flow rate of $5.1Nm^3/hr$. This shows that the plasma-catalyst system is as effective at lower flow rates as it is at higher flow rates. Furthermore, the SED is significantly lower at higher flow rates, meaning that more gas can be treated with similar NO_x removal efficiencies then at lower flow rates.

The NO_x removal efficiencies are also lower than the previous test at 23°C without the addition of CH_4, as shown in Figures 5-12 to 5-15 ($[CH_4]/[NO]$ ratio = 0 for previous test). This result was expected as the addition of CH_4 should have allowed for the formation of aldehydes in the NTP reactor but could not activate the sodium zeolite-Y catalyst at low gas temperatures. As well, the plasma energy may be more effectively used to dissociate CH_4 then generating N^* and N_2^* radicals, hence NO_x removal may not be enhanced as has been observed by Ambridge et al [77]. However with no direct measurement of aldehydes during the experiment, the presence of aldehydes cannot be confirmed or refuted. The results of this experiment are similar to the results of the previous experiment without CH_4 at 65°C. Both experiments had maximum NO_x removal efficiencies of approximately 50%.
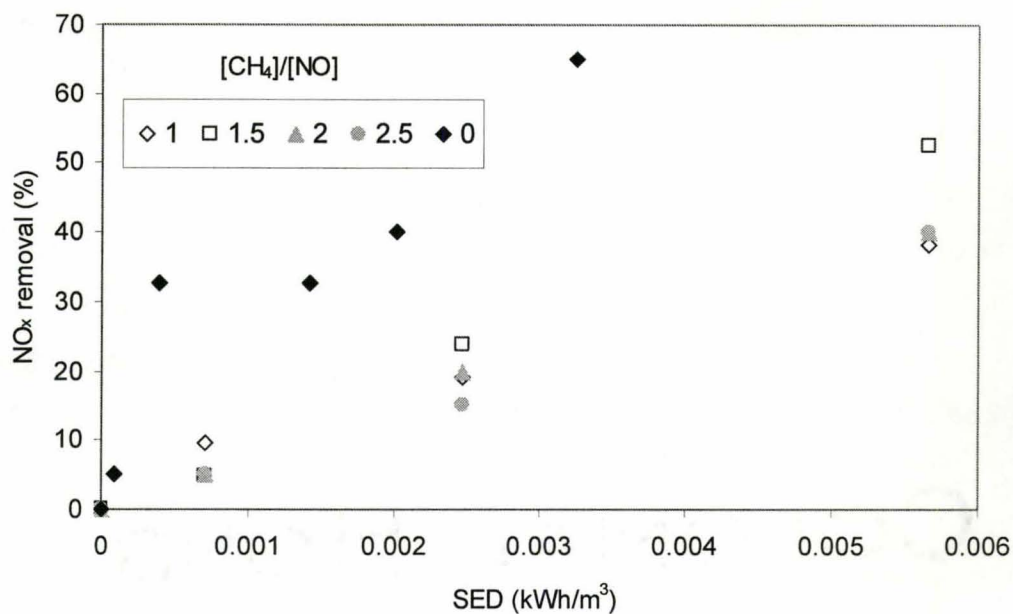
Figure 5-12: NO_x removal versus SED for non-thermal plasma-catalyst for gas a flow rate of $3.4Nm^3/hr$ for various CH_4 to NO ratios
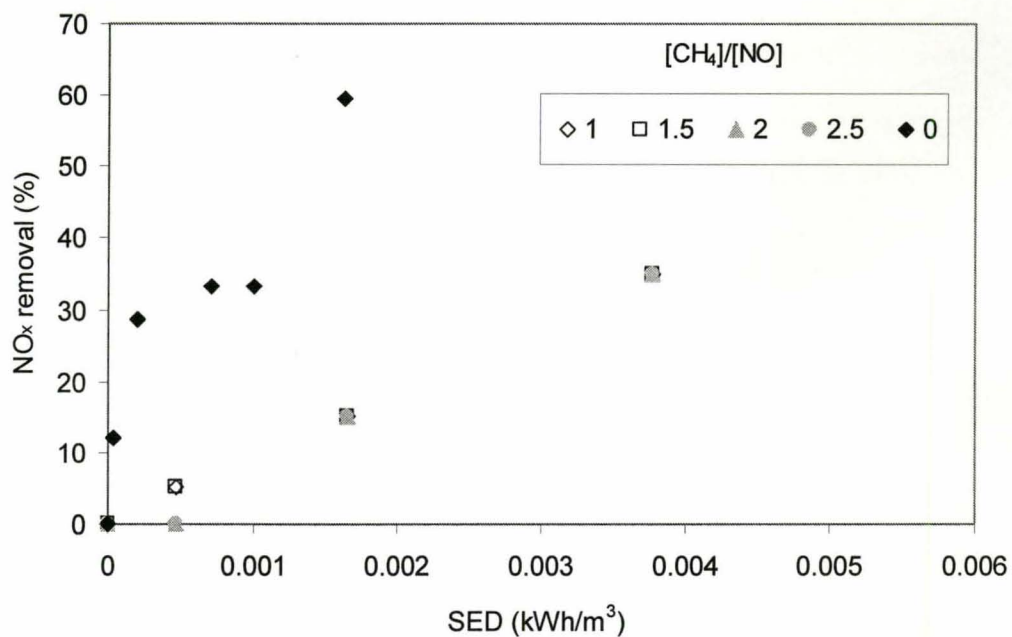
Figure 5-13: NO_x removal versus SED for non-thermal plasma-catalyst for gas a flow rate of $5.1Nm^3/hr$ for various CH_4 to NO ratios
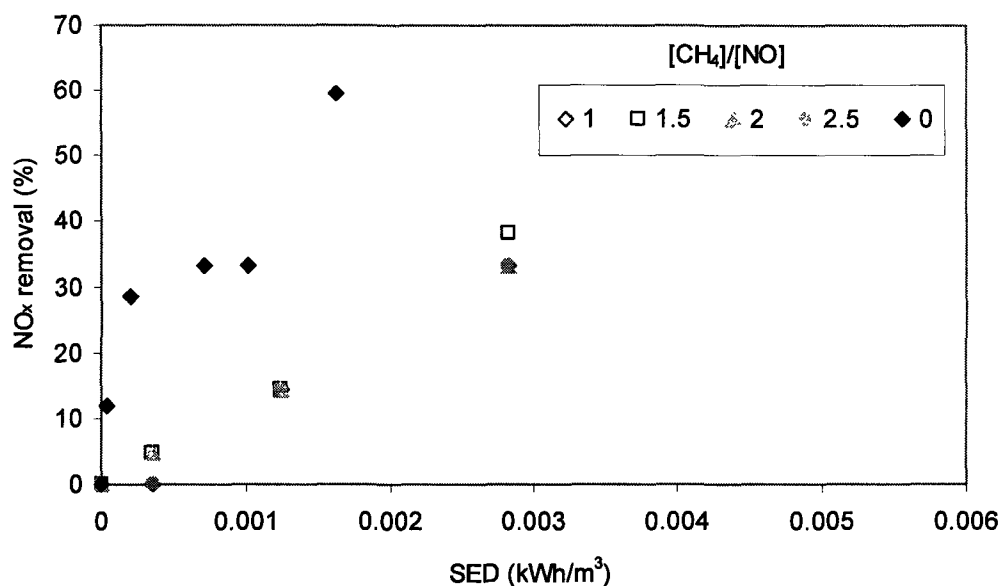
Figure 5-14: NO_x removal versus SED for non-thermal plasma-catalyst for gas a flow rate of $6.8Nm^3/hr$ for various CH_4 to NO ratios
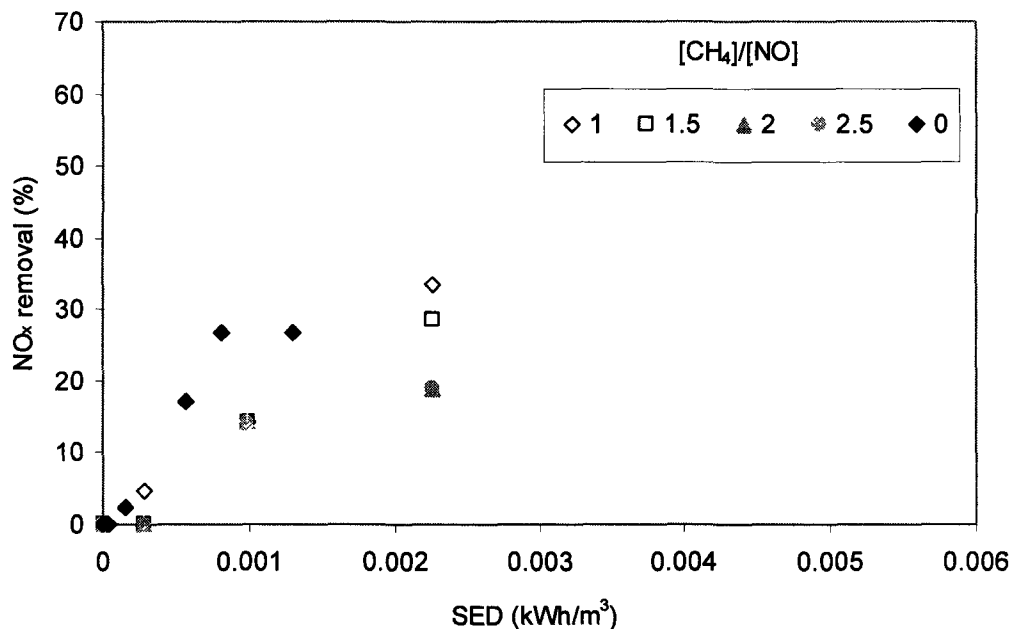
Figure 5-15: NO_x removal versus SED for non-thermal plasma-catalyst for gas a flow rate of $8.5Nm^3/hr$ for various CH_4 to NO ratios

Figures 5-16 to 5-19 show the energy efficiency of NO_x removed ($g[NO_x]$/kWh) versus the SED for flow rates of $3.4Nm^3$/hr, $5.1Nm^3$/hr, $6.8Nm^3$/hr and $8.5Nm^3$/hr, respectively. The energy efficiency of NO_x removed varies between a minimum of 2.4g/kWh at a flow rate of $3.4Nm^3$/hr with a CH_4 to NO ratio of 1.5 to a maximum of 7.2g/kWh at a flow rate of $5.1Nm^3$/hr with a CH_4 to NO ratio of 1.5. This shows that the mass of NO_x removed per kWh varies less depending on flow rate, demonstrating that the plasma-catalyst is as effective at higher flow rates as it is a lower flow rates, which have increased residence times. It can also be observed that the maximum mass of NO_x removed per kWh occurs at the highest flow rate, showing again that the plasma catalyst is efficient at high flow rates. The mass of NO_x removed per kWh during this experiment was very similar to the previous test without CH_4 at 65°C, both tests being in the range of 0-10 gNO_x/kWh at a SED of approximately 0.001 kWh/m^3.
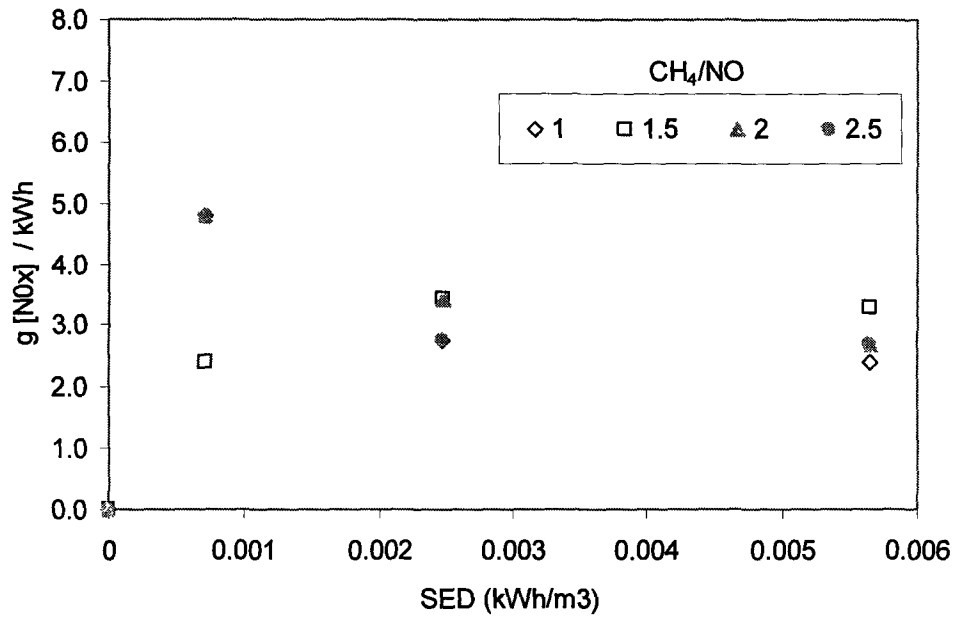
Figure 5-16: Energy efficiency of NO$_x$ removal versus SED for non-thermal plasma-catalyst for gas a flow rate of 3.4Nm^3/hr for various CH$_4$ to NO ratios
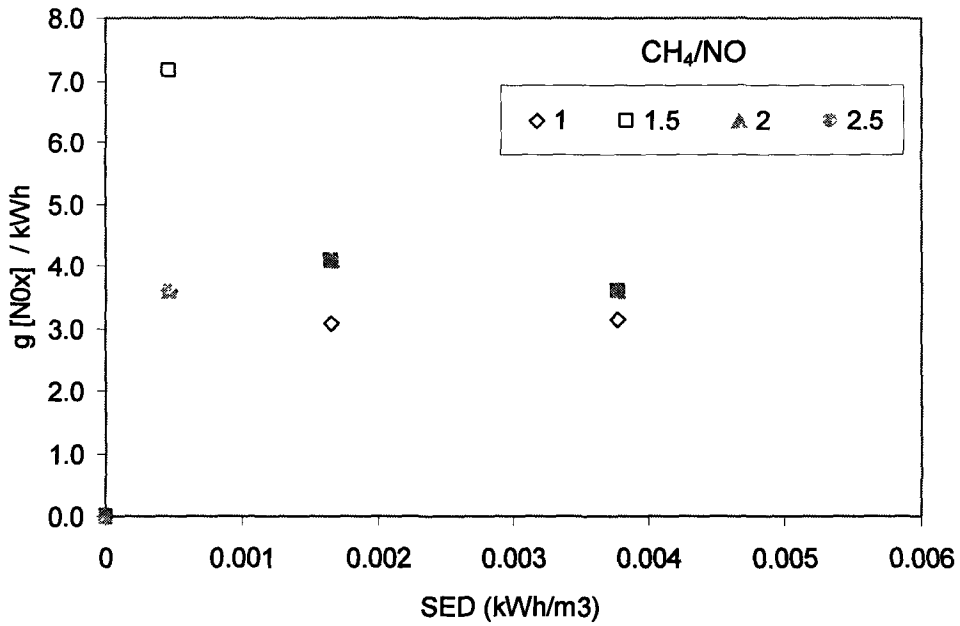
Figure 5-17: Energy efficiency of NO$_x$ removal versus SED for non-thermal plasma-catalyst for gas a flow rate of 5.1Nm^3/hr for various CH$_4$ to NO ratios
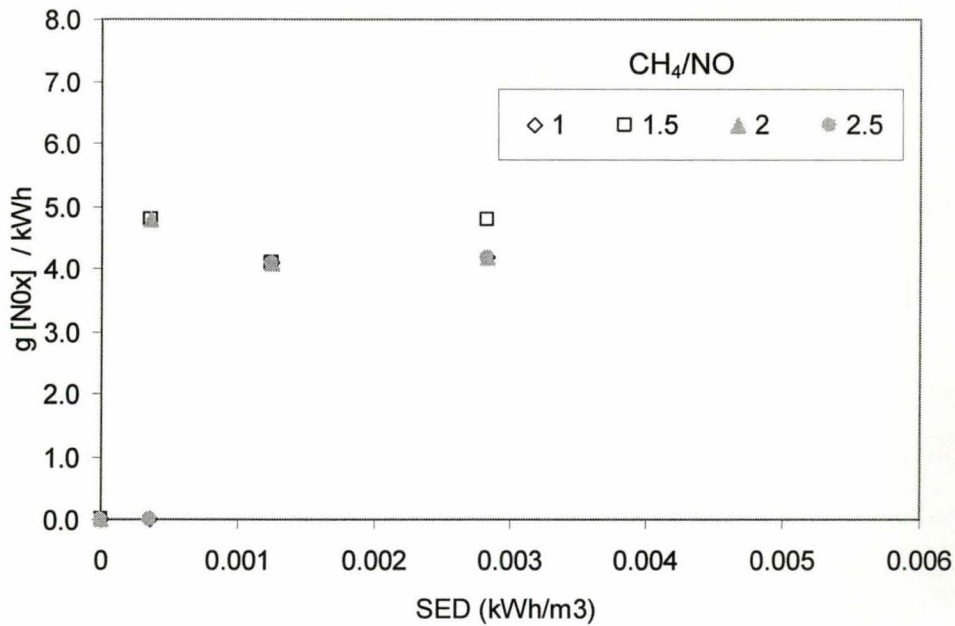
Figure 5-18: Energy efficiency of NO_x removal versus SED for non-thermal plasma-catalyst for gas a flow rate of $6.8Nm^3/hr$ for various CH_4 to NO ratios
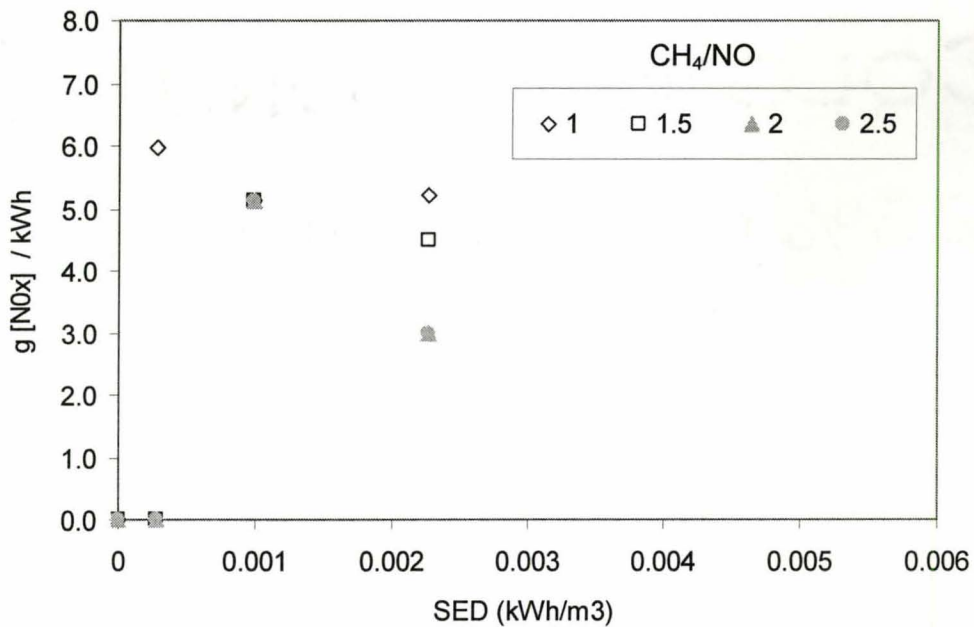
Figure 5-19: Energy efficiency of NO_x removal versus SED for non-thermal plasma-catalyst for gas a flow rate of $8.5Nm^3/hr$ for various CH_4 to NO ratios

# Chapter 6 – Conclusions and Recommendations

6.1 Conclusions

6.1.1 Natural Gas Micro-Gas Turbine Flue Gas Characterizations

6.1.1.1 Single Stage Combustion Type Micro-Gas Turbine

This study has focused on the characterization of two different types of micro-gas turbines, a single stage combustion type MGT and a dual stage combustion type MGT. The flue gas emissions for both MGTs were characterized for volatile organic compounds (VOCs), particulate matter (PM), nitrogen oxides (NO_x), hydrocarbons (HC), carbon monoxide (CO), oxygen (O_2), carbon dioxide (CO_2), aldehydes and ozone (O_3).

For the single stage combustion type (Elliott TA-80R 80kW) MGT it was observed that the oxygen concentration decreased with increasing power to a minimum of 18.5% and the amount of CO_2 increased with increasing load to a maximum concentration of 1.9% at a full load of 101.2kW for natural gas combustion. For propane combustion the same trends were observed for O_2 and CO_2 with the minimum concentration of O_2 being 18.2% and the maximum concentration for CO_2 being 1.8% at a full load of 85.6kW. The concentration of CO decreased with increasing load for both natural gas and propane combustion. The minimum CO concentration for natural gas combustion was 3ppm at a full of load of 101.2kW and the minimum for propane combustion was 35ppm at a full load of 85.6kW. The maximum CO concentrations at start up were 238ppm and 387ppm for natural gas and propane, respectively.

The VOC concentrations for the single stage combustion type MGT were observed to be relatively stable at all loads. The VOC concentration for natural gas combustion varied between 100-120ppm and between 150-170ppm for propane combustion. The hydrocarbon concentration for both natural gas combustion and propane combustion decreased with

increasing load. For natural gas and propane combustion the HC concentration range was between 0.03% and 0.05%.

The concentration of NO_x for the single stage combustion type MGT was observed to increase with increasing load for both natural gas and propane combustion. The maximum NO_x concentration for natural gas combustion was observed to be 15ppm at a full load of 101.2kW. The maximum NO_x concentration for propane combustion was higher then natural gas combustion at 17ppm at a full load of 85.6kW. The particulate matter mass concentration was observed to decrease with increasing load for natural gas combustion, but it was observed to increase with increasing load for propane combustion. The maximum PM concentration for natural gas combustion was observed to be $0.87mg/m^3$ at a load of 10kW. The maximum PM concentration for propane gas combustion was observed to be $1.8mg/m^3$ at a load of 85.6kW. ESEM analysis found that the majority of particles greater then $1\mu m$ were between $1-7\mu m$ for both propane and natural gas combustion. Propane combustion had a greater number of particles larger $20\mu m$ when compared to natural gas combustion.

FTIR adsorption spectroscopy analysis from the single stage combustion type MGT found that the most common identifiable compounds in the flue gas for both propane and natural gas combustion were the hydrocarbons CH_4, C_2H_2, C_2H_4 and C_2H_6. Nitrogen dioxide was also present in three samples. Ozone and aldehydes were also measured at steady state, but were observed to be below the detection limit of the instrument, 0.025ppm and 4ppm, respectively.

6.1.1.2 Dual Stage Combustion Type Micro-Gas Turbine

As the dual stage combustion type (Ingersoll-Rand Powerworks 70kW) MGT did not have the ability to vary load, the characterization focused on cold start, warm start and steady state emissions. The O_2 concentration during steady state at a full load of 70kW was observed to be 18.9% and the CO_2 concentration was observed to be 1.4%. The CO concentration was observed to be at a maximum at cold start up with a concentration of 25ppm, while at full load it varied between 0-1ppm, the detection limit of the instrument. The VOC concentration was observed to be between 80-140ppm at steady state operation, with a maximum occurring during cold start up of 200ppm. The NO_x concentration was also found to have a maximum at the cold start up of the MGT, with a concentration of 16ppm and ranged between 0-1ppm at full load steady state operation, again at the detection limit of the instrument.

A nano-sized particle size distribution was determined to have a bimodal shape with a significant amount of particles smaller than 29nm present. As well the mean particle diameter was observed to be 35nm. FTIR adsorption spectroscopy trace gas analysis from the dual stage combustion type MGT found that the most common identifiable compounds in the flue gas were the hydrocarbons CH_4, C_2H_2, C_2H_4 and C_2H_6. As well ammonia was observed to be present in all flue gas samples. Ozone and aldehydes were also measured at steady state, but were observed to be below the detection limit of the instrument, 0.025ppm and 4ppm, respectively.

6.1.2 Plasma-Catalyst System

Plasmas-catalyst system was first tested for pressure characteristics. The plasma-catalyst system was found top have a pressure drop of 220Pa at $10Nm^3/hr$. The pressure drop across the trench type NTP had good agreement with theoretical values, being on the same order of magnitude. The maximum power injected to the trench type NTP reactor was 13 watts at an applied voltage of 20kV. It was observed that the power injected to the trench type NTP reactor did not have a significant change with air flow rate or air temperature. At 20kV, the trench type NTP reactor was established to have the maximum NO to NO_2 conversion at 75% at a flow rate of 3.4 Nm^3/hr and a SED of 3.25 x 10^{-3} kW/m^3. The minimum NO to NO_2 conversion of 35% occurred at a flow rate of $8.5Nm^3/hr$ and a SED of 1.3 x10^{-3} kW/m^3.

Of all experiments conducted, the plasma-catalyst system was observed to have a maximum NO_x removal efficiency of 65% at 23°C for the simulated MGT exhaust gas without methane. The maximum NO_x removal observed at a gas temperature of 65°C during the test using compressed NO was approximately 50%. In the simulated MGT exhaust gas treatment with methane, the maximum NO_x removal efficiency was observed to be 52% at 23°C with 30ppm of injected CH_4 (CH_4 to NO ratio of 1.5). It was observed during the test with NO and CH_4 that the removal of NO_x increased with increasing SED. It was also seen the concentration of CH_4 did not have a large impact on the NO_x removal efficiency in most cases at 23°C. At all flow rates, expect $8.5Nm^3/hr$, the maximum NO_x removal occurred with a CH_4 concentration of 30ppm. The NO_x removal by mass per kilowatt-hour was observed to be similar between the test with CH_4 and without CH_4 at 65°C, having removals of between 0-10g[NO_x]/kWh at similar SEDs.

6.2 Recommendations for Future Work

The trench type NTP reactor has shown promising results for both the conversion of NO to NO_2 and NO_x removal with the sodium zeolite reactor. However the maximum NO_x removal observed in this study for the plasma-catalyst system was 65% and will need to be much higher to meet future emission regulations. Hydrocarbons other than CH_4 should be tested with compressed NO to determine the most effective hydrocarbon to activate the catalyst. The plasma-catalyst system should also be placed into an oven in order to ensure the sodium zeolite-Y reactor is at the minimum temperature for effective operation. The oven will also keep the temperature of the natural gas combustion loop above the dew point, avoiding condensation and corrosion within the plasma-catalyst. Testing also needs to be completed using natural gas combustion with the plasma-catalyst system to test the effectiveness of the plasma-catalyst in operating conditions closer to those of MGT exhausts. The trench type reactor should also be modified to have two or more reactors in series or parallel to increase the efficiency of flue gas treatment.

References

[1]   D. Smith, "Distributed generation: the power to choose," *Power Engineering*, vol. 105, no.3, pp. 32-35, 2001.

[2]   M. Hanley, "Sprint takes on the power of turbines," *Telephony*, vol. 244, no.9, pp. 40-43, 2003.

[3]   P. Fairley, "Power to the People," *Technology Review*, vol. 140, no.4, pp. 70 to 77, 2001.

[4]   Anonymous, "Two California companies set an example with the use of microturbines," *Pollution Engineering*, vol. 33, no.8, pp. 7, 2001.

[5]   S. Mraz, "A microturbine in every house," *Machine Design*, vol. 74, no.5, pp. 84, 2002.

[6]   G. Powers, E. Weber, M. Irvine, and P. Baldwin, "A New Class of Small, NG Turbines are Arriving," *Plant Engineering*, vol. 51, no.13, pp. A9-A12, 1997.

[7]   P. Hull, "Continuous Power - or Not, As You Prefer," *Distributed Energy: the Journal for Onsite Power Solutions*, vol. Jan/Feb, 2004, pp. unknown.

[8]   "Product Datasheet: Capstone C60 Microturbine," Capstone Corporation, 2004.

[9]   "National Emission Guidelines for Stationary Combustion Turbines," Canadian Council of the Ministers of the Environment Publication CCME-EPC/AITG-49E, December 1992.

[10]   "Product Datasheet: Ingersoll-Rand Powerworks 70L Series Microturbine," Ingersoll-Rand Energy Systems, 2004.

[11]   "Product Datasheet:: Elliott TA-80R 80kkW CHP Microturbine," Elliott Energy Systems, 2004.

[12]   "Guideline A-5: Atmospheric Emissions for Stationary Combustion Turbines," Ministry of the Environment of Ontario, March 1994.

[13]   "Thermal Power Generation Emissions - National Guidelines for New Stationary Sources Discussion Document," Environment Canada, December 2001.

[14]   Noel De Nevers, *Air Pollution Control Engineering*, Second ed. Toronto: McGraw-Hill, 2000.

[15]   "Distributed Energy Program," Air Resources Board of California 2004.

[16]   "Guidance for the Permitting of Electrical Generation Technologies," Air Resources Board of California, July 2002.

[17]   "Distributed Generation Certification of Capstone Turbine Corporation's C60 Microturbine," Air Resources Board of California, Executive Order DG-002, February 25 2003.

[18]   "Distributed Generation Certification of Ingersoll-Rand Energy Systems 70LM PowerWorks Microturbine," Air Resources Board of California Executive Order DG-004, May 30 2003.

[19]   Anonymous, "Integrated Pollution Prevention and Control: Draft Reference Document on the Best Available Techniques for Large Combustion Plants," European Commission March 2003.

[20]   "NOx: How nitrogen oxides affect the way we live and breath," Office of Air Quality Planning and Standards, EPA-456/F-98-005, September 1998.

[21]   E. Sher (Editor), "Handbook of Air Pollution from Internal Combustion Engines: Pollutant Formation and Control." Toronto: Academic Press, 1998.

[22]   H. Peavey, D. Rowe, and G. Tchobanoglous., *Environmental Engineering*. Toronto: McGraw-Hill, 1985.

[23]   S. Masuda and H. Nakao "Control of NOx by Positive and Negative Pulsed Corona Discharge", IEEE Transactions on Industrial Applications, vol.26, pp.374-381, 1990.

[24]   A. Mizuno, K. Shimizu, A. Chakrabarti, L. Dascalescu, and S. Furuto, "NOx Removal Process Using Pulsed Discharge Plasma," *IEEE Transactions on Industry Applications*, vol. 31, no.5, pp. 957-963, 1995.

[25]   L. Bromberg, D. R. Cohn, M. Koch, R. M. Patrick, and P. Thomas, "Decomposition of dilute concentrations of carbon tetrachloride in air by an electron beam generated plasma," *Physics Letters A*, vol. 173, pp. 293-299, 1993.

[26]   Y. Nakagawa, S. Adachi, A.Kohchi, and J. Nagasawa, "Application of Pulse High-Energy Electron Beams for Decomposition of Chlorofluorocarbon in Atmospheric-Pressure Air," *Japanese Journal of Applied Physics*, vol. 34, Part 2, no.6B, pp. 793-796, 1995.

[27]   I. Maezono and J.S. Chang. "Reduction of CO_2 from Combustion Flue Gases by Corona Torch", IEEE Transactions on Industrial Applications, vol.26, pp.651-655, 1990.

[28]   T. Yamamoto, P. Lawless, and L. Sparks, "Triangle-Shaped DC Corona Discharge Device for Molecular Decomposition," *IEEE Transactions on Industry Applications*, vol. 25, no.4, pp. 743-749, 1989.

[29]   W. Niessen, O. Wolf, R. Schruft, and M. Neiger, "The influence of ethene on the conversion of NOx in a dielectric barrier discharge," *Journal of Applied Physics D: Applied Physics*, vol. 31, pp. 542-550, 1998.

[30]   H. Ma, P. Chen, M. Zhang, X. Lin, and R. Ruan, "Study of SO2 Removal Using Non-Thermal Plasma Induced by Dielectric Barrier Discharge," *Plasma Chemistry and Plasma Processing*, vol. 22, no.2, pp. 239-254, 2002.

[31]   K. Urashima and J.-S. Chang, "Removal of Volatile Organic Compounds from Air Streams and Industrial Flue Gases by Non-

Thermal Plasma Technology," *IEEE Transactions on Dielectrics and Electrical Insulation*, vol. 7, no.5, pp. 602-614, 2000.

[32]   T. G. Beuthe and J.-S. Chang, "Chapter 9," in *Handbook of Electrostatic Processes*, J.-S. Chang, A. Kelly, and J. Crowley, Eds. New York: Marcel Dekker, 1995, pp. 147-193.

[33]   S. Agnihotri, M. Cal, and J. Prien, "Destruction of 1,1,1-Trichloroethane Using Dielectric Barrier Discharge Nonthermal Plasma," *Journal of Environmental Engineering*, pp. 349-355, 2004 (March).

[34]   J.-S. Chang, P. Lawless, and T. Yamamoto, "Corona Discharge Processes," *IEEE Transactions on Plasma Science*, vol. 19, no.6, pp. 1152-1166, 1991.

[35]   K. Takaki, M. Shimizu, S. Mukaigawa, and T. Fujiwara, "Effect of Electrode Shape in Dielectric Barrier Discharge Plasma Reactor for NOx Removal," *IEEE Transactions on Plasma Science*, vol. 32, no.1, pp. 32-38, 2004.

[36]   "Standard Test Methods for Measurement of Energy and Integrated Charge Transfer Due to Partial Discharges (Corona) Using Bridge Techniques," in *2002 Annual Book of ASTM Standards, Section 10, Electrical Insulation and Electronics*, vol. 10.02: American Society of Testing & Materials, 2002.

[37]   R. Feng, G. Castle, and S. Jayaram, "Automated System for Power Measurement in the Silent Discharge," *IEEE Transactions on Industry Applications*, vol. 34, no.3, pp. 563-570, 1998.

[38]   "EPA's Environmental Technology Verification Program," Environmental Protection Agency EPA600/F-04/064, June 2004.

[39]   "Environmental Technology Verification Report: Honeywell Energy Systems, Parallon 75kW Turbogenerator," Environmental Protection Agency, SRI/USEPA-GHG-VR10, September 2001.

[40]   "Environmental Technology Verification Report: Combined Heat and Power at a Commercial Supermarket - Capstone 60kW Microturbine CHP System," Environmental Protection Agency 2003.

[41]   "Environmental Technology Verification Report: Ingersoll-Rand Power Systems Inc., IR Powerworks 70kW Microturbine System," Environmental Protection Agency SRI/USEPA-GHG-VR21, April 2003.

[42]   K. Shimizu, T. Harano, and T. Oda, "Effect of Water Vapor and Hydrocarbons in Removing NOx by Using Plasma and Catalyst," *IEEE Transactions on Industry Applications*, vol. 37, no.2, pp. 464-471, 2001.

[43]   J. Hoard and R. Tonkyn, "Two-Stage Plasma Catalysis for Diesel NO_x Emission Control," *Journal of Advanced Oxidation Technology*, vol. 6, no.2, pp. 158-165, 2003.

[44]   A. Khacef and R. Tonkyn, "Two-Stage Plasma Catalysis for Diesel NOx Emission Control," *Journal of Applied Physics D: Applied Physics*, vol. 6, no.2, pp. 158-165, 2003.

[45]   J. Y. Park, I. Tomicic, G. F. Round, and J.-S. Chang, "Simultaneous removal of NOx and SO2 from NO-SO2-CO2-N2-O2 gas mixtures by corona radical shower systems," *Journal of Applied Physics D: Applied Physics*, vol. 32, pp. 1006-1011, 1999.

[46]   K. Urashima, J.-S. Chang, and T. Ito, "Reduction of NOx from Combustion Flue Gases by Superimposed Barrier Discharge Plasma Reactor," *IEEE Transactions on Industry Applications*, vol. 33, no.4, pp. 897-886, 1997.

[47]   H. H. Kim, G. Prieto, K. Takashima, S. Katasura, and A. Mizuno, "Performance evaluation of discharge plasma process for gaseous pollutant removal," *Journal of Electrostatics*, vol. 55, pp. 25-41, 2002.

[48]	M. B. Chang and S. C. Yang, "NO/NOx Removal with C_2H_2 as Additive via Dielectric Barrier Discharges," *AIChE Journal*, vol. 47, no.5, pp. 1126-1233, 2001.

[49]	J.-S. Chang, "Simultaneous Removal of NO_x, SO_x and VOCs from Engine Combustion Generated Waste Gas Streams by Non-Thermal Plasma Technologies," presented at International Symposium Plasma 2001: Research and Application of Plasmas, Warsaw, Poland, 2001.

[50]	K. Takaki and T. Fujiwara, "Multipoint Barrier Discharge Process for Removal of NOx from Diesel Engine Exhaust," *IEEE Transactions on Plasma Science*, vol. 29, no.3, pp. 518-523, 2001.

[51]	R. Dorai, K. Hassouni, and M. Kushner, "Interaction between soot particles and NOx during dielectric barrier discharge plasma remediation of simulated diesel exhaust," *Journal of Applied Physics D: Applied Physics*, vol. 88, no.10, pp. 6060-6071, 2000.

[52]	M. Higashi, S. Uchida, N. Suzuki, and K. Fujii, "Soot Elimination and NOx and SOx Reduction in Diesel-Engine Exhaust by a Combination of Discharge Plasma and Oil Dynamics," *IEEE Transactions on Plasma Science*, vol. 20, no.1, pp. 1-12, 1992.

[53]	J. O. Chae, "Non-thermal plasma for diesel exhaust treatment," *Journal of Electrostatics*, vol. 57, pp. 251-262, 2003.

[54]	T. Yamamoto, C. L. Yang, M. Beltrna, and Z. Kravets, "Plasma-Assisted Chemical Process for NOx Control," *IEEE Transactions on Industry Applications*, vol. 36, no.3, pp. 923-927, 2000.

[55]	J.-S. Chang, P. Looy, M. Arquilla, I. Kamiya, and R. Sinko, "Ozone and the Other Gaseous By-products Generated from Dry Air by Trench Type Barrier Discharge Plasma Reactor," *Journal of Advanced Oxidation Technology*, vol. 2, no.2, pp. 274-277, 1997.

[56] R. Dorai and M. Kushner, "Consequences of propane and propane on plasma remediation of NOx," *Journal of Applied Physics D: Applied Physics*, vol. 88, no.6, pp. 3739-3747, 2000.

[57] T. Yamamoto, M. Okubo, T. Nagaoka, and K. Hayakawa, "Simultaneous Removal of NO_x, SO_x, and CO_2 at Elevated Temperature Using Plasma-Chemical Hybrid Process," *IEEE Transactions on Industry Applications*, vol. 38, no.5, pp. 1168-1173, 2002.

[58] H. H. Kim, K. Tsunoda, S. Katsura, and A. Mizuno, "A Novel Plasma Reactor for NOx Control Using Photocatalyst and Hydrogen Peroxide Injection," *IEEE Transactions on Industry Applications*, vol. 35, no.6, pp. 1306-1310, 1999.

[59] K. Shimizu and T. Oda, "DeNO$_x$ Process in Flue Gas Combined with Nonthermal Plasma and Catalyst," *IEEE Transactions on Industry Applications*, vol. 35, no.6, pp. 1311-1322, 1999.

[60] J. H. Kwak, J. Szanyi, and C. Peden, "Nonthermal plasma-assisted catalytic NOx reduction over Ba-Y, FAU: the effect of catalyst preparation," *Journal of Catalysis*, vol. 220, pp. 291-298, 2003.

[61] T. Oda, T. Kato, T. Takahashi, and K. Shimizu, "Nitric Oxide Decomposition in Air by Using Nonthermal Plasma Processing with Additives and Catalyst," *IEEE Transactions on Industry Applications*, vol. 34, no.2, pp. 268-272, 1998.

[62] J. Hoard, T. Wallington, J. Ball, M. Hurley, K. Wodzisz, and L. Balmer, "Role of Methyl Nitrate in Plasma Exhaust Treatment," *Environmental Science and Technology*, vol. 33, pp. 3427-3437, 1999.

[63] H. Miessner, K.-P. Francke, R. Rudolph, and T. Hammer, "NOx removal in excess oxygen by plasma-enhanced selective catalytic reduction," *Catalysis Today*, vol. 75, pp. 325-330, 2002.

[64] H. Miessner, K.-P. Francke, and R. Rudolph, "Plasma-enhanced HC-SCR of NOx in the presence of excess oxygen," *Applied Catalysis B: Environmental*, vol. 36, pp. 53-62, 2002.

[65] P. Kilpinen, P. Glarborg, and M. Hupa, "Reburning Chemistry: A Kinetic Modeling Study," *Industrial & Engineering Chemistry Research*, vol. 31, pp. 1477-1490, 1992.

[66] J.-S. Chang, K. Urashima, M. Arquilla, and T. Ito, "Reduction of NOx From Combustion Flue Gases by Corona Discharge Activated Methane Radical Injections," *Combustion Science and Technology*, vol. 133, pp. 31-47, 1998.

[67] C.-H. Lin and H. Bai, "Energy-Effectiveness of Nonthermal Plasma Reactors for Toluene Vapor Destruction," *Journal of Environmental Engineering*, pp. 648-654, 2001 (July).

[68] K.-P. Francke, H. Miessner, and R. Rudolph, "Plasmacatalytic processes for environmental problems," *Catalysis Today*, vol. 59, pp. 411-416, 2000.

[69] Y.-H. Song, M. S. Cha, Y. Kim, S. J. Kim, S.-Y. Han, and K.-I. Choi, "Synergetic Effects of Non-thermal Plasma and Catalysts on VOCs Decomposition," *Journal of Advanced Oxidation Technology*, vol. 6, no.1, pp. 11-16, 2003.

[70] Y.-H. Song, S. J. Kim, K.-I. Choi, and T. Yamamoto, "Effects of adsorption and temperature on a nonthermal plasma process for removing VOCs," *Journal of Electrostatics*, vol. 55, pp. 189-201, 2002.

[71] Z. Falkenstein, "Effects of O_2 concentration on the removal efficiency of volatile organic compounds with dielectric barrier discharges in Ar and N_2," *Journal of Applied Physics D: Applied Physics*, vol. 85, No.1, pp. 525-529, 1999.

[72]   T. Ohkubo, D. Li, D. Yakushiji, S. Kanazawa, and Y. Nomoto, "Decomposition of VOC in Air Using Streamer Corona Discharge Reactor Combined with Catalyst," *Journal of Advanced Oxidation Technology*, vol. 6, no.1, pp. 75-79, 2003.

[73]   H. M. Lee and M. B. Chang, "Removal of Gaseous Acetaldehyde via a Silent Discharge Reactor Packed with Al_2O_3 Beads," *Journal of Advanced Oxidation Technology*, vol. 6, no.1, pp. 48-54, 2003.

[74]   T. Oda, T. Takahashi, and K. Yamaji, "Nonthermal Plasma Processing for Dilute VOCs Decomposition," *IEEE Transactions on Industry Applications*, vol. 38, no.3, pp. 873-878, 2002.

[75]   T. Oda and K. Yamaji, "Dilute Tricholoroethylene Decomposition in Air by Using Non-Thermal Plasma-Catalyst Effect," *Journal of Advanced Oxidation Technology*, vol. 6, no.1, pp. 93-99, 2003.

[76]   J. T. Richardson, Y. Peng, and D. Remue, "Properties of ceramic foam catalyst supports: pressure drop," *Applied Catalysis A: General*, vol. 204, no.1, pp. 19-32, 2000.

[77]   S. Ambridge, Y. Uchida, K. Urashima, D. Ewing, and J.-S. Chang, "Oxidation of NOx and Hydrocarbon Emissions from Diesel Engines," presented at 53rd Canadian Chemical Engineering Conference, Hamilton, Canada, 2003.

7401   23